Max-Planck-Institut für Metallforschung
Stuttgart

Nitriding of Iron-based Alloys; the Role of Excess Nitrogen

Santosh S. Hosmani

Dissertation
an der
Universität Stuttgart

Bericht Nr. 187
Juni 2006

Max-Planck-Institut für Metallforschung
Stuttgart

Nitriding of Iron-based Alloys; the Role of Excess Nitrogen

Santosh S. Hosmani

Dissertation
an der
Universität Stuttgart

Bericht Nr. 187
Juni 2006

Nitriding of Iron-based Alloys; the Role of Excess Nitrogen

von der Fakultät Chemie der Universität Stuttgart
zur Erlangung der Würde eines Doktors der
Naturwissenschaften (Dr. rer. nat.) genehmigte Abhandlung

vorgelegt von

Santosh S. Hosmani

aus Belagam/Indien

Hauptberichter:	Prof. Dr. Ir. E. J. Mittemeijer
Mitberichter:	Prof. Dr. F. Aldinger
Mitprüfer:	Prof. Dr. H. Bertagnolli

Tag der Einreichung:	31.03.2006
Tag der mündlichen Prüfung:	14.06.2006

MAX-PLANCK-INSTITUT FÜR METALLFORSCHUNG STUTTGART
INSTITUT FÜR METALLKUNDE DER UNIVERSITÄT STUTTGART

2006

Contents

1. Introduction 9
1.1. General introduction about nitriding 9
1.2. Basics about equilibrium solubility of nitrogen in α-Fe 9
1.3. Nitriding of Fe-Me alloys and occurrence of excess nitrogen 12
1.4. Outline of thesis 14
References 15

2. The kinetics of the nitriding of Fe-7wt.%Cr alloys; the role of the nitriding potential 17
2.1. Introduction 18
2.2. Theoretical background 18
2.2.1. Nitriding potential 18
2.2.2. Nitriding characteristics of Fe-Cr alloys; discontinuous coarsening and excess nitrogen 19
2.2.3. Model for growth kinetics 20
2.3. Experimental 25
2.3.1. Specimen preparation 25
2.3.2. Nitriding 25
2.3.3. Specimen characterisation 26
2.3.3.1. Light and scanning electron microscopy 26
2.3.3.2. Hardness measurement 26
2.3.3.3. X-ray diffraction (XRD) 26
2.3.3.4. Electron probe microanalysis (EPMA) 27
2.4. Results and evaluation 27
2.4.1. Phase analysis 27
2.4.2. Morphology of the nitrided zone 28
2.4.3. Hardness-depth profiles 31
2.4.4. Concentration-depth profiles; excess nitrogen 32
2.4.5. Thickness of nitrided zone 35
2.5. Kinetics of nitrided layer growth 37
2.6. Conclusions 40
Acknowledgements 41
References 42

3. Microstructure of the "white layer" formed on nitrided Fe-7wt.%Cr alloys 45
3.1. Introduction 46
3.2. Experimental 46
3.2.1. Specimen preparation 46
3.2.2. Nitriding 47
3.2.3. Specimen characterisation 47
3.2.3.1. Light and scanning electron microscopy 47
3.2.3.2. X-ray diffraction (XRD) 48
3.2.3.3. Electron probe microanalysis (EPMA) 48
3.3. Results and discussion 48
3.3.1. Light optical microscopy 48
3.3.2. X-ray diffraction analysis 49
3.3.3. Electron probe microanalysis; quantitative phase analysis 51

3.4. Conclusions …….. 54
Acknowledgements …….. 54
References …… 55

4. Nitriding behavior of Fe–4wt%V and Fe–2wt%V alloys …… 57
4.1. Introduction …….. 58
4.2. Experimental ……. 58
4.2.1. Specimen preparation …… 58
4.2.2. Nitriding ……. 59
4.2.3. Specimen characterisation ……. 59
4.2.3.1. Light and scanning electron microscopy …… 59
4.2.3.2. Hardness measurement ……... 60
4.2.3.3. X-ray diffraction (XRD) ……. 60
4.2.3.4. Electron probe microanalysis (EPMA) ……... 60
4.3. Precipitation behavior; “continuous” versus “discontinuous” …….. 61
4.3.1. Nitriding of Fe-4wt.%V ……. 61
4.3.2. Nitriding of Fe-2wt.%V ……. 66
4.4. Discussion ……. 68
4.4.1. Precipitation morphology …….. 68
4.4.2. Excess nitrogen …….. 69
4.4.3. Growth kinetics of the nitrided layers …… 70
4.5. Conclusions …….. 73
Acknowledgements …….. 74
References …… 75

5. Nitrogen uptake by an Fe-V alloy; quantitative analysis of excess nitrogen ……. 77
5.1. Introduction …….. 78
5.2. Theoretical background …… 79
5.2.1. Nitrogen uptake in Fe-V alloys …….. 79
5.2.1.1. Nitrogen adsorbed at the precipitate-matrix interfaces ……... 80
5.2.1.2. Nitrogen dissolved in the strained iron lattice …… 80
5.2.2. The nitrogen absorption isotherm …….. 82
5.3. Experimental ……. 84
5.3.1. Specimen preparation …… 84
5.3.2. Nitriding ……. 84
5.3.3. Determination of nitrogen absorption isotherms ……... 85
5.4. Results and discussion …….. 86
5.4.1. Pre-nitriding ……... 86
5.4.2. De-nitriding …… 88
5.4.3. Nitrogen absorption isotherms ……... 89
5.4.3.1. Interfacial, adsorbed nitrogen, $[N]_{interface}$ …… 91
5.4.3.2. Dissolved nitrogen, $[N]^0_\alpha + [N]_{strain}$ ……. 92
5.4.3.3. Concluding remarks on excess nitrogen ……. 94
5.5. Conclusions …….. 95
Acknowledgements …….. 96
References …… 97

6. Kinetics of nitriding Fe-2wt.%V alloy; mobile and immobile excess nitrogen ……. 99
6.1. Introduction …….. 100

6.2. Model for the kinetics of diffusion zone growth: theoretical background ……... 100
6.2.1. Nitrogen uptake in Fe-Me alloys ……... 100
6.2.2. Modelling the nitrogen depth profile of the diffusion zone of nitrided Fe-Me alloys ……... 102
6.3. Experimental ……. 107
6.3.1. Specimen preparation …… 107
6.3.2. Nitriding ……. 108
6.3.3. Specimen characterisation ……. 108
6.3.3.1. Light microscopy …… 108
6.3.3.2. Hardness measurement ……... 109
6.3.3.3. Electron probe microanalysis (EPMA) ……... 109
6.4. Results and discussion …….. 109
6.4.1. Morphology of the nitrided zone ……... 109
6.4.2. Nitrogen concentration depth profiles: excess nitrogen …… 110
6.4.3. Model fitting: the effect of temperature on excess nitrogen and nitrogen diffusivity …….. 113
6.5. Conclusions …….. 117
References …… 119

7. Zusammenfassung ……. 121
7.1. Einleitung …….. 121
7.2. Experimentelles ……...……. 121
7.3. Ergebnisse und Diskussion …...……...……. 122
7.3.1. Mikrostruktur der Nitrierschicht …… 122
7.3.2. Überschussstickstoff; Absorptionsisothermen ……..……. 125
7.3.3. Wachstumskinetik nitrierter Schichten ……...……... 126

Curriculum Vitae ……... 131

Acknowledgements …….. 133

Chapter 1

Introduction

1.1 General introduction about nitriding

Nitriding is a thermochemical surface process by which nitrogen is introduced into the surface region of workpieces. Nitriding improves the fatigue strength, the tribological properties and/or the corrosion resistance.

Nitrided regions can be subdivided into (i) the compound layer adjacent to the surface composed of iron nitrides, and (ii) the diffusion zone underneath, where nitrogen is either dissolved or precipitate as alloying element nitrides (Fig. 1.1). The improvement of corrosion and wear properties can be attributed to the compound layer, whereas the diffusion zone improves the fatigue properties, if precipitation of alloying element nitrides takes place.-

There are several nitriding methods: e.g. plasma nitriding, salt bath nitriding and gaseous nitriding. The most well-known method to introduce nitrogen into a (ferritic) workpiece is gaseous nitriding. An eminent advantage of gaseous nitriding is the precise control of the chemical potential of nitrogen in the nitriding atmosphere.

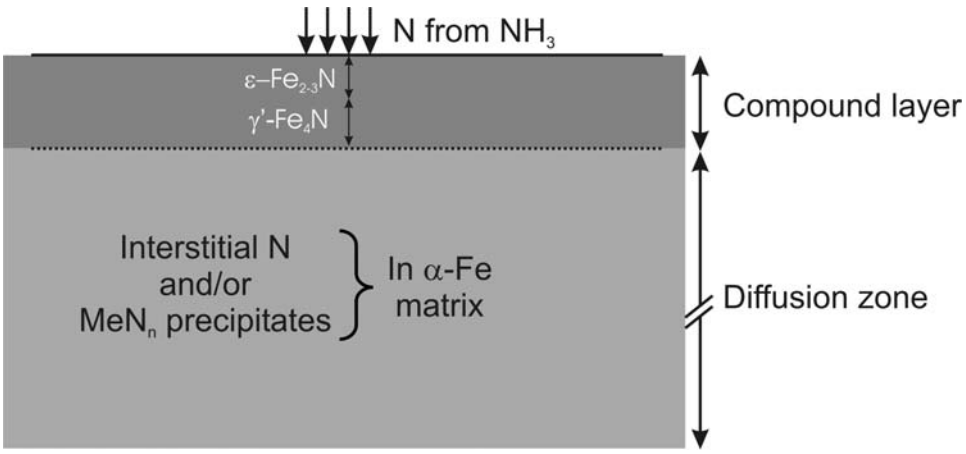

Fig. 1.1: Schematic presentation of the surface region of a nitrided iron/iron-based alloy.

1.2 Basics about equilibrium solubility of nitrogen in α-Fe

Nitriding in NH_3/H_2 gas mixture is equivalent to nitriding in N_2 at a pressure of a number of thousands atm (thermodynamic argument [1]) and is possible due to the slow thermal

decomposition of NH_3 (kinetic argument [2]). Therefore the Fe-N phase diagram established in contact with NH_3/H_2 gas mixture is not the phase diagram for its pure components Fe and N_2 at atmospheric pressure, but, it represents the phase diagram for Fe and NH_3/H_2 gas mixture.

The chemical potential of nitrogen in a gas phase, $\mu_{N,g}$, consisting of an NH_3/H_2 gas mixture can be defined on the basis of the hypothetical equilibrium:

$$NH_3 \Leftrightarrow \frac{3}{2}H_2 + \frac{1}{2}N_2$$

where,

$$\mu_{N,g} \equiv \frac{1}{2}\mu_{N_2} = \mu_{NH_3} - \frac{3}{2}\mu_{H_2}$$

If the standard states refer to unit pressure and if ideal gases or constant fugacity coefficients can be assumed it holds:

$$\mu_{N,g} = \frac{1}{2}\left[G^0_{N_2} + RT\ln p_{N_2}\right] = \left[\left(G^0_{NH_3} + RT\ln p_{NH_3}\right) - \left(\frac{3}{2}G^0_{H_2} + RT\ln p^{3/2}_{H_2}\right)\right]$$

$$= G^0_{NH_3} - \frac{3}{2}G^0_{H_2} + RT\ln\left(\frac{p_{NH_3}}{p^{3/2}_{H_2}}\right)$$

$$= G^0_{NH_3} - \frac{3}{2}G^0_{H_2} + RT\ln(r_n) \qquad (1.1)$$

where p_{N_2}, p_{HN_3} and p_{H_2} are partial pressure of N_2, NH_3 and H_2 respectively; G is Gibbs-free energy per mole and superscript 0 indicates the standard state; r_n is nitriding potential. From Eq. (1.1), at constant temperature $\mu_{N,g}$ depends only on r_n. If equilibrium is attained between an imposed NH_3/H_2 gas mixture and Fe-N phase (i.e. in present study "say" α-Fe), the chemical potential of nitrogen in α-Fe is equal to that in the gas phase: $\mu_{N,\alpha-Fe} = \mu_{N,g}$. By variation of the NH_3/H_2 gas mixture (i.e. variation nitriding potential) at a certain temperature and determination of the equilibrium nitrogen content in the α-Fe phase the so-called nitrogen absorption isotherm for Fe in α-phase region can be determined.

A solution of nitrogen in ferrite can be described considering a regular solution of nitrogen on its own sublattice [3]. The nitrogen content on the interstitial sublattice is so low that excess enthalpy does not need to be taken into account [3]. So now the Gibbs-free energy for one mole Fe-N (α phase) (from Ref. [3] and any text-book related to phase transformation: e.g. Ref. [4]) reads:

$$G_{Fe-y_{N,\alpha}} = G^0_{Fe} + y_{N,\alpha-Fe}\cdot G^0_{N,\alpha-Fe} + RT\left[y_{N,\alpha-Fe}\cdot\ln(y_{N,\alpha-Fe}) + (1-y_{N,\alpha-Fe})\cdot\ln(1-y_{N,\alpha-Fe})\right]$$

(1.2)

where $y_{N,\alpha-Fe}$ is the fraction of sites of 'interstitial sublattice' that is occupied by N atoms (i.e. occupancy of nitrogen sublattice for α-Fe phase). A general representation of the chemical potential [4] of nitrogen in ferrite:

$$\mu_{N,\alpha-Fe} \equiv N_{Av}\left(\frac{\partial G^{|}_{Fe-y_{N,\alpha}}}{\partial y_{N,\alpha-Fe}}\right) = \left(\frac{\partial G_{Fe-y_{N,\alpha}}}{\partial y_{N,\alpha-Fe}}\right) \tag{1.3}$$

where the symbol $G^{|}$ refers to the Gibbs-free energy of the whole system; and symbol G denotes to the molar free energy which is independent of the size of the system. N_{Av} is Avogadro's number.

Now from Eq. (1.2) and (1.3), the chemical potential of nitrogen in ferrite, $\mu_{N,\alpha-Fe}$, is:

$$\mu_{N,\alpha-Fe} = G^0_{N,\alpha-Fe} + RT\ln\left[\frac{y_{N,\alpha-Fe}}{1-y_{N,\alpha-Fe}}\right] \tag{1.4}$$

For equilibrium between NH_3/H_2 gas mixture and ferrite: $\mu_{N,\alpha-Fe} = \mu_{N,g}$, equating Eq. (1.1) and (1.4):

$$G^0_{N,\alpha-Fe} + RT\ln\left[\frac{y_{N,\alpha-Fe}}{1-y_{N,\alpha-Fe}}\right] = G^0_{NH_3} - \frac{3}{2}G^0_{H_2} + RT\ln(r_n)$$

i.e. $$G^0_{N,\alpha-Fe} - G^0_{NH_3} + \frac{3}{2}G^0_{H_2} = RT\ln(r_n) - RT\ln\left[\frac{y_{N,\alpha-Fe}}{1-y_{N,\alpha-Fe}}\right] \tag{1.5}$$

Let, ΔG^0 be the change in standard Gibbs-free energy for the solubility of nitrogen in ferrite in equilibrium with NH_3/H_2 gas mixture:

$$NH_3 - \frac{3}{2}H_2 \Leftrightarrow [N]_\alpha \tag{1.6}$$

For the above reaction (Eq. (1.6)) ΔG^0 is,

$$\Delta G^0 = G^0_{N,\alpha-Fe} - G^0_{NH_3} + \frac{3}{2}G^0_{H_2} = -RT\ln\left(\frac{a^0_n}{p^0_{NH_3}\cdot(p^0_{H_2})^{-3/2}}\right) \tag{1.7a}$$

In the standard state, activity of dissolved N in ferrite, $a^0_n = 1$ and let $[p^0_{NH_3}\cdot(p^0_{H_2})^{-3/2}]$ be r^0_n (where r^0_n is reference nitriding potential for α-Fe phase). So Eq. (1.7a) becomes,

$$\Delta G^0 = G^0_{N,\alpha-Fe} - G^0_{NH_3} + \frac{3}{2}G^0_{H_2} = RT\ln\left(r^0_n\right) \tag{1.7b}$$

From Eqs. (1.5) and (1.7b),

$$RT\ln(r_n^0) = RT\ln(r_n) - RT\ln\left[\frac{y_{N,\alpha-Fe}}{1-y_{N,\alpha-Fe}}\right]$$

i.e.

$$\left[\frac{y_{N,\alpha-Fe}}{1-y_{N,\alpha-Fe}}\right] = \left[\frac{r_n}{r_n^0}\right] \tag{1.8}$$

Since the occupancy of nitrogen for α-Fe phase ($y_{N,\alpha-Fe}$) is very small, the denominator in left-hand-side of Eq. (1.8) can be replaced by 1:

$$\therefore \quad y_{N,\alpha-Fe} = \frac{r_n}{r_n^0} \tag{1.9}$$

According to Eq. (1.9) the equilibrium nitrogen content in α-Fe at a certain temperature depends linearly on the nitriding potential. Such simple straightforward relations do not occur for other Fe-N phases, like γ'-Fe_4N_{1-x} and ε-Fe_2N_{1-z} (see Refs. [2, 3] for details).

1.3 Nitriding of Fe-Me alloys and occurrence of excess nitrogen

During nitriding, if the iron matrix (substrate) contains alloying elements with a relatively high affinity for nitrogen, like Ti, V, Cr, Mn and Al, alloying element nitride precipitates can develop (in the "diffusion zone"), which leads to a pronounced increase of the hardness. The increase in e.g. hardness or fatigue resistance depends on the chemical composition of the precipitates, their coherency with the matrix, their size and their morphology.

If a Fe-Me (Me= Ti, V, Cr etc) alloy is nitrided such that no iron nitrides can be formed at the surface (i.e. the nitriding potential is sufficiently low [1, 2]), only a diffusion zone containing MeN_n precipitates develops ("internal nitriding"). The nitrided zone is composed of alloying element nitride precipitates and surrounding α-Fe (ferrite) matrix containing nitrogen at octahedral interstitial sites. For MeN_n precipitate in α-Fe the nitride platelets have the orientation $(001)_{\alpha\text{-Fe}}$ // $(001)_{MeNn}$, which is compatible with the Bain orientation relationship (e.g. see Ref. [5] for VN).

Nitrided Fe-Me alloys have a considerable capacity for the uptake of so-called excess nitrogen (i.e. more nitrogen than necessary for (i) precipitation of all alloying element as nitride, $[N]_{MeN_n}$, and (ii) equilibrium saturation of the ferrite matrix, $[N]_\alpha^0$). The total amount of excess nitrogen can be divided into two types: mobile and immobile excess nitrogen (see below).

A significant part of the excess nitrogen in nitrided binary iron-based alloys is adsorbed at the nitride/matrix interfaces, $[N]_{interface}$. A MeN_n precipitate with excess nitrogen adsorbed at

the interface with the matrix can be regarded as a MeN_X compound, i.e. (X-n) nitrogen atoms per MeN_X molecule are bonded / adsorbed to the coherent faces of the particle / platelet. The amount of nitrogen at the precipitate / matrix interface is called immobile excess nitrogen as it does not take part in kinetic process.

The coherent MeN_n precipitates induce strain fields in the surrounding ferrite matrix and thereby influence the nitrogen solubility of the ferrite matrix [6]. A MeN_n precipitate developing in the ferrite matrix experiences a positive volume misfit. Then, supposing fully elastic accommodation, the treatment by Eshelby [7] for a finite matrix shows that a positive dilation of the matrix occurs. The matrix lattice dilation generated by the misfitting nitrides, induced by the hydrostatic component of the image-stress field of finite bodies, provides a geometrical understanding for the occurrence of enhanced solubility of nitrogen. This dilation is not a direct function of temperature. The actually occurring, temperature dependent amount of excess nitrogen (at strain fields: $[N]_{strain}$) can then be estimated applying the thermodynamics of (hydrostatically) stressed solids [6]. The amount of nitrogen at strain fields is called mobile excess nitrogen as it takes part in the diffusion (kinetic) process.

Total nitrogen uptake by nitrided Fe-Me system can be subdivided (for easy understanding) as shown in Fig. 1.2. Nitrogen absorption isotherms (cf. section 1.2) can be a useful tool to understand the various kinds of differently (chemically) bonded nitrogen.

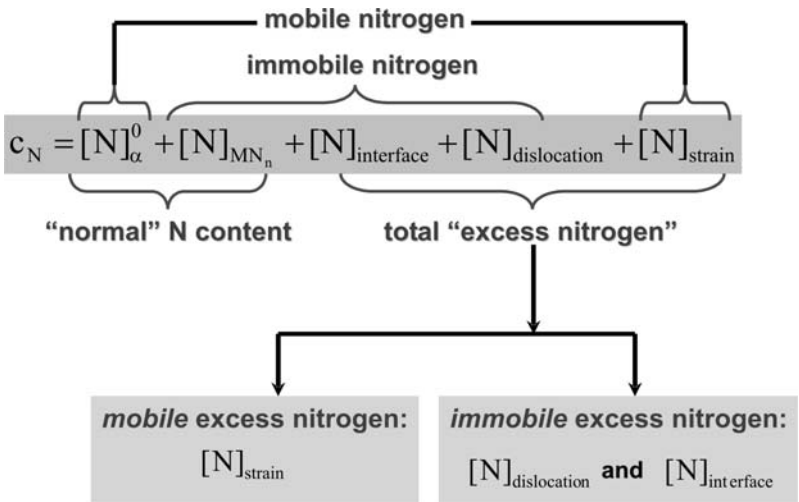

Fig. 1.2: Flow chart indicating subdivision of nitrogen uptake in nitrided Fe-Me alloys. The amount of $[N]_{dislocation}$ can be neglected in recrystallized samples due to the relatively low dislocation densities.

1.4 Outline of thesis

In Chapter 2 the kinetics of the nitriding of Fe-7wt.%Cr alloy was studied as function of the nitriding potential, recognizing that Cr is an important alloying element for nitriding steels. The nitriding potential has a direct effect on the amount of dissolved nitrogen in ferrite (including mobile excess nitrogen) and thereby on the nitriding kinetics. A satisfactory quantitative description of the kinetics of the nitriding process has not been presented until now. Recently (2003-2004) our group has proposed a model to describe the nitriding kinetics that for the first time incorporated the role of the so-called excess nitrogen in the nitrided zone [8]. This model was applied to the experimental nitrogen concentration depth profiles for Fe-7wt.%Cr at different nitriding potentials.

Chapter 3 is devoted to an analysis of the microstructure of the compound layer / "white layer" on Fe-7wt.%Cr alloy. For the first time a quantitative (phase) analysis of such a white layer was carried out, demonstrating the presence of a dispersed CrN phase within a γ' iron-nitride matrix and providing an understanding for the evolution of the compound layer.

Chapter 4 deals with nitriding of Fe-V alloys. In this work upon nitriding Fe-V alloys two precipitation morphologies was observed for the first time: near the surface of nitrided Fe-4wt.%V alloys a lamellar microstructure composed of α-Fe and VN lamellae occurs; at larger depths in the nitrided zone very finely dispersed, submicroscopical VN precipitates occur. The nitriding kinetics was determined and analyzed. Significant amounts of mobile and immobile excess nitrogen in Fe-V alloys were observed.

In Chapter 5 nitrogen absorption isotherms of Fe-2wt.%V alloys were determined experimentally to study the differences in chemical bonding for various types of absorbed nitrogen. Until now the direct compositional analysis of the coherent, extremely tiny, thin nitride precipitate platelets has appeared impossible. Doubts were expressed that the composition of the nitrides would not be purely MeN (here VN) but (Me, Fe)N, which would simply explain the observation of excess nitrogen. The study was performed to investigate in detail the various types and their amounts of absorbed nitrogen, and thereby also to settle the nature of the excess nitrogen, at least for the Fe-V alloys considered here.

Chapter 6 presents a diffusion model to calculate nitrogen concentration depth profiles. The presence of mobile and immobile excess nitrogen is considered in this model. Application of the model to nitrogen concentration-depth profiles as a function of temperature for Fe-2wt.%V alloy demonstrated that the nitriding temperature has significant influence on the amounts of mobile and immobile excess nitrogen.

References

[1] Mittemeijer EJ, Slycke JT. Surface Engineering 1996;12:152.

[2] Mittemeijer EJ, Somers MAJ. Surface Engineering 1997;13:483.

[3] Kooj BJ. PhD Thesis Delft University of Technology, The Netherlands 1995.

[4] Porter DA, Easterling KE. Van Nostrand Reinhold (UK) Co. Ltd. 1981.

[5] Bor TC, Kempen ATW, Tichelaar FD, Mittemeijer EJ, van der Giessen E. Phil Mag A 2002;82:971.

[6] Somers MAJ, Lankreijer RM, Mittemeijer EJ. Phil Mag A 1989;59:353.

[7] Eshelby JD. Solid State Physics 1956;3:79.

[8] Schacherl RE, Graat PCJ, Mittemeijer EJ. Metall Mater Trans A 2004;35:3387.

Chapter 2

The kinetics of the nitriding of Fe-7wt.%Cr alloys; the role of the nitriding potential

S.S. Hosmani, R.E. Schacherl and E.J. Mittemeijer

Abstract

The nitriding behaviour of the Fe-7wt.%Cr alloy was studied at 580 °C in a gas mixture of ammonia and hydrogen. The nitriding potential was varied from 0.03 to 0.818 $atm^{-1/2}$. Microstructural analysis of the nitrided specimens was performed by applying light microscopy, hardness measurements, X-ray diffraction, and electron probe microanalysis. The nitrided zone is composed of both regions with finely dispersed small chromium-nitride (CrN) precipitates (continuous precipitates) in ferrite (α-Fe) grains and, mainly near the surface, regions where the precipitates have discontinuously coarsened leading to a lamellar CrN/α-Fe morphology. The nitrogen content within the nitrided zone is larger than expected on the basis of the chromium content and the solubility of nitrogen in (stress-free) ferrite: excess nitrogen occurs. The hardness maximum in the nitrided zone and the nitriding depth increases with increasing nitriding potential as long as no iron-nitride layer developed at the surface of the specimens. To describe the evolution of the nitrogen concentration-depth profile of the nitrided layers a numerical model was applied that has as important (fit) parameters: the surface nitrogen content, the solubility product of chromium and nitrogen dissolved in the ferrite matrix, and a parameter defining the composition of the precipitated chromium nitride. The nitriding depth depends roughly linearly on the square root of the nitriding potential. Analysis of the concentration-depth profile data demonstrated that the amount of excess nitrogen considerably influences the nitriding kinetics.

2.1 Introduction

Nitriding is a well-known thermochemical surface treatment to improve the fatigue, tribological and/or anti-corrosion properties of iron-based (steel) workpieces. One method to introduce nitrogen in a workpiece is by gaseous nitriding, involving that nitrogen, from dissociating NH_3 at temperatures in the range 450 – 590 °C, enters the workpiece through its surface. Nitriding in NH_3/H_2 gas mixtures is equivalent to nitriding in N_2 at a pressure of a number of thousands atm (thermodynamic argument [1]) and is possible due to the slow thermal decomposition of NH_3 (kinetic argument [2]).

If strong nitride forming alloying elements, like Ti, Al, V and Cr, are present, alloying-element nitride precipitates can develop upon nitriding [3, 4], which causes large increase in the hardness. Many nitriding steels contain chromium as an important alloying element. Therefore study of nitriding of iron-chromium alloys is of practical interest. The gaseous nitriding of iron-chromium alloys has been subject of several investigations [5-11]. However, a satisfactory quantitative description of the kinetics of the nitriding process has not been presented until now. Recently our group has proposed a model to describe the nitriding kinetics that for the first time incorporated the role of the so-called excess nitrogen [12] in the nitrided zone [13]. The model was applied to experiments performed at one nitriding potential. However, the nitriding potential is expected to have a direct effect on the amount of dissolved nitrogen (including excess nitrogen) and thereby on the nitriding kinetics.

In the present work, gaseous nitriding of iron-chromium alloys has been performed as a function of the "nitriding potential". A model is presented that quantitatively describes the observed kinetics; thereby opening the route to automated process control of the nitriding process.

2.2 Theoretical background

2.2.1 Nitriding potential

The "nitriding potential", r_N, is defined as follows,

$$r_n \equiv \frac{p_{NH_3}}{p_{H_2}^{3/2}} \tag{2.1}$$

where, p_{NH_3} and p_{H_2} are the partial pressures of NH_3 and H_2, respectively. Nitriding in a NH_3-H_2 gas mixture can be presented as [1]:

$$NH_3 \Leftrightarrow [N] + \frac{3}{2}H_2 \tag{2.2}$$

where [N] represents N dissolved in the ferrite grains of the iron-chromium alloy. Thus, if local equilibrium occurs at the surface of the specimen, the activity of nitrogen in the specimen at its surface, a_N^S, and the chemical potential of nitrogen in the gas phase are both governed by r_n, irrespective of the total pressure of the NH_3-H_2 gas mixture. Thus it holds for a_N^S

$$a_N^S = K^{(1)}\left(\frac{p_{NH_3}}{p_{H_2}^{3/2}}\right) = K^{(1)} r_N \tag{2.3}$$

where $K^{(1)}$ is the equilibrium constant for reaction (2.2). Hence, by controlled variation of the gas composition in the nitriding atmosphere, the activity of nitrogen at the surface and thereby the concentration of dissolved nitrogen at the surface can be varied [2].

In the case of nitriding pure iron, (layers of) iron nitrides can be formed at the surface if the nitriding potential is high enough ("external nitriding"). Thus, depending on the applied nitriding temperature and nitriding potential the hexagonal ε-Fe_2N_{1-Z} and/or the cubic $\gamma^{|}$-Fe_4N_{1-X} phases can develop. Below the iron-nitride layers always a zone of α-Fe with nitrogen dissolved in the octahedral interstitial sites of the body centred cubic Fe parent lattice is present: the so-called diffusion zone.

The critical nitriding potential above which the first iron nitride ($\gamma^{|}$-Fe_4N_{1-X}) develops is well known for pure iron [1, 2, 14]. This value can have the same importance for the nitriding of Fe-Cr alloys, because upon nitriding all Cr precipitates as chromium nitride leaving a pure α-Fe matrix containing the dissolved, mobile nitrogen, that is responsible for the continuation of the nitriding process experienced by the specimen.

2.2.2 Nitriding characteristics of Fe-Cr alloys; discontinuous coarsening and excess nitrogen

Because of the relatively strong N-Cr interaction, upon nitriding chromium nitrides are formed within the nitrogen containing diffusion zone ("internal nitriding") [15, 16]. In ferritic iron-chromium alloys containing less than 20 wt.% Cr, nitriding starts with the formation of face centered cubic CrN precipitates [5, 7, 16] which are coherent (or semicoherent) and very small (submicroscopical; i.e. not visible with light microscopy). This stage is associated with relatively high hardness values because of the strain fields induced by the misfit between the (coherent) chromium nitride and α-Fe [15-17].

It has been observed [7, 18] that upon nitriding Fe-Cr alloys a surplus uptake of nitrogen occurs: "excess nitrogen". Excess nitrogen is the amount of nitrogen which exceeds the

"normal" capacity of nitrogen uptake. This normal capacity for nitrogen uptake consists in the case of a Fe-Cr alloy of:

- the amount of nitrogen dissolved interstitially in the unstrained α-Fe matrix and
- the amount of nitrogen, which is incorporated in the CrN precipitates.

The difference between the total amount of nitrogen in the nitrided zone and this normal capacity is defined as "excess" nitrogen. Three types of "excess" nitrogen are distinguished: (i) nitrogen which is trapped at dislocations (in particular for deformed alloys [19]), (ii) nitrogen which is adsorbed at matrix/precipitate interfaces and (iii) nitrogen which is (additionally) dissolved in the strained α-Fe matrix. Such excess nitrogen was found in nitrided Fe-Cr alloys [7, 18, 20].

Coarsening of the chromium-nitride precipitates can take place either by the continuous growth of the initial chromium-nitride particles and/or by the (simultaneous) formation of chromium-nitride and α-Fe lamellae (discontinuous coarsening). This last discontinuous coarsening reaction initiates at grain boundaries and can be described as [7]:

$$\alpha^{|} + \beta^{|} \rightarrow \alpha + \beta \qquad (2.4)$$

where $\beta^{|}$ denotes coherent CrN precipitates in a supersaturated matrix ($\alpha^{|}$). The reaction consists of replacing submicroscopical, coherent, CrN precipitates by CrN lamellae ($\beta^{|} \rightarrow \beta$) under simultaneous elimination of the supersaturation of the matrix ($\alpha^{|} \rightarrow \alpha$). The driving force for this transformation is the decrease of the interfacial area between chromium nitride and α-Fe, the decrease (of the extent) of the stress fields surrounding the initially coherent chromium-nitride precipitates which have become incoherent with the α-Fe matrix and the loss of nitrogen supersaturation [15, 16]. Because of their relatively coarse microstructure and relaxed misfit at the α-Fe/CrN interfaces, the discontinuously coarsened areas show relatively low hardness values [15-17].

2.2.3 Model for growth kinetics

The first proposals to describe diffusion zone growth upon nitriding are based on a simple model originally meant for "internal oxidation" [21]. Applying this model to internal nitriding, the following assumptions must hold:

(i) The nitrogen dissolved in the ferrite matrix (α) exhibits Henrian behaviour. This implies that the diffusion coefficient of nitrogen in the ferrite matrix is independent of the dissolved nitrogen content.

(ii) The reaction of dissolved nitrogen with dissolved Cr, leading to the nitride CrN, takes place only and completely at a sharp interface between the nitrided zone and the not nitrided core.

(iii) The amount of nitrogen which is required for building up the concentration profile in the ferrite matrix of the nitrided zone is negligible in comparison to the amount of nitrogen which is consumed at the reaction interface.

(iv) Diffusion of Cr can be neglected and is not nitriding-rate determining.

(v) Local equilibrium prevails at the nitriding medium / specimen interface, so that the surface concentration $c^S_{N_\alpha}$ is equal to the lattice solubility of nitrogen, as given by the chemical potential of nitrogen in the nitriding atmosphere.

If these conditions are satisfied, it follows for the nitriding depth, z, at constant temperature:

$$z^2 = \left(\frac{2 \cdot c^S_{N_\alpha} \cdot D_N}{c_{Cr}} \right) \cdot t \tag{2.5}$$

where c_{Cr} is the atomic concentration of substitutional solute Cr originally dissolved and D_N is the diffusivity of nitrogen.

This model has been often used to predict the case depth of the nitrided zone [3, 7, 10]. However, a sharp interface between nitrided and unnitrided zone, as required by the model, does not occur in reality (see section 2.4.4). Further, a major simplification of reality in the model is that the solubility of nitrogen in the ferrite matrix is taken as that pertaining to unstrained, pure α-Fe: the presence of excess nitrogen dissolved in the α-Fe matrix is not accounted for. These shortcomings of the simple model have been overcome in the numerical model proposed recently in Ref. [13]. The essence of this model is summarised briefly below.

It is essential to distinguish between *mobile* excess nitrogen, i.e. nitrogen dissolved in the ferrite lattice, and *immobile* excess nitrogen, i.e. nitrogen trapped at dislocations and adsorbed at the nitride/matrix interfaces. Mobile excess nitrogen will enhance the extent of the diffusion zone, whereas immobile excess nitrogen will decrease the extent of the nitrided zone.

The inward diffusion of nitrogen in the α-Fe matrix can be described with Fick's second law:

$$\frac{\partial c_{N_\alpha}(z,t)}{\partial t} = D_N \cdot \frac{\partial^2 c_{N_\alpha}(z,t)}{\partial z^2} \tag{2.6}$$

$c_{N_\alpha}(z,t)$ is the nitrogen dissolved in the α-Fe matrix at the depth z at time t and at temperature T. D_N is the diffusion coefficient of nitrogen in α-Fe, which can be taken as concentration

independent [1, 2]. The formation of nitrides of possibly present alloying elements removes dissolved, mobile nitrogen from the matrix, which nitrogen then is trapped as immobile nitrogen in the nitrides formed. The formation of CrN can be expressed with the following equation:

$$Cr_\alpha + N_\alpha \Leftrightarrow CrN \tag{2.7}$$

where Cr_α and N_α denote alloying element (i.e. Cr) and nitrogen dissolved in the α-Fe matrix. The equilibrium constant of the above reaction, K_e, obeys

$$K_e = \frac{1}{[Cr_\alpha]\cdot[N_\alpha]} = \frac{1}{K_{CrN}} \quad \text{with} \quad K_{CrN} = [Cr_\alpha]\cdot[N_\alpha] \tag{2.8}$$

where $[Cr_\alpha]$ and $[N_\alpha]$ denote the concentrations of dissolved Cr and dissolved N in the α-Fe matrix and K_{CrN} is the corresponding solubility product of Cr_α and N_α. The precipitation of CrN will take place at a certain location if there it holds

$$[Cr_\alpha][N_\alpha] > K_{CrN} \tag{2.9}$$

In solving Fick's second law (Eq. (2.6)) it must be tested at every location (depth z) for every time (step) if the solubility product, K_{CrN}, is surpassed. If this is the case, precipitation of CrN, at the location considered, should be allowed for until $[Cr_\alpha][N_\alpha] = K_{CrN}$. Thereby a numerical finite difference solution method (explicit method) is naturally suggested to solve Fick's second law, subject to the prevailing boundary conditions [22, 23]. The algorithm for the numerical model for the nitriding kinetics adopted here is described in Ref. [13].

In this work the effect of the nitriding potential on the nitriding kinetics is considered by taking the nitrogen lattice solubility at the surface, $c^S_{N_\alpha}$, as a fit parameter (i.e., it is not assumed that $c^S_{N_\alpha}$ is equal to the equilibrium nitrogen solubility of (unstrained) ferrite), because the nitriding potential has a direct effect on the amount of dissolved nitrogen (including mobile excess nitrogen). The presence of immobile excess nitrogen is recognised by replacing the stoichiometric parameter n (= 1) in equilibrium CrN_n by b=n+x (= 1+x), with x expressing as the contribution of immobile excess nitrogen. The fit parameters in the numerical model as applied here thus are: $c^S_{N_\alpha}$, b and K_{CrN}.

The importance of the nitriding potential and the effects of both mobile and immobile excess nitrogen for the nitriding kinetics can be demonstrated by simulations using the numerical model. A Fe-7 wt.% Cr alloy is considered, which is nitrided at 580 °C for 4h. The

solid lines in Fig. 2.1a show the resulting nitrogen-concentration depth profiles as calculated for different nitriding potentials for the case that neither mobile nor immobile excess nitrogen is present in the nitrided layer. This means that (i) the surface nitrogen content $c^S_{N_\alpha}$ is equal to the solubility of nitrogen in pure, unstrained ferrite, in accordance with the applied nitriding parameters (r_n = 0.03, 0.08, 0.11, 0.16 $atm^{-1/2}$ at 580 °C; for data on $c^S_{N_\alpha}$, see Ref. [2]) and (ii) that b is equal to n=1 (no immobile excess nitrogen). Evidently, the nitriding depth increases with increasing nitriding potential, reflecting the consequence of an overall concentration gradient of dissolved nitrogen increasing with nitriding potential (Fig. 2.1a).

If only the existence of mobile excess nitrogen is assumed, as expressed by higher values for $c^S_{N_\alpha}$, a significantly larger extent (depth) of the nitrided zone occurs as compared to the absence of mobile excess nitrogen (see dashed line vs. full line in Fig. 2.1b). If only the existence of immobile excess nitrogen is assumed, as expressed by a value of b larger than n (=1 for the present case of CrN precipitation), a smaller penetration depth of nitrogen occurs (see the dotted line vs. full line in Fig. 2.1b). The above used values for $c^S_{N_\alpha}$ and b are realistic values (see section 2.5).

If the nitriding time has been too short to establish local equilibrium (at the surface of the substrate), of the gas atmosphere with the solid substrate (i.e. surface concentration smaller than lattice solubility of nitrogen, as given by the chemical potential of nitrogen in the nitriding atmosphere), due to finite rate of dissociation of NH_3 at low nitriding potentials [24, 25], as expressed by a value for $c^S_{N_\alpha}$ lower than corresponding to equilibrium, a significantly smaller thickness of the nitrided zone occurs. This could be misinterpreted as the absence of excess nitrogen.

The transition of the nitrided zone to the unnitrided zone (i.e. the reaction front) becomes less sharp as the solubility product, K_{CrN}, increases [13]. Relatively large K_{CrN} values imply that (at the reaction front) not all dissolved Cr reacts with nitrogen to chromium nitride and thus the extent of the nitrided zone is larger for larger K_{CrN}, although in association with a more gradual transition between the nitrided zone and the not nitrided core of the sample. The solubility product, K_{CrN}, should not depend on nitriding potential, nitriding time and chromium content at constant temperature.

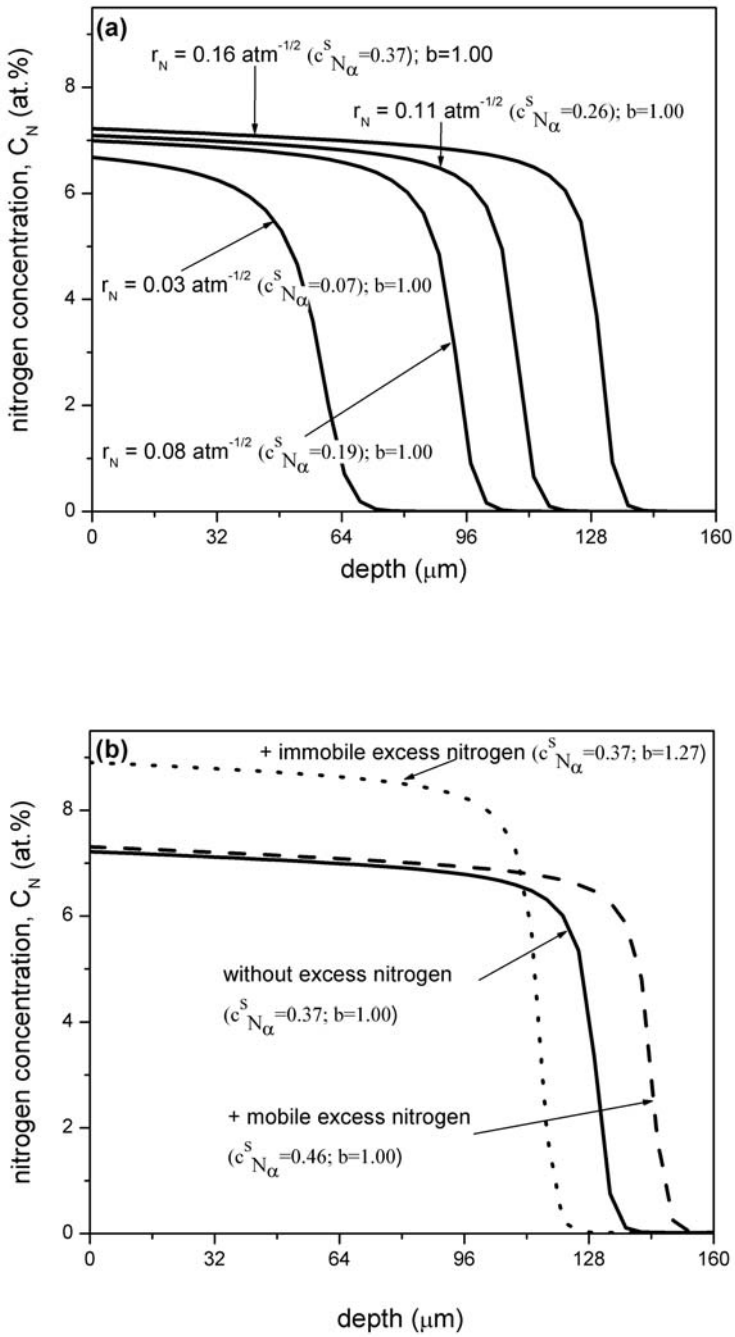

Fig. 2.1: Fe-7 wt.% Cr alloy sheet nitrided at 580 °C for 4h. (a) Effect of nitriding potential on the development of the nitrogen concentration-depth profile in the absence of excess nitrogen. (b) Effect of mobile and immobile excess nitrogen on the development of the nitrogen concentration-depth profile for $r_n = 0.16$ atm$^{-1/2}$.

2.3 Experimental

2.3.1 Specimen preparation

Fe-7wt.%Cr alloys were prepared from pure Fe (99.98 wt.%) and pure Cr (99.999 wt. %) in an inductive furnace under argon atmosphere (99.999 vol. %). The Cr content of the alloys was verified employing X-ray fluorescence analysis. The melt process was performed in an Al_2O_3 crucible.

After casting the alloys have a cylindrical shape with a diameter of 10 mm and a length of 100 mm. The cast alloys were cold rolled to sheets with a thickness of 1.2 +/-0.1 mm. The obtained sheets were cut into rectangular pieces of lateral dimensions 1.5x1.5 cm^2. These pieces were subsequently cleaned in an ultrasonic bath filled with ethanol and encapsulated in a silica tube filled with argon (purity: 99.999 vol.%) up to a pressure of 750 Torr. The encapsulated samples were annealed for 1h at 700 °C (within the α-phase region of the Fe-Cr diagram) to get a recrystallized grain structure. Before nitriding the samples were ground, polished (last step: 1μm diamond paste) and cleaned in an ultrasonic bath filled with ethanol.

2.3.2 Nitriding

For nitriding a sample was suspended at a quartz fibre in a vertical quartz tube (of inner diameter 28 mm) nitriding furnace. To start the nitriding process the sample was placed in the middle of the nitriding furnace. The nitriding experiments were performed at 580 °C (= 853 K) in an ammonia/hydrogen gas flux (purity: H_2: 99.999 vol. %, NH_3: >99.998 vol. %). The fluxes of both gases were adjusted with mass flow controllers. The nitriding parameters used are given in Table 2.1. The Fe-7wt.%Cr specimens which were nitrided at 580 ^{0}C at $r_n \leq 0.16$ $atm^{-1/2}$ were nitrided below the critical nitriding potential for (γ') iron-nitride formation (see section 2.2.1). For nitriding potentials higher than 0.19 $atm^{-1/2}$, formation of (γ') iron-nitride can be expected at the surface of the specimen. After the nitriding, the samples were quenched in water.

Table 2.1: Applied nitriding parameters (T = 580 °C; t = 4h). Inner diameter of quartz tube furnace: 28 mm.

expected phase upon nitriding pure iron	H_2 flow (ml/min)	NH_3 flow (ml/min)	nitriding potential r_n ($atm^{-1/2}$)
α	99	1	0.01
	97	3	0.03
	92	8	0.08
	90	10	0.11
	87	13	0.16
γ^{I}	84	16	0.21
	79	21	0.30
	69	31	0.54
	61	39	0.82

2.3.3 Specimen characterisation

2.3.3.1 Light and scanning electron microscopy

For light microscopical investigation, pieces were cut from the samples and prepared to cross sections, by subsequent embedding (Konduktomet, Buehler GmbH), polishing (last step: 1 µm diamond paste) and etching with 2.5% nital (2.5 vol.% HNO_3 in ethanol) for about 5 s. These cross sections were investigated with light optical microscopy applying a Leica DMRM microscope. The light micrographs were recorded with a digital camera (Jenoptik Progres 3008).

For scanning electron microscopy (SEM) the same (etched) cross-sections were used as for light microscopy. The SEM micrographs were taken with a Jeol JSM 6300F operating at 3 or 5 kV.

2.3.3.2 Hardness measurement

Hardness-depth profiles were obtained by carrying out hardness measurements across the cross-sections of the nitrided specimens using a Leitz Durimet hardness tester, applying a load of 100 g. The hardness values presented are average values of 4 measurements.

2.3.3.3 X-ray diffraction (XRD)

To determine which phases are present after nitriding, XRD was applied using a Philips X'Pert diffractometer. Measurements were made using Cu Kα and Co Kα radiations and employing the Bragg-Brentano geometry with a graphite monochromator in the diffracted

beam. The diffraction angle (2Θ) range scanned was 10 – 150°, with a step size of 0.05°. The X-ray diffractograms were recorded from specimen surfaces as obtained after nitriding. To identify the phases from the positions of the diffraction peaks the data from the JCPDS data base were used [26].

2.3.3.4 Electron probe microanalysis (EPMA)

To determine the composition of the nitrided zones of the samples after nitriding, EPMA was performed employing a Cameca SX100 instrument. Cross-sections of the nitrided alloys, similar to those as described above for light and scanning electron microscopy, were analysed, but in this case no etching after polishing was applied. A focussed electron beam at an accelerating voltage of 15 kV and a current of 100 nA was applied. To obtain the element contents in the specimens, the intensity of the characteristic Fe Kβ, Cr Kβ, N Kα, and O Kα X-ray emission peaks was determined at points along lines across the cross-sections (single measurement points at a distance of 2 μm). The intensities obtained from the nitrided samples were divided by the intensities obtained from standard samples of pure Fe (Fe Kβ), pure Cr (Cr Kβ), andradite/$Ca_3Fe_2(SiO_4)_3$ (O Kα), and γ'-Fe_4N (N Kα). Concentration values were calculated from the intensity ratios applying the $\Phi(\rho z)$ approach according to Ref. [27].

2.4 Results and evaluation

2.4.1 Phase analysis

X-ray diffractograms, recorded from the nitrided specimen surface, are presented in Fig. 2.2. The X-ray diffractograms of the Fe-7wt.%Cr specimens nitrided at $r_n \leq 0.16$ $atm^{-1/2}$, reveal the presence of α-Fe and CrN (Figs. 2.2a and b). The X-ray diffractograms of the samples nitrided at $r_n \geq 0.21$ $atm^{-1/2}$ show the presence of α-Fe, CrN and Fe_4N_{1-X} (Figs. 2.2c and d). The intensities of the diffraction peaks of Fe_4N_{1-X} increase for increasing r_n (Figs. 2.2c and d).

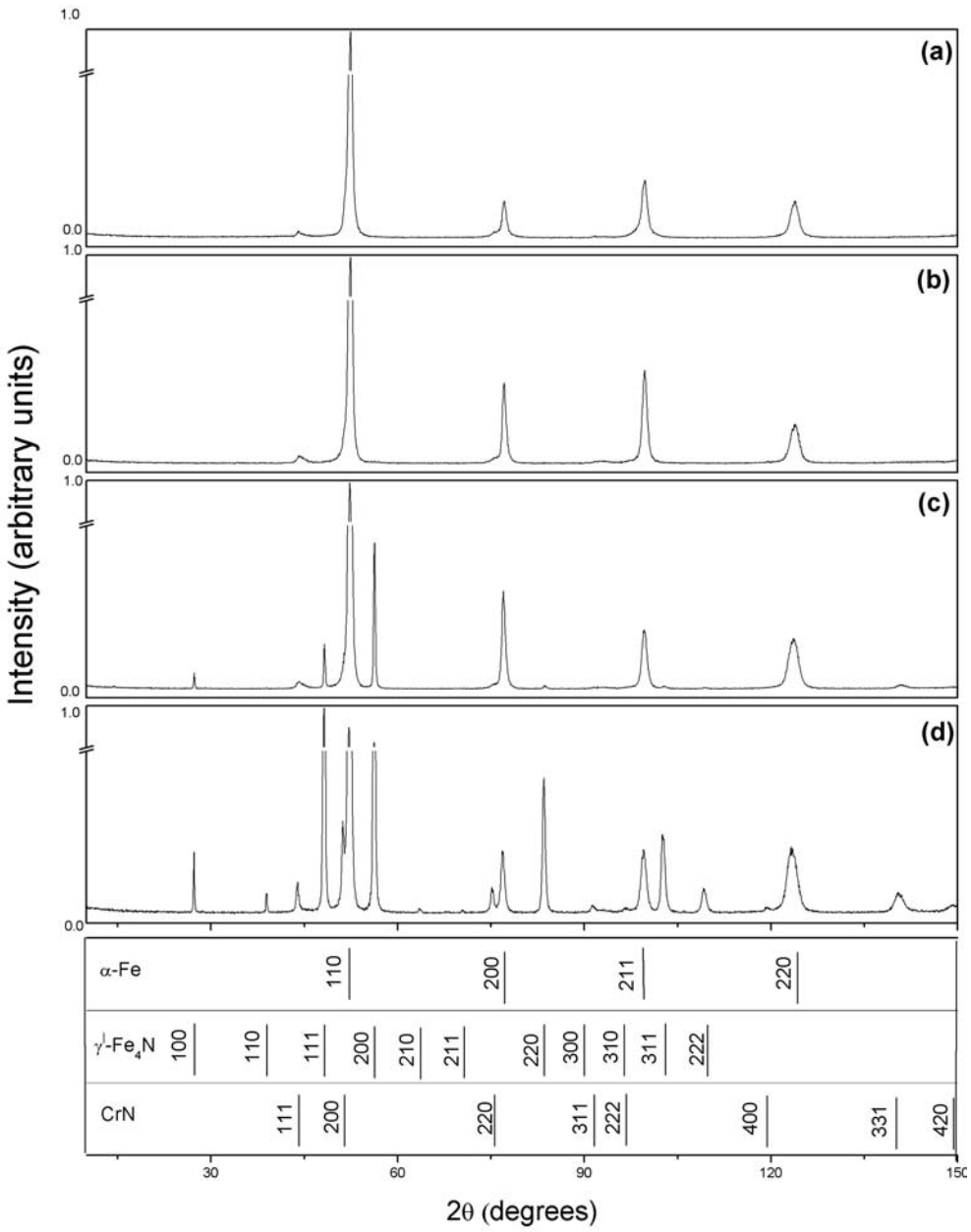

Fig. 2.2: X-ray diffractograms recorded from the surface of Fe-7wt.%Cr specimens, nitrided at 580 °C for 4h at (a) $r_n = 0.03\ atm^{-1/2}$; (b) $r_n = 0.16\ atm^{-1/2}$; (c) $r_n = 0.21\ atm^{-1/2}$ and (d) $r_n = 0.82\ atm^{-1/2}$. The positions of the α-Fe, CrN and Fe_4N_{1-X} reflections have been indicated.

2.4.2 Morphology of the nitrided zone

Light optical micrographs of the cross sections of the Fe-7wt.%Cr specimens nitrided at 580 °C for 4hr and at different nitriding potentials are shown in Fig. 2.3. Evidently the thickness of the nitrided zone increases distinctly with increasing nitriding potential upto 0.16 $atm^{-1/2}$. Further increase of the nitriding potential causes no significant increase of the thickness of the nitrided zone.

Dark regions occur (mainly) near the specimen surface and bright regions occur (mainly) near the centre of the specimen (Fig. 2.3). For nitriding potentials ≥ 0.21 $atm^{-1/2}$, at the surface a thin "white" layer occurs (Figs. 2.3b-d), which is composed of $\gamma^{|}$-Fe_4N_{1-X} as indicated by the X-ray diffractograms (Figs. 2.2c and d). This $\gamma^{|}$-Fe_4N_{1-X} layer becomes thicker for increases nitriding potential (Figs. 2.3b-d). This is compatible with the X-ray diffraction results showing that the intensities of the diffraction peaks of $\gamma^{|}$-Fe_4N_{1-X} increase for increasing r_n (Figs. 2.2c and d).

These microscopical observations, supported by hardness- and concentration-depth profile data reported in sections 2.4.3 and 2.4.4, can be interpreted as follows (see also begin of section 2.2). Initially the chromium nitride is formed as finely dispersed precipitates, which are probably coherent with the α-Fe matrix and undetectable by light microscopical analysis [7, 16]. On prolonged nitriding a coarsening of the CrN precipitates occurs, driven by the reduction of the Gibbs energy as a result of relaxation of the internal stress field, the reduction of precipitate/matrix interfacial area and the loss of nitrogen supersaturation. This coarsening can occur either as a continuous growth of the precipitates, i.e. a gradual increase of the size and decrease of the number of precipitates or it can take place as a discontinuous transformation of the former continuous precipitates: a lamellar (α-Fe/CrN) microstructure nucleating at and growing from grain boundaries / the surface into the bulk of the grains containing the submicroscopical CrN precipitates [7] (see SEM micrograph shown in Fig. 2.4). Thus, upon nitriding of Fe-Cr alloys two reaction fronts can be expected, the first one is due to inward diffusion of nitrogen and the reaction of Cr and N to finely dispersed CrN precipitates, and the second one is due to the subsequent coarsening of the precipitates. The resulting depth dependent morphology of the specimen depends on the nitriding conditions (temperature, nitriding potential, time) and the specimen conditions (as composition, grain size, state of residual stress) [16].

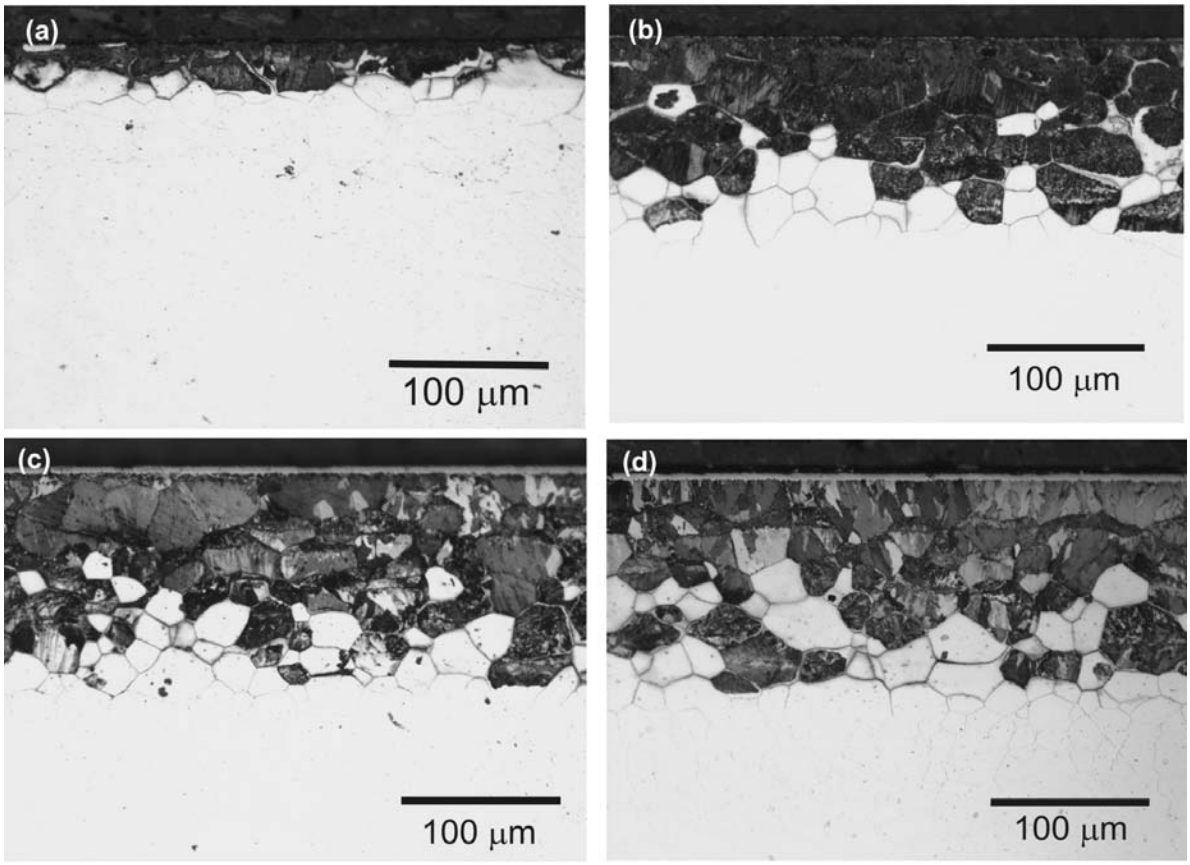

Fig. 2.3: Light optical micrographs of etched cross sections of Fe-7wt.%Cr specimens, nitrided at 580 °C for 4h at (a) $r_n = 0.03\ atm^{-1/2}$; (b) $r_n = 0.21\ atm^{-1/2}$; (c) $r_n = 0.54\ atm^{-1/2}$ and (d) $r_n = 0.82\ atm^{-1/2}$.

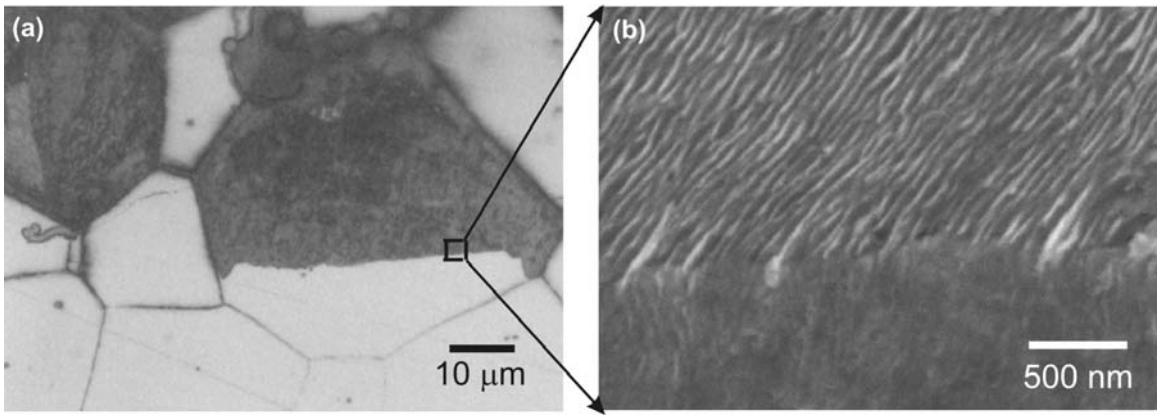

Fig. 2.4: An original grain of the Fe-7wt.%Cr alloy, after nitriding partially transformed by the discontinuous coarsening reaction (4h nitriding at 580 °C for nitriding potential 0.16 $atm^{-1/2}$). (a) Optical micrograph; (b) SEM micrograph of the region indicated in (a). The SEM micrograph clearly reveals the lamellar morphology of the part of the grain that had experienced the discontinuous coarsening.

2.4.3 Hardness-depth profiles

The brighter grains, containing the finely dispersed (submicroscopic) CrN precipitates, exhibit a microhardness much higher than measured for the darker grains containing the discontinuously coarsened CrN: see Fig. 2.5 showing that the hardness values close to the surface where the discontinuously transformed grains occur, are lower than the peak-hardness values which occur within the bright grains at larger layer depths.

The peak-hardness value increases with the nitriding potential for $r_n \leq 0.16$ atm$^{-1/2}$ (Figs. 2.5a and c). The nitrogen contents (circular dots in Fig. 2.5c) at the depths of peak-hardness at different nitriding potentials, as determined by electron probe microanalysis (EPMA), are nearly constant. A possible interpretation of this phenomenon may be as follows. As the nitriding potential increases (for $r_n \leq 0.16$ atm$^{-1/2}$; i.e. in the absence of an iron-nitride ($\gamma^{|}$) layer at the surface), the solubility of nitrogen at the nitriding temperature in α-Fe at the sample surface increases. Consequently, the driving force for CrN precipitation increases. This may lead to a large number of (even) smaller CrN particles, resulting in an increase of the peak hardness value with nitriding potential for $r_n \leq 0.16$ atm$^{-1/2}$.

The depth of hardening (see also sections 2.4.4 and 2.4.5) increases with nitriding potential for $r_n \leq 0.16$ atm$^{-1/2}$ (Fig. 2.5a).

For the specimens nitrided at nitriding potentials ≥ 0.21 atm$^{-1/2}$, a ($\gamma^{|}$) iron-nitride layer is formed at the surface (Figs. 2.2c, d and Figs. 2.3b-d). Then it can be expected that the solubility of nitrogen at the nitriding temperature in α-Fe at the interface of $\gamma^{|}$-Fe_4N_{1-X} layer and diffusion zone is constant [1, 2], i.e. independent of the nitriding potential, and thus the amount of precipitated CrN particles is constant as well, leading to peak hardness independent of r_n (Fig. 2.5b).

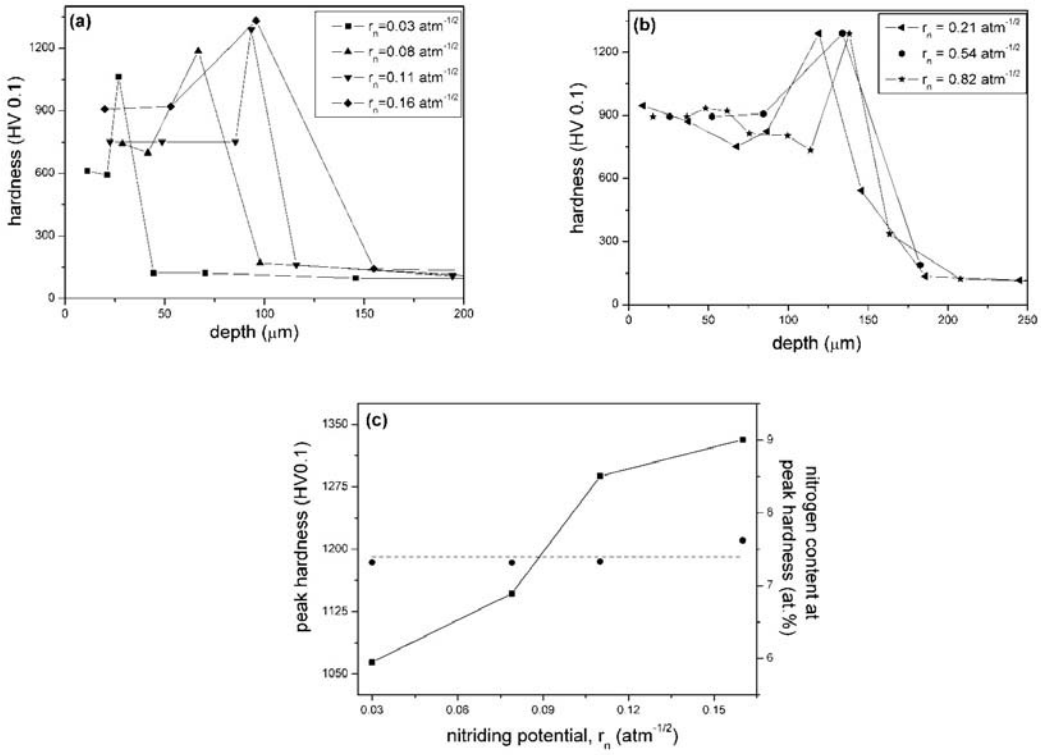

Fig. 2.5: Hardness-depth profiles for Fe-7wt.%Cr specimens nitrided at 580 ^{0}C for 4h at nitriding potentials (a) $r_n \leq 0.16$ atm$^{-1/2}$ and (b) $r_n \geq 0.21$ atm$^{-1/2}$. (c) Peak-hardness values (square dots and full line) for $r_n \leq 0.16$ atm$^{-1/2}$. The dashed horizontal line in (c) represents the average of nitrogen contents shown by circular dots at the depth locations of peak hardness for $r_n \leq 0.16$ atm$^{-1/2}$.

2.4.4 Concentration-depth profiles; excess nitrogen

The nitrogen concentration-depth profiles, as determined by EPMA, for Fe-7wt.%Cr specimens nitrided at 580 °C for 4h at $r_n \leq 0.16$ atm$^{-1/2}$ are shown in Fig. 2.6. Clearly, a practically constant nitrogen concentration occurs within the nitrided zone. The discontinuously transformed regions within the diffusion zone have no distinct influence on the nitrogen content: the regions of discontinuous precipitation and continuous precipitation cannot be distinguished in the concentration-depth profiles recorded for the nitrided zone, which contrasts with the results obtained from microscopical analysis and hardness measurements. Both the level of nitrogen uptake and the nitriding depth increase with nitriding potential for $r_n \leq 0.16$ atm$^{-1/2}$ (Fig. 2.6).

The EPMA results for the Fe-7wt.%Cr samples nitrided at $r_n \geq 0.21$ atm$^{-1/2}$ show a relatively high nitrogen content near the surface (Fig. 2.7) which is due to the $\gamma^{|}$-Fe_4N_{1-X} surface layer (see sections 2.4.1 and 2.4.2). The depth of nitriding is practically constant for $r_n \geq 0.21$ atm$^{-1/2}$ (Fig. 2.7), which parallels the results obtained from the hardness measurements (section 2.4.3).

Irregularities superimposed on the composition-depth profiles can be observed (Fig. 2.7). A local increase of the N content is always associated with a decrease of the Fe content at the same depth and (not always) an increase of the Cr content at the same depth at the same depth (see, for example, the dashed vertical lines in Figs. 2.7b and d). This is ascribed to the occurrence of CrN precipitates at grain boundaries and pores (containing N_2 gas) at grain boundaries [16].

The EPMA analysis of all nitrided specimens shows that the nitrogen concentration in the nitrided zone is larger than compatible with (i) the precipitation of all chromium as CrN, and (ii) the equilibrium solubility of nitrogen in the (remaining) ferrite matrix. The "normal" amount of nitrogen (according to (i) and (ii)), which should be present in the nitrided zone if no excess nitrogen would occur, has been indicated in Fig. 2.6 as well. The difference between the experimentally obtained total amount of nitrogen in the nitrided zone and this normal capacity is defined as "excess" nitrogen (also see section 2.2.2).

The equilibrium solubility of nitrogen in stress-free ferrite, $c^{S,0}_{N_\alpha}$, is calculated according to data in Refs. [1 and 2]. The experimental amount of surface nitrogen content in ferrite, $c^{S}_{N_\alpha}$, for Fe-7wt.%Cr specimens nitrided at $r_n \leq 0.16$ atm$^{-1/2}$ has been determined by EPMA (obtained as average value from the (first) three data points closest to the surface, after subtracting the amount of nitrogen contained in CrN from the total measured N concentration) (see Table 2.2). The difference between $c^{S}_{N_\alpha}$ and $c^{S,0}_{N_\alpha}$ gives the total amount of "excess" nitrogen (Table 2.2).

A similar approach is followed for the cases where an iron-nitride (γ') layer is present at the surface ($r_n \geq 0.21$ atm$^{-1/2}$). The experimental amount of nitrogen content in ferrite at the γ'/α-Fe interface, $c^{S}_{N_\alpha}$, is obtained by EPMA (obtained as average value from the (first) three data points closest to the γ'/α-Fe interface, after subtracting the amount of nitrogen contained in CrN from the total measured N concentration) (see Table 2.2).

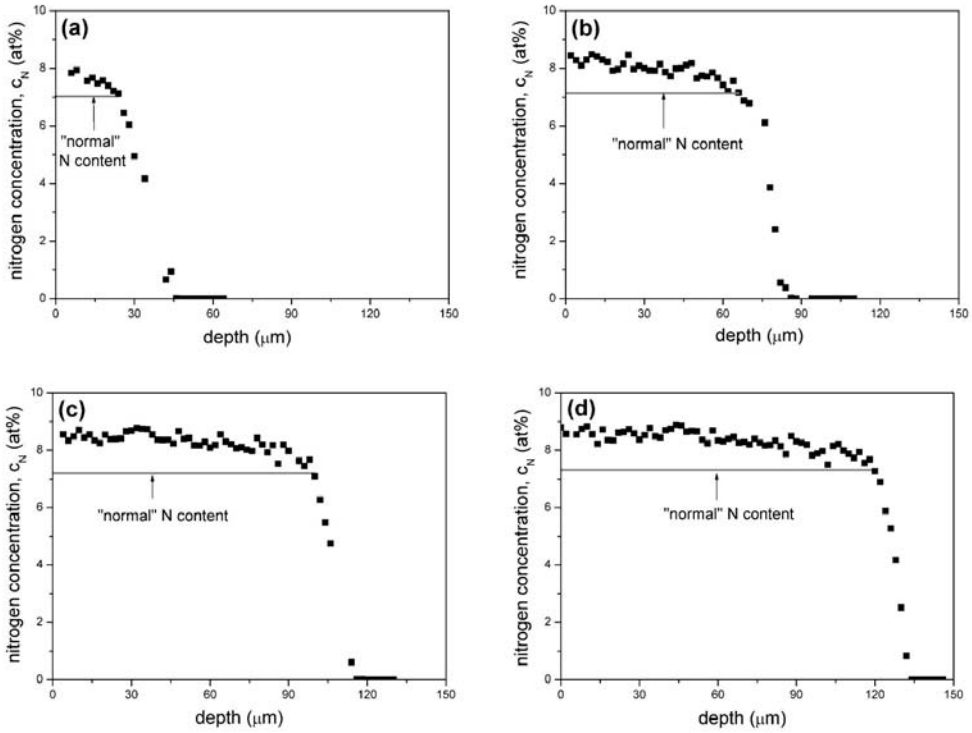

Fig. 2.6: Nitrogen concentration-depth profiles as measured with EPMA (black dots) for Fe-7wt.%Cr specimens nitrided at 580 °C for 4h at nitriding potentials (a) $r_n = 0.03$ atm$^{-1/2}$; (b) $r_n = 0.08$ atm$^{-1/2}$; (c) $r_n = 0.11$ atm$^{-1/2}$ and (d) $r_n = 0.16$ atm$^{-1/2}$. The horizontally drawn lines in these figures indicate the "normal" capacity for nitrogen uptake, i.e. the sum of the amount of nitrogen required for the formation of CrN, plus the amount of nitrogen dissolved in the unstrained ferrite matrix which is in equilibrium with the nitriding atmosphere.

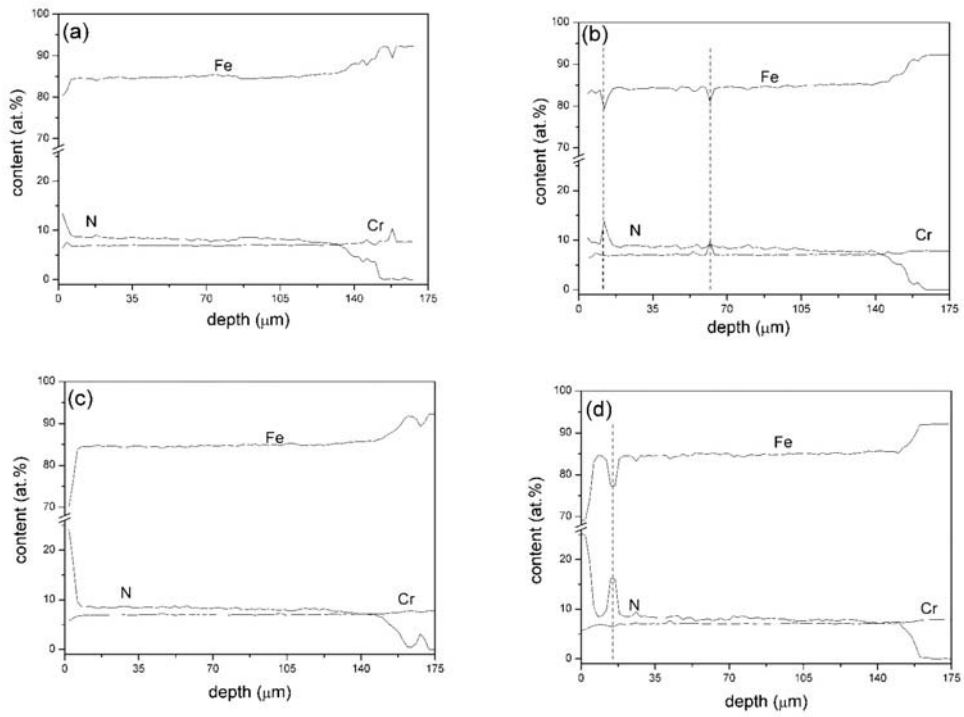

Fig. 2.7: N, Cr and Fe concentration-depth profiles as measured with EPMA for Fe-7wt.%Cr specimens nitrided at 580 °C for 4h at nitriding potentials (a) $r_n = 0.21$ atm$^{-1/2}$; (b) $r_n = 0.30$ atm$^{-1/2}$; (c) $r_n = 0.54$ atm$^{-1/2}$ and (d) $r_n = 0.82$ atm$^{-1/2}$.

Table 2.2: The experimental amount of nitrogen in ferrite at the surface, $c^{S}_{N_\alpha}$, the equilibrium solubility of nitrogen in stress-free ferrite, $c^{S,0}_{N_\alpha}$, and the total amount of excess nitrogen ($=c^{S}_{N_\alpha} - c^{S,0}_{N_\alpha}$), as a function of nitriding potential for Fe-7wt.%Cr specimens nitrided at 580 °C for 4h.

expected phase upon nitriding pure iron	r_n ($atm^{-1/2}$)	$c^{S}_{N_\alpha}$ (from EPMA data) (at%)	$c^{S,0}_{N_\alpha}$ (from literature) (at%)	total amount of excess nitrogen (at%)
α	0.03	1.1	0.07	1.0
	0.08	1.3	0.19	1.1
	0.11	1.6	0.26	1.3
	0.16	1.9	0.37	1.5
γ'	0.21	1.7	0.39	1.3
	0.30	1.8	0.39	1.4
	0.54	1.5	0.39	1.1
	0.82	1.7	0.39	1.3

2.4.5 Thickness of nitrided zone

The extent of the nitrided regions of the Fe-7wt.%Cr specimens as determined by the concentration-depth profiles and by the hardness-depth profiles can be compared. To this end the following definitions are employed:

- *Nitriding depth from concentration profiles*: the depth where the atomic nitrogen content reaches half the atomic chromium content present in the alloys [20].
- *Nitriding depth from hardness profiles*: the depth where the hardness value equals the average of the maximum (peak value) and the minimum (unnitrided core region) hardness [15].

On this basis the comparative presentation shown in Fig. 2.8 has been obtained. The straight line drawn with slope 1 in this figure demonstrates that the two measures of depth are fully compatible.

The actual nitrided layer thickness as obtained from the concentration-depth profiles has been plotted as a function of nitriding potential in Fig. 2.9a. A strong increase of the nitriding depth is observed for $r_n \leq 0.16$ $atm^{-1/2}$. This observation can be evaluated as follows. If, at constant temperature, the nitriding potential increases, the concentration of nitrogen dissolved interstitially in the α-Fe matrix at the surface (equilibrium solubility + excess nitrogen) increases (section 2.4.4), as long as the nitriding potential is below the critical value for iron-nitride formation at the surface. Therefore the overall concentration gradient, in the ferrite matrix of the nitrided zone containing precipitated CrN, increases with nitriding potential and

consequently, (according to Fick's first law) a larger nitrided layer thickness results. Henry's law holds for the nitrogen dissolved in α-Fe [1] and hence it follows from Eq. (2.3) that $c_{N_\alpha}^S \sim a_N^S \sim r_n$. Then, considering the highly simplified model yielding Eq. (2.5), it can be suggested that the nitriding depth must be approximately proportional to $(r_n)^{1/2}$. From the results as plotted in Fig. 2.9b, it follows that this crude prediction indeed agrees well with the experimental data.

If "local equilibrium" may be assumed at the nitride-layer/substrate interface (see discussion in Ref. [2]), a constant value would occur for the equilibrium solubility of nitrogen in the ferrite matrix at the interface (and also for the amount of excess nitrogen). Hence, beyond the critical nitriding potential, the nitrided layer thickness does not depend on nitriding potential (Fig. 2.9a).

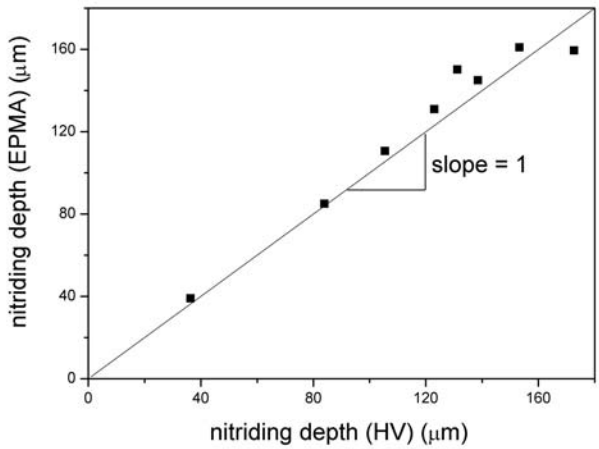

Fig. 2.8: Nitriding depth as determined from the nitrogen concentration-depth profiles versus the nitriding depth as determined from the hardness-depth profiles for different nitriding potentials.

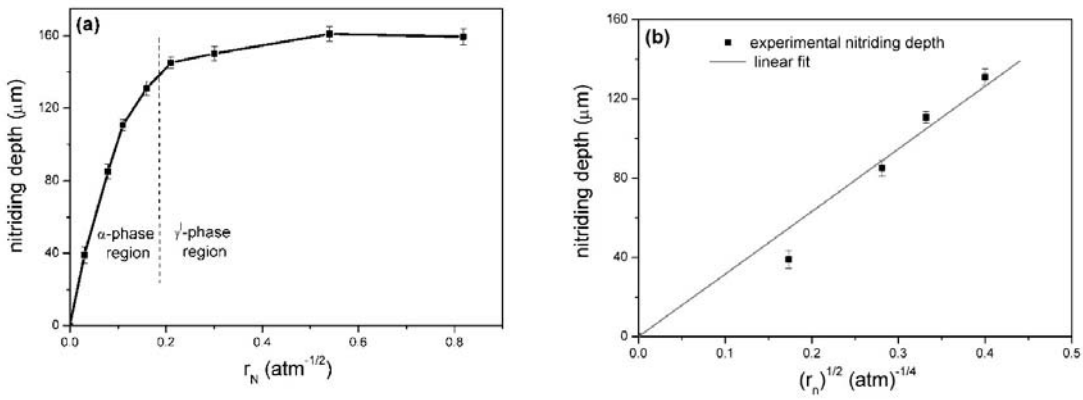

Fig. 2.9: (a) Nitriding depth as a function of the nitriding potential, r_n, for Fe-7wt.%Cr specimens nitrided at 580 °C for 4h. (b) Nitriding depth data for $r_n \leq 0.16$ atm$^{-1/2}$ versus $(r_n)^{1/2}$. The straight line in figure (b) indicates the linear fit to the experimental data. The resulting fit yields: nitriding depth = $315.8 \cdot (r_n)^{1/2}$; where nitriding depth is expressed in μm and r_n in atm$^{-1/2}$.

2.5 Kinetics of nitrided layer growth

Nitrogen concentration-depth profiles, as calculated using the numerical model described in section 2.2.3, were fitted to the experimentally determined nitrogen concentration-depth profiles for Fe-7wt.%Cr specimens nitrided at 580 °C for 4h at values of $r_n \leq 0.16$ atm$^{-1/2}$. To determine optimal values for the fitting parameters K_{CrN}, b=n+x (with n=1) and $c^S_{N_\alpha}$ (see section 2.2.3), a two step fitting procedure has been applied as follows.

Four nitrogen concentration-depth profiles were measured for Fe-7wt.%Cr specimens nitrided at 580 °C for each value of r_n. First, the nitrogen concentration-depth profiles were fitted individually. At constant temperature the solubility product K_{CrN} should not depend on nitriding time, nitriding potential and Cr content. Accordingly, the average value of K_{CrN}, determined from the 16 nitrogen concentration-depth profiles thus analysed, provided the value of K_{CrN} at 580 °C: $K_{CrN} \approx 0.02$ nm^{-6}. Using this value of K_{CrN}, the second, definitive fittings were performed, where only $c^S_{N_\alpha}$ and b were the fit parameters. Examples of thus fitted nitrogen concentration-depth profiles are shown in Fig. 2.10. The results (averages of 4 data for each r_n) obtained for the surface nitrogen content, $c^S_{N_\alpha}$, and the nitride-particle composition parameter, b, have been gathered in Table 2.3.

At low nitriding potentials (r_n=0.03 atm$^{-1/2}$ and 0.08 atm$^{-1/2}$), the value of $c^S_{N_\alpha}$ is slightly lower than equilibrium solubility of nitrogen in the ferrite [2] (see Table 2.3). This observation can be explained as follows. A significantly large finite period of time is necessary, at relatively low nitriding potential, to establish local equilibrium (at the surface of the substrate) of the gas atmosphere with the solid substrate. This effect has been observed for the nitriding of pure iron and is due to the finite rate of dissociation of NH_3 [24, 25]. The effect can be stronger for an iron-chromium alloy at low r_n, because in the presence of Cr much more N has to be taken up before saturation at the surface can be attained. Apparently, for the Fe-7wt.%Cr specimens nitrided for 4h at low nitriding potentials, the nitriding time applied is too small to achieve saturation at the surface. At relatively large nitriding potential (r_n=0.11 atm$^{-1/2}$ and 0.16 atm$^{-1/2}$), it appears that saturation at the surface bas been established; the solubility of nitrogen in the pure iron matrix of the nitrided Fe-7wt.%Cr specimens is higher than as expected for pure iron (Table 2.3). This indicates the presence of *mobile* excess nitrogen (i.e. dissolved nitrogen) that contributes to the (further) growth of the nitrided zone.

The values obtained for the stoichiometric parameter, b, are clearly larger than one (Table 2.3), which indicates the presence of *immobile* excess nitrogen in the nitrided zone. The origins of this immobile excess can be discussed as follows:

(i) It may be suggested that this immobile excess N is due to N (originally) adsorbed at the faces of the submicroscopical, coherent nitride particles [12]. At a later stage of nitriding, where practically the whole, or large parts of, the nitrided zone have experienced the discontinuous coarsening reaction, this N may no longer be accommodated at the interface of the CrN (now lamellae) with the α-Fe (now lamellae) and thus this N could have segregated (e.g. at grain boundaries) leading to porosity (N_2 formation), as has been detected (see Ref. [16]). Also then, this N cannot contribute to further nitriding and is accounted for in the kinetic model as immobile nitrogen.

(ii) In earlier work on nitrided Fe-Cr [7, 12, 18] it has been concluded that in case of CrN in α-Fe (and in contrast with, e.g., TiN in α-Fe or VN in α-Fe) no nitrogen adsorbs at the faces of the coherent CrN platelets. Further, as compared with the data for $c^S_{N_\alpha}$ obtained here, a much higher value of dissolved excess N has been deduced for an α-Fe matrix containing only submicroscopical, coherent CrN platelets: $c^S_{N_\alpha}$ values more than three times larger than the equilibrium solubility for α-Fe occur [7, 12]. The present, much lower values for mobile excess N suggest that the largest part of this originally mobile excess N is no longer dissolved in the α-Fe matrix upon continued nitriding (note the pronounced extent of the discontinuous coarsening; see section 2.4.2) and could have segregated (see further under (i)). Thereby this part of the excess nitrogen is accounted for in the kinetic model as immobile nitrogen.

The amounts of mobile and immobile excess nitrogen concentrations are larger for the Fe-7wt.%Cr specimens nitrided at r_n=0.16 $atm^{-1/2}$ than at r_n=0.11 $atm^{-1/2}$. This observation can be interpreted as follows. With increasing nitriding potential, the solubility of nitrogen at the nitriding temperature in the ferrite matrix at the sample surface increases and, consequently, the driving force for CrN precipitation increases. This may lead to a larger number of (even) smaller CrN particles for larger nitriding potential (see section 2.2.2), resulting in a larger nitride/matrix interfacial area (associated with “trapped”, immobile excess nitrogen) and more pronounced nitride/matrix misfit-strain fields (associated with dissolved, mobile excess nitrogen).

It should be recognized that the quantitative subdivision of the amount of excess nitrogen in mobile and immobile excess nitrogen, as established in this work, does not directly depend

on the absolute accuracy of the total amounts of nitrogen content as measured by EPMA: The amount of mobile excess nitrogen content, as determined by fitting (see Fig. 2.10), depends not in the first place on the level of total nitrogen content, but depends largely on the depth of the nitrided zone (a change of only 0.04 at. % mobile N leads to a change of nitriding depth of about 10µm (see also Fig. 2.1b), which is very well experimentally determinable); the much larger amount of immobile excess nitrogen then makes up for the remaining much larger part of the excess nitrogen.

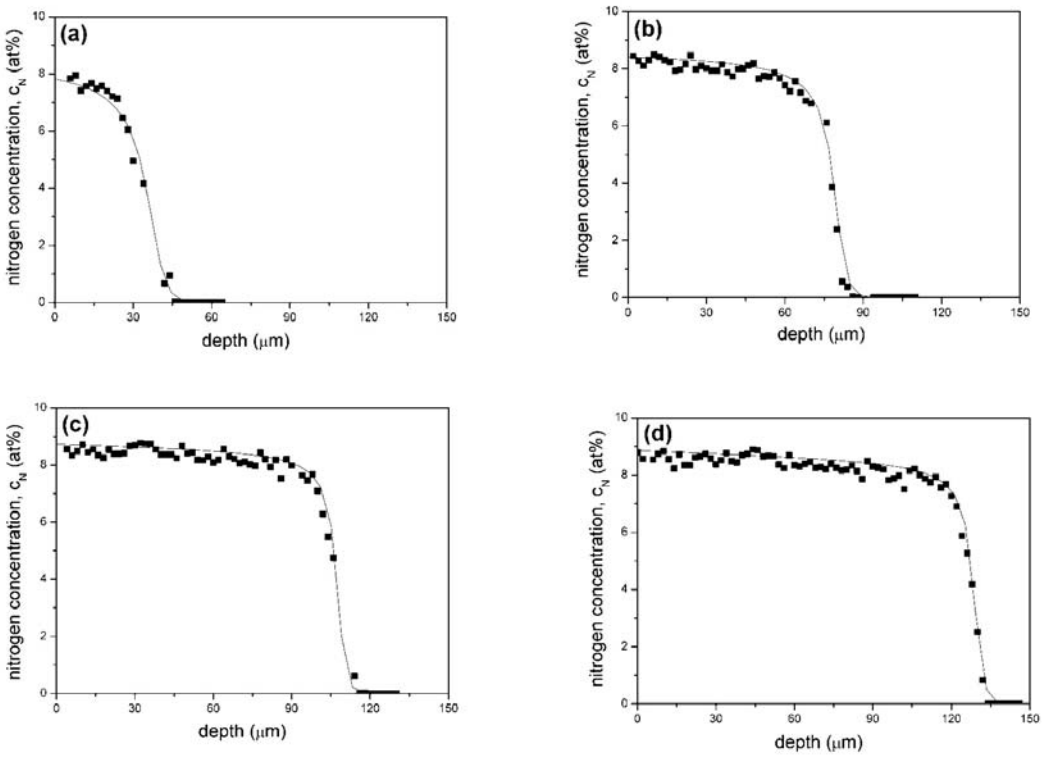

Fig. 2.10: Nitrogen concentration-depth profiles of nitrided Fe-7wt.%Cr specimens, as measured with EPMA (black dots) and as calculated profiles (lines) by the numerical model applying the parameters: (a) $c^S_{N_\alpha}$ = 0.03 at.%; b = 1.23; K_{CrN} = 0.02 for r_N = 0.03 $atm^{-1/2}$. (b) $c^S_{N_\alpha}$ = 0.17 at.%; b = 1.23; K_{CrN} = 0.02 for r_N = 0.08 $atm^{-1/2}$. (c) $c^S_{N_\alpha}$ = 0.32 at.%; b = 1.25; K_{CrN} = 0.02 for r_N = 0.11 $atm^{-1/2}$. (d) $c^S_{N_\alpha}$ = 0.45 at.%; b = 1.27; K_{CrN} = 0.02 for r_N = 0.16 $atm^{-1/2}$.

Table 2.3: Nitrogen uptake by the Fe-7wt.%Cr specimens nitrided at 580 °C for 4h and for various values of the nitriding potentials, r_n. Nitrogen content in the ferrite matrix at specimen surface, $c^S_{N_\alpha}$, and the stoichiometric parameter, b (in CrN_b), as obtained from fitting the numerical model to the experimentally determined nitrogen concentration-depth profiles. The amount of total excess nitrogen in the surface region of the specimen as determined by EPMA, the equilibrium solubility of nitrogen in the stress-free ferrite, $c^{S,0}_{N_\alpha}$, and the deduced amounts of immobile excess nitrogen and mobile excess nitrogen.

expected phase upon nitriding pure iron	r_n ($atm^{-1/2}$)	total excess nitrogen (from EPMA) (at%)	$c^S_{N_\alpha}$ (from fit) (at%)	$c^{S,0}_{N_\alpha}$ (see Ref. [2]) (at%)	b (from fit)	immobile excess nitrogen (from fit and EPMA) (at.%)	mobile excess nitrogen (from fit) (at.%)
α	0.03	1.0	0.03	0.07	1.23	1.0	0
	0.08	1.1	0.17	0.19	1.23	1.1	0
	0.11	1.3	0.32	0.26	1.25	1.3	0.06
	0.16	1.5	0.46	0.37	1.27	1.5	0.09

2.6 Conclusions

The nitriding potential has a great influence on the depth of the nitrided zone developing upon the nitriding of Fe-Cr alloys. The nitriding depth depends approximately linearly on the square root of the nitriding potential. For Fe-7wt.%Cr alloys nitrided at 580 °C, the nitriding depth = $315.8 \cdot (r_n)^{1/2}$; where nitriding depth is expressed in μm and r_n in $atm^{-1/2}$. The dependence of the nitriding kinetics on the nitriding potential becomes marginal as soon as a closed iron-nitride layer has formed on the surface, which occurs beyond a critical nitriding potential.

The occurrence of excess nitrogen in the nitrided zone has a pronounced influence on the kinetics of the nitriding process and, in contrast with earlier attempts, accordingly must be considered in any quantitative modelling of the nitriding kinetics.

Analysis of the nitriding kinetics demonstrated the occurrence of two kinds of excess nitrogen: immobile excess nitrogen adsorbed at the nitride/matrix interface and mobile excess nitrogen dissolved in the α-Fe matrix.

The nitriding depth can be assessed equally well from the hardness-depth profiles and from the nitrogen concentration-depth profiles. It should however be recognized that, strong variations of hardness occur in the nitrided zone, as a result of morphological variation in the chromium-nitride precipitation process (submicroscopical, fine chromium nitride precipitates

or lamellae of chromium nitride), whereas the nitrogen concentration-depth profile is insensitive to such effects.

Until now, in commercial practice the nitriding potential has been ignored as a tool to control the nitriding kinetics. The present results demonstrate that the nitriding depth can be changed strongly and controlled very well for cases of nitriding where no iron-nitride (compound) layer forms at the surface (i.e. r_n is smaller than a specific critical value), provided the composition of the nitriding atmosphere can be governed (e.g. by application of a sensor as described in Ref. [2]).

Acknowledgements

We are grateful to Mrs. S. Haug for assistance with the electron probe microanalysis measurements.

References

[1] Mittemeijer EJ, Slycke JT. Surface Engineering 1996;12:152.

[2] Mittemeijer EJ, Somers MAJ. Surface Engineering 1997;13:483.

[3] Lightfoot BJ, Jack DH. Proceedings of the conference on heat treatment 1973. The Metals Society, London; 1975. p. 59-65.

[4] Jack KH. Proceedings of the conference on heat treatment; 1973. The Metals Society London; 1975. p. 39.

[5] Mortimer B, Grieveson P, Jack KH. Scandinavian Journal of Metallurgy 1972;1:203.

[6] Mittemeijer EJ, Vogels ABP, van der Schaaf PJ. Journal of Materials Science 1980;12:3129.

[7] Hekker PM, Rozendaal HCF, Mittemeijer EJ. Journal of Materials Science 1985;20:718.

[8] Takada J, Ohizumi Y, Miyamura H, Kuwahara H, Kikuchi S, Tamura I. Journal of Materials Science 1986;21:2493.

[9] Ustinovshikov Y, Ruts A, Bannykh O, Blinov V, Kostina M. Materials Science and Engineering A 1999;262:82.

[10] Alves Jr. C, de A. Rodrigues J, Martinelli AE. Materials Science and Engineering A 2000;279:10.

[11] Gemma K, Ohtsuka T, Fujiwara T, Kawakami M. Journal of Materials Science 2001;36:5231.

[12] Somers MAJ, Lankreijer RM, Mittemeijer EJ. Philosophical Magazine A 1989;59:353.

[13] Schacherl RE, Graat PCJ, Mittemeijer EJ. Met. & Mat. Trans. A 2004;35:3387.

[14] Lehrer E. Zeitschrift fuer Elektrochemie 1930;36:383.

[15] Mittemeijer EJ. Journal of Metals 1985;September:16.

[16] Schacherl RE, Graat PCJ, Mittemeijer EJ. Zeitschrift fuer Metallkunde 2002;93:468.

[17] van Wiggen PC, Rozendaal HCF, Mittemeijer EJ. Journal of Materials Science 1985;20:4561.

[18] Mittemeijer EJ, Rozendaal HCF, Colijn PF, van der Schaaf PJ, Furnee RTh. Proceedings of the Conference on Heat Treatment 1981. Birmingham, UK, (The Metals Society London, 1983). p. 107.

[19] Biglari MH, Brakman CM, Mittemeijer EJ, van der Zwaag S. Philosophical Magazine A 1995;72:931.

[20] Schacherl RE, Graat PCJ, Mittemeijer EJ. Nitriding of Fe-Cr Alloys with High Chromium Contents. In: Proceedings of the Symposium on Nitriding (10-12 April 2002 Aachen, Germany), (Eds.) J. Grosch and E.J. Mittemeijer. Arbeitsgemeinschaft Wärmebehandlung und Werkstofftechnik (AWT), Schlangenbad, Germany; 2002. p. 51.

[21] Meijering JL. Advances in Material Research. Advances in Material Research, vol. 5. New York: Wiley Interscience; 1971. p. 1.

[22] Sun Y, Bell T. Materials Science and Engineering A 1997;224:33.

[23] Crank J. The Mathematics of Diffusion. Oxford: Clarendon Press; 1975. p. 137.

[24] Rozendaal HCF, Mittemeijer EJ, Colijn PF, van der Schaaf PJ. Metall. Trans. A 1983;14:395.

[25] Friehling PB, Poulsen FW, Somers MAJ. Zeitschrift fuer Metallkunde 2001;92:589.

[26] JCPDS-International Center for Diffraction Data (1999), PCPDFWIN, Version 202.

[27] Pouchau JL, Pichoir F. La Recherche Aérospatiale 1984;13(3):167.

Chapter 3

Microstructure of the “white layer” formed on nitrided Fe-7wt.%Cr alloys

S.S. Hosmani, R.E. Schacherl and E.J. Mittemeijer

Abstract

The formation of a compound, “white” layer on the surface of Fe-7wt.%Cr alloy, by exposure to a gas mixture of ammonia and hydrogen at 580 ºC, was investigated. The microstructure of the surface layer was analyzed employing light and scanning electron microscopy, X-ray diffraction and electron probe microanalysis. For the first time a quantitative (phase) analysis of such a white layer was carried out, demonstrating the presence of a dispersed CrN phase within a $\gamma^{|}$ iron-nitride matrix.

3.1 Introduction

Nitriding is a well-known thermochemical surface treatment to improve the fatigue, tribological and/or anti-corrosion properties of iron-based (steel) workpieces. One method to introduce nitrogen in a workpiece is by gaseous nitriding, involving that nitrogen, from dissociating NH_3 at temperatures in the range 450 – 590 ºC, enters the workpiece through its surface. Nitriding in NH_3/H_2 gas mixtures is equivalent to nitriding in N_2 at a pressure of a number of thousands atm (thermodynamic argument [1]) and is possible due to the slow thermal decomposition of NH_3 (kinetic argument [2]).

Gaseous nitriding of iron-chromium alloys has been subject of several investigations [3-13]. The attention was devoted to the development of (chromium) nitrides within the nitrided, ferritic zone close to the surface, which so-called diffusion zone is responsible for the enhancement of the fatigue resistance. However, under normal nitriding conditions a compound layer develops at the surface of the nitrided workpiece, which hard and so-called "white layer" (named so because of its appearance after etching) can possibly cause drastic improvement of tribological and anti-corrosion properties.

Against this background, the present work is devoted to an analysis of the microstructure of this "white layer" on Fe-7wt.%Cr alloy, recognizing that Cr is an important alloying element for nitriding steels.

3.2 Experimental

3.2.1 Specimen preparation

Fe-7wt.%Cr alloys were prepared from pure Fe (99.98 wt.%) and pure Cr (99.999 wt. %) in a Al_2O_3 crucible in an inductive furnace under argon atmosphere (99.999 vol. %). The amounts of chromium and impurities like oxygen, nitrogen, carbon and sulphur were determined by chemical analysis (inductive-coupled plasma-optic emission spectroscopy) of the produced alloys. The alloy compositions thus determined are shown in Table 3.1.

Table 3.1: Amounts of chromium and light element impurities for the Fe-7wt%Cr alloy.

Alloy	Cr (wt.%)	O (µg/g)	N (µg/g)	C (µg/g)	S (µg/g)
Fe-7wt.%Cr	7.10 ± 0.08	138 ± 10	< 5	6 ± 2	7 ± 3

After casting the alloys had a cylindrical shape with a diameter of 10 mm and a length of 100 mm. The cast alloys were cold rolled to sheets with a thickness of 1.2 ± 0.1 mm. The

obtained sheets were cut into rectangular pieces of lateral dimensions 1.5x1.5 cm^2. These pieces were subsequently cleaned in an ultrasonic bath filled with ethanol and encapsulated in a silica tube filled with argon (purity: 99.999 vol.%) up to a pressure of 750 Torr. The encapsulated samples were annealed for 1h at 700 °C (within the α-phase region of the Fe-Cr diagram) to get a recrystallized grain structure. Before nitriding the samples were ground, polished (last step: 1μm diamond paste) and cleaned in an ultrasonic bath filled with ethanol.

3.2.2 Nitriding

For nitriding a specimen was suspended at a quartz fibre in the vertical quartz tube (of inner diameter 28 mm) of the nitriding furnace. To start the nitriding process the specimen was placed in the middle of the nitriding furnace. The nitriding experiments were performed at 580 °C ± 1°C (=853 K ±1K) in an ammonia/hydrogen gas flux (purity: H_2: 99.999 vol. %, NH_3: >99.998 vol. %). The fluxes of both gases were adjusted with mass flow controllers and amounted to 61 ml/min hydrogen and 39 ml/min ammonia (i.e. the nitriding potential (= $\frac{p_{NH_3}}{p_{H_2}^{3/2}}$, with p as partial pressure) equalled 0.82 $atm^{-1/2}$). Under these nitriding conditions iron nitride (γ'-Fe_4N) is formed on the surface of a pure iron specimen [2, 14]. The specimen was nitrided for 48h. After nitriding the specimen was quenched in water flushed with N_2 gas.

3.2.3 Specimen characterisation

3.2.3.1 Light and scanning electron microscopy

For light microscopical investigation, pieces were cut from the samples and prepared to cross sections, by subsequent embedding (Konduktomet, Buehler GmbH), polishing (last step: 1 μm diamond paste) and etching with 2.5% nital (2.5 vol.% HNO_3 in ethanol) for about 5 s. These cross sections were investigated with light optical microscopy applying a Leica DMRM microscope. The light micrographs were recorded with a digital camera (Jenoptik Progres 3008).

For scanning electron microscopy (SEM) the same (etched) cross-sections were used as for light microscopy. The SEM micrographs were taken with a Jeol JSM 6300F operating at 3 or 5 kV.

3.2.3.2 X-ray diffraction (XRD)

To determine which phases are present before and after nitriding, XRD was applied using a Philips X'Pert diffractometer. Measurements were made using Cu Kα and Co Kα radiations and employing the Bragg-Brentano geometry with a graphite monochromator in the diffracted beam. The diffraction angle (2Θ) range scanned was 10 – 150°, with a step size of 0.05°. The X-ray diffractograms were recorded from specimen surfaces as obtained after nitriding. To identify the phases from the positions of the diffraction peaks the data from the JCPDS data base were used [15].

3.2.3.3 Electron probe microanalysis (EPMA)

To determine the composition of the nitrided zones of the specimens after nitriding, EPMA was performed employing a Cameca SX100 instrument. Cross-sections of the nitrided alloys, similar to those as described above for light and scanning electron microscopy, were analysed, but in this case no etching after polishing was applied. A focussed electron beam at an accelerating voltage of 15 kV and a current of 100 nA was applied. To obtain the element contents in the specimens, the intensities of the characteristic Fe Kβ, Cr Kβ, N Kα, and O Kα X-ray emission peaks were determined at points along lines across the cross-sections (single measurement points at a distance of 2 μm). The intensities obtained from the nitrided samples were divided by the intensities obtained from standard samples of pure Fe (Fe Kβ), pure Cr (Cr Kβ), andradite/$Ca_3Fe_2(SiO_4)_3$ (O Kα), and γ'-Fe_4N (N Kα). Concentration values were calculated from the intensity ratios applying the $\Phi(\rho z)$ approach according to Ref. [16].

3.3 Results and Discussion

3.3.1 Light optical microscopy

Metallographic investigations of the cross section of the nitrided Fe-7wt.%Cr specimens revealed the formation of a white layer at the surface of the specimen. The thickness of the layer varies from 6.0 – 21.3 μm (see Fig. 3.1). A poly-phase nature of the compound layer is not apparent. At the edges of the specimen the formation of a massive layer can be observed (see Fig. 3.2). The nitrided zone below the white layer is composed of grains exhibiting a discontinuous (dark grains) and a continuous (bright grains) chromium-nitride precipitate morphology (see Refs. [5, 10, 11-13] for discussion of precipitation morphology).

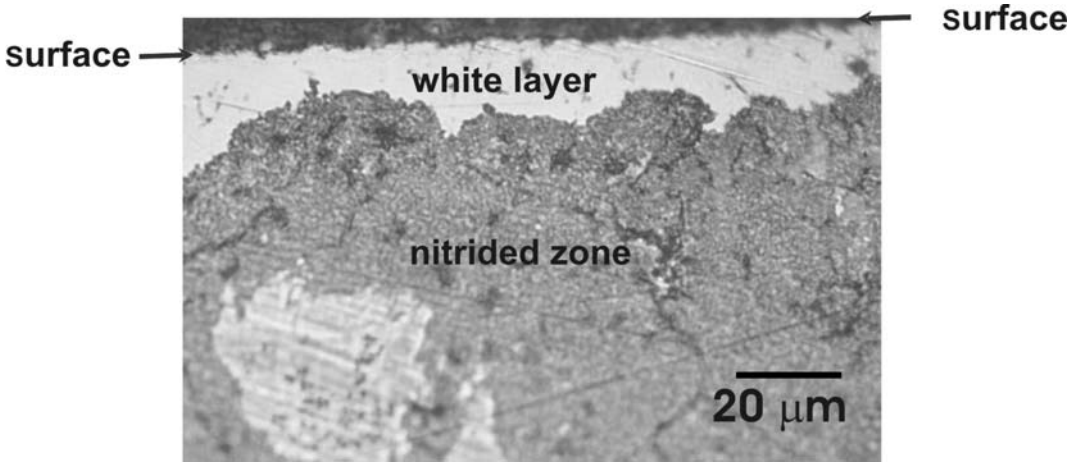

Fig. 3.1: (a) Light optical micrograph of the cross section of a nitrided Fe-7wt.%Cr specimen, nitrided at 580 ºC for 48h at a nitriding potential of 0.82 $atm^{-1/2}$.

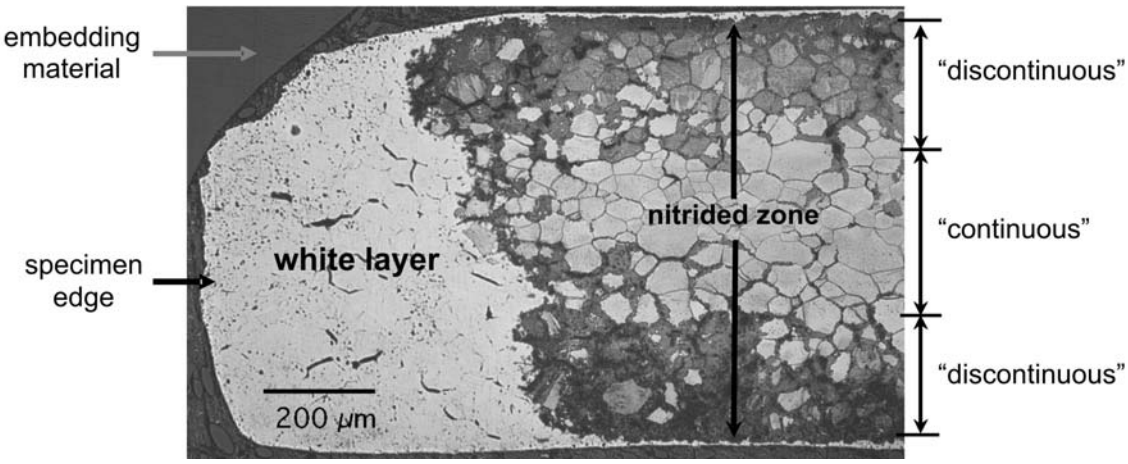

Fig. 3.2: Light optical micrograph of the cross-section at the edge of the specimen of a Fe-7wt.%Cr specimen, nitrided at 580 ºC for 48h at a nitriding potential of 0.82 $atm^{-1/2}$.

3.3.2 X-ray diffraction analysis

X-ray diffractograms, recorded from the nitrided specimen surface, are presented in Fig. 3.3. The X-ray diffractograms were recorded employing CoK_α (λ = 1.79 Å) (see Fig. 3.3a) and CuK_α (λ = 1.54 Å) (see Fig. 3.3b) radiation. The intensity values on the ordinate represent the ratio of the intensity of the reflection considered and the intensity of the $\gamma^{|}$-Fe_4N (111) reflection.

Both X-ray diffractograms of the nitrided Fe-7wt.%Cr specimen show the presence of α-Fe, CrN and $\gamma^{|}$-Fe_4N. However, the α-Fe reflections of the X-ray diffractogram recorded with CuK_α radiation show a distinctly lower intensity in comparison with the corresponding ones

recorded with CoK_α radiation. The penetration depth (and thus the information depth) is, in particular for iron-based materials, much less for CuK_α than for CoK_α (for discussion and quantification, see Ref. [17]). Therefore the strong difference in relative intensities of the α-Fe reflections between the diffractograms recorded with CuK_α and CoK_α radiations, suggest that the α-Fe reflections originate from the substrate underneath the "white layer". Whilst the intensities of the α-Fe reflections almost disappear, upon changing from CoK_α to CuK_α, the CrN reflections remain clearly visible.

It is concluded that CrN phase is present in the compound layer that is dominated by the γ'-Fe_4N phase (see also section 3.3.3).

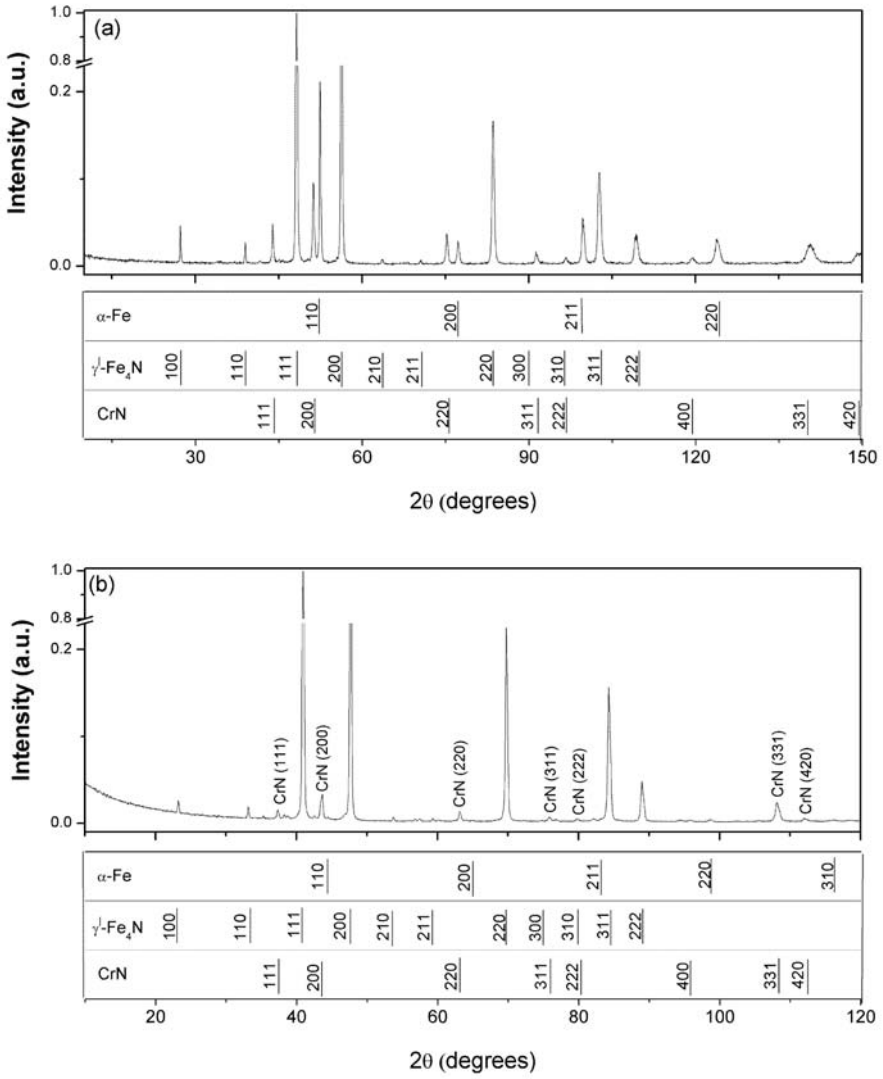

Fig. 3.3: X-ray diffractograms recorded from the surface of a Fe-7wt.%Cr specimen, nitrided at 580 ºC for 48h at a nitriding potential of 0.82 $atm^{-1/2}$ by using (a) CoKα (λ = 1.79 Å) radiation and (b) CuKα (λ = 1.54 Å) radiation.

3.3.3 Electron probe microanalysis; quantitative phase analysis

Results of EPMA are shown in Fig. 3.4a for a series of point measurements within the compound layer at the edge of the specimen (cf. Fig. 3.2); the corresponding backscattered electron (BSE) image is shown in Fig. 3.4b. The location of the line along which the EPMA measurements were made has been indicated by the black dashed line. If it is assumed that chromium would not form any nitrides and would be present as a dissolved component in the $\gamma^{|}$ phase, then the nitrogen content (under the given nitriding conditions: cf. section 3.2.2) should be around 19.9 at.% (see Ref. [2]), corresponding to $(Fe, Cr)_4N$. However, the average nitrogen content within the compound layer is 24.2 at.% (see also Fig. 3.5).

The N, Cr and Fe concentrations, as measured with EPMA, within the compound layer are shown in Table 3.2. If it is assumed that all chromium in the compound layer is present as CrN, then the nitrogen uptake (i.e. 24.2 at.%) minus the chromium content of the layer (i.e. 6.0 at.%), gives the amount of nitrogen (i.e. 24.2 – 6.0 = 18.2 at.%) associated with Fe (69.8 at.%). On the basis of the X-ray diffractograms (Fig. 3.3) it is concluded that these amounts of Fe and N must be present as $\gamma^{|}$-Fe_4N phase. Taking the experimental values for the Fe and N contents (69.8 at.% and 18.2 at.%) the content of N in this $\gamma^{|}$ - phase equals ($\frac{18.2 \times 100}{69.8 + 18.2}$=) 20.7 at.%, which is very close to (but slightly larger than; see below) the composition expected for Fe_4N_{1-x} (x = 0.04 corresponding to 19.9 at.% N) under the given nitriding conditions (see Ref. [2]). It is concluded that chromium is not incorporated significantly in the $\gamma^{|}$ phase.

At the edges of the sample, within the compound layer and in particular in the transition region compound layer / diffusion zone, islands of dark contrast in the BSE image can be observed (see the squares in Fig. 3.4b and Fig. 3.5a), which, according to EPMA measurements, possess a distinctly lower nitrogen content (8.3 at.%) than their surroundings (see Fig. 3.5c). The composition of these islands suggests that they are composed of α-Fe and CrN precipitates.

On the basis of the above results, the following picture emerges for the development of the compound layer: Upon gaseous nitriding, nitrogen diffuses through ferrite grains by bulk diffusion which causes the formation of CrN precipitates in particular at grain boundaries, due to a relatively easy nucleation there. When the solubility of nitrogen in the ferrite matrix, surrounding the precipitates, exceeds the nitrogen solubility limit, formation of $\gamma^{|}$-Fe_4N phase can occur. Thus the transformation process ferrite substrate → compound layer starts at the

grain boundaries and progresses towards the centre of the originally ferrite grains. The ferrite phase surrounding the misfitting CrN particles will be strained [18]. Therefore some excess nitrogen can be taken up (enhanced nitrogen solubility of ferrite) [13, 18]. This may explain the slight excess of N observed (20.7 at.% N versus 19.9 at.% N; see above). During the phase transformation of α-Fe (surrounding the CrN precipitates) to Fe_4N, relaxation of the internal misfit strain fields, in the α-Fe matrix surrounding the CrN precipitates, occurs. Thereby the capacity for excess N uptake is lost and the excess nitrogen may segregate at grain boundaries (cf. Ref. [10, 11]). These nitrogen atoms coagulate to molecular nitrogen gas, $2[N] \rightarrow N_2$, thereby causing voids at the grain boundaries (see within the white layer at the edge of specimen in Fig. 3.2).

From the above it follows that in particular at the layer / substrate interface, where the (inward) growth of the layer occurs, some α-Fe regions may be observed which have to be considered as the remains of transforming grains which are on their way of becoming part of the compound layer.

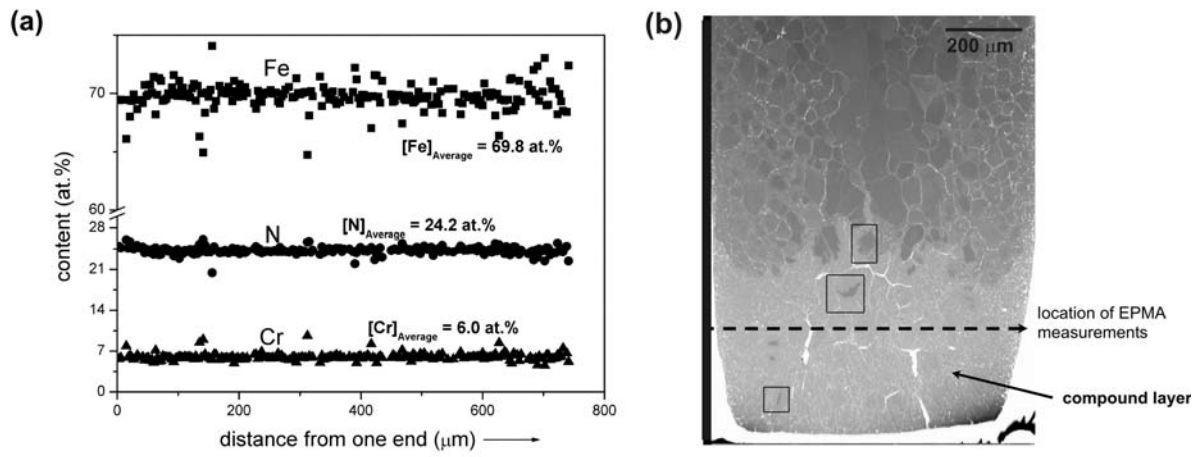

Fig. 3.4: (a) EPMA results for a series of point measurements within the compound layer, formed at the edge of Fe-7wt.%Cr specimen nitrided at 580 ºC for 48h at a nitriding potential of 0.82 $atm^{-1/2}$. (b) Backscattered electron image showing the location of the EPMA point measurements (taken along the dashed line) for the results shown in (a).

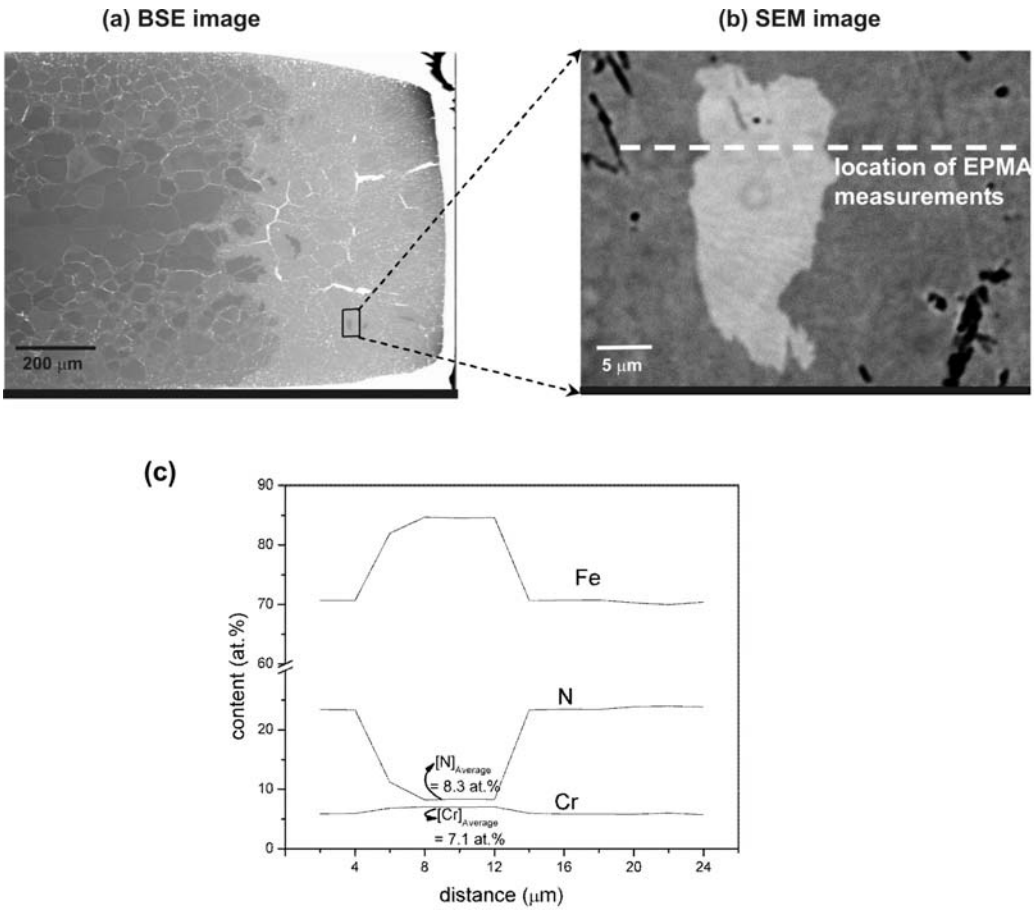

Fig. 3.5: (a) Backscattered electron image of the compound layer, at the edge of a Fe-7wt.%Cr specimen nitrided at 580 ºC for 48h at a nitriding potential of 0.82 $atm^{-1/2}$. (b) Enlargement of dark area shown in (a). (c) EPMA results for a series of point measurements along a (dashed) line shown in (b).

Table 3.2: N, Cr and Fe concentrations in the compound layer as determined by EPMA for a Fe-7wt.%Cr specimen nitrided at 580 ºC for 48h at 0.82 $atm^{-1/2}$ (see also Fig. 3.4); see further text.

Element content in the compound layer (from EPMA)				**N in $\gamma^{\prime}$ - phase (at.%)**
(1)	**(2)**	**(3)**	**(4)=(1)-(2)**	
$[N]_{total}$ (at.%)	**[Cr] (at.%)**	**[Fe] (at.%)**	**N associated with Fe (assuming that all Cr is present as CrN) (at.%)**	
24.2	6.0	69.8	18.2	$\frac{(4)}{(3)+(4)} \times 100$ = 20.7

3.4 Conclusions

The compound layer developing during gaseous nitriding on the surface of iron-based ferritic Fe-Cr alloy is composed of iron nitride and chromium nitride. Chromium is not taken up significantly in the iron nitride.

In particular near the layer / substrate interface enclosed α-Fe regions occur as remains of originally ferritic grains transforming into (largely) iron nitride by a substrate → compound layer transformation process that progresses from the grain boundaries to the interior of the grains.

Acknowledgements

We are grateful to Mrs. S. Haug (Max Planck Institute for Metals Research) for assistance with the electron probe microanalysis measurements.

References

[1] Mittemeijer EJ, Slycke JT. Surface Engineering 1996;12:152.

[2] Mittemeijer EJ, Somers MAJ. Surface Engineering 1997;13:483.

[3] Mortimer B, Grieveson P, Jack KH. Scandinavian Journal of Metallurgy 1972;1:203.

[4] Mittemeijer EJ, Vogels ABP, van der Schaaf PJ. Journal of Materials Science 1980;12:3129.

[5] Hekker PM, Rozendaal HCF, Mittemeijer EJ. Journal of Materials Science 1985;20:718.

[6] Takada J, Ohizumi Y, Miyamura H, Kuwahara H, Kikuchi S, Tamura I. Journal of Materials Science 1986;21:2493.

[7] Ustinovshikov Y, Ruts A, Bannykh O, Blinov V, Kostina M. Materials Science and Engineering A 1999;262:82.

[8] Alves Jr. C, de A. Rodrigues J, Martinelli AE. Materials Science and Engineering A 2000;279:10.

[9] Gemma K, Ohtsuka T, Fujiwara T, Kawakami M. Journal of Materials Science 2001;36:5231.

[10] Hosmani SS, Schacherl RE, Mittemeijer EJ. Materials Science and Technology 2005;21:113. (Chapter 2).

[11] Schacherl RE, Graat PCJ, Mittemeijer EJ. Zeitschrift fuer Metallkunde 2002;93:468.

[12] Schacherl RE, Graat PCJ, Mittemeijer EJ. Nitriding of Fe-Cr Alloys with High Chromium Contents. In: Proceedings of the Symposium on Nitriding (10-12 April 2002 Aachen, Germany), (Eds.) J. Grosch and E.J. Mittemeijer. Arbeitsgemeinschaft Wärmebehandlung und Werkstofftechnik (AWT), Schlangenbad, Germany; 2002. p. 51.

[13] Schacherl RE, Graat PCJ, Mittemeijer EJ. Met. & Mat. Trans. A 2004;35:3387.

[14] Lehrer E. Zeitschrift fuer Elektrochemie 1930;36:383.

[15] JCPDS-International Center for Diffraction Data (1999), PCPDFWIN, Version 202.

[16] Pouchau JL, Pichoir F. La Recherche Aérospatiale 1984;13(3):167.

[17] Delhez R, de Keijser ThH, Mittemeijer EJ. Surface Engineering 1987;3:331.

[18] Somers MAJ, Lankreijer RM, Mittemeijer EJ. Philosophical Magazine A 1989;59:353.

Chapter 4

Nitriding behavior of Fe–4wt%V and Fe–2wt%V alloys

S.S. Hosmani, R.E. Schacherl and E.J. Mittemeijer

Abstract

The nitriding behavior of Fe–4wt%V and Fe–2wt%V alloys was investigated by exposing these alloys to a gas mixture of ammonia and hydrogen at 580 °C. The microstructure of the nitrided specimens was analyzed employing light and scanning electron microscopy, hardness measurements, and X-ray diffraction. To determine the elemental composition of the nitrided zone electron probe microanalysis (EPMA) was applied. The nitrided zone of the Fe–4wt%V specimens comprised many grains exhibiting a lamellar morphology characterized by a lamellar spacing of 20–40 nm. Such a lamellar microstructure was absent in the nitrided zone of the Fe–2wt%V specimens. These morphological results, together with the obtained hardness and X-ray diffraction data, demonstrate that a discontinuous coarsening reaction occurs in nitrided Fe–4wt%V alloy. Such a reaction was not observed before for nitrided Fe–V alloys. EPMA showed the uptake of excess nitrogen in the nitrided zone. The discontinuously transformed regions contain less nitrogen than the not transformed regions. The effect of these phenomena on the nitriding kinetics was analyzed and discussed.

4.1 Introduction

Nitriding is a well-known thermochemical surface treatment to improve the fatigue, tribological and/or anti-corrosion properties of iron-based (steel) workpieces. One method to introduce nitrogen in a (ferritic) workpiece is by gaseous nitriding, involving that nitrogen, from dissociating NH_3 at temperatures in the range 450–590 ºC, enters the workpiece through its surface. Nitriding in NH_3/H_2 gas mixtures is equivalent to nitriding in N_2 at a pressure of a number of thousands atm (thermodynamic argument [1]) and is possible due to the slow thermal decomposition of NH_3 (kinetic argument [2]).

If strong nitride forming alloying elements, like Ti, Al, V and Cr, are present, alloying element nitride precipitates can develop upon nitriding, which can cause large increase of the hardness (e.g. see for Fe-Ti, Refs. [3-5], for Fe-Al, Refs. [6-11], for Fe-V, Refs. [12-19], for Fe-Cr, Refs. [20-24]). The resulting increase in hardness depends on the chemical composition of the precipitates, their coherency with the matrix, their size and their morphology.

A number of investigations have been devoted to nitrided iron-vanadium alloys [12-19]. Only finely distributed, plate-like precipitates of vanadium nitride were observed until now (typically about 40 Å long with a thickness of about 10 Å, precipitated along $\{001\}_\alpha$ matrix planes) (e.g. see Ref. [17]). In the present work it has been shown that a discontinuous precipitation morphology of vanadium nitride can occur, which has been observed before only for nitrided Fe-Cr alloys [20-24]. The results obtained show that nitrided Fe-V alloys have a considerable capacity for the uptake of so-called excess nitrogen (i.e. more nitrogen than necessary for precipitation of all vanadium as nitride and equilibrium saturation of the ferrite matrix). Finally, the nitriding kinetics have been determined and analyzed.

4.2 Experimental

4.2.1 Specimen preparation

Fe-4wt.%V and Fe-2wt.%V alloys were prepared from pure Fe (99.98 wt.%) and pure V (99.80 wt. %) in a Al_2O_3 crucible in an inductive furnace under argon atmosphere (99.999 vol. %). The amounts of vanadium and impurities like oxygen, nitrogen, carbon, sulphur in the produced alloys were determined by chemical analysis (inductive-coupled plasma-optic emission spectroscopy). The alloy compositions are shown in Table 4.1.

Table 4.1: Amounts of vanadium and light element impurities for the two alloys used in this work.

Alloy	V (wt.%)	V (at.%)	O (µg/g)	N (µg/g)	C (µg/g)	S (µg/g)
Fe-2wt.%V	2.04 ± 0.05	2.23	142 ± 10	< 6	6 ± 2	6 ± 3
Fe-4wt.%V	4.05 ± 0.07	4.42	155 ± 10	< 6	6 ± 3	5 ± 2

After casting the alloys have a cylindrical shape with a diameter of 10 mm and a length of 100 mm. The cast alloys were cold rolled to sheets with a thickness of 1.0 mm and 0.2 mm. The obtained sheets were cut into rectangular pieces of lateral dimensions 1.5 x 1.5 cm^2. These pieces were annealed for 2h at 700 ºC (within the α-phase region of the Fe-V diagram) to obtain a recrystallized grain structure. After annealing the grains of both alloys had an average diameter of about 55 µm. Before nitriding the samples were ground, polished (last step: 1µm diamond paste) and cleaned in an ultrasonic bath filled with ethanol.

4.2.2 Nitriding

For nitriding a sample was suspended at a quartz fiber in a vertical quartz tube of inner diameter 28 mm in the nitriding furnace. To start the nitriding process the sample was placed in the middle of the nitriding furnace. The nitriding experiments were performed at 580 ºC (= 853 K) in an ammonia/hydrogen gas flux (purity: H_2: 99.999 vol. %; NH_3: >99.998 vol. %). The fluxes of both gases were adjusted with mass flow controllers and amounted to 455 ml/min hydrogen and 45 ml/min ammonia (i.e. the nitriding potential (= $\frac{p_{NH_3}}{p_{H_2}^{3/2}}$, with p as partial pressure) equalled 0.103 $atm^{-1/2}$). Under these nitriding conditions no iron nitrides can be formed. Thin specimens (thickness of 0.2 mm) of Fe-4wt.%V were nitrided for 24h. This nitriding treatment resulted in throughout nitrided specimens. Thick specimens (thickness of 1.0 mm) of both Fe-4wt.%V and Fe-2wt.%V were nitrided for 10h. At the end of the nitriding process, the samples were quenched in water.

4.2.3 Specimen characterization

4.2.3.1 Light and scanning electron microscopy

For light microscopical investigation, pieces were cut from the samples and prepared to cross sections, by subsequent embedding (Konduktomet, Buehler GmbH), polishing (last step: 1 µm diamond paste) and etching with 2.5% nital (2.5 vol.% HNO_3 in ethanol) for about 5 s. These cross sections were investigated with light optical microscopy applying a Leica DMRM

microscope. The light micrographs were recorded with a digital camera (Jenoptik Progres 3008).

For scanning electron microscopy (SEM) the same (etched) cross-sections were used as for light microscopy. The SEM micrographs were taken with a Jeol JSM 6300F operating at 3 or 5 kV.

4.2.3.2 Hardness measurement

Hardness-depth profiles were obtained by carrying out hardness measurements across the cross-sections of the nitrided specimens using a Leitz Durimet hardness tester, applying a load of 100 g. The hardness values presented are average values of 4 measurements.

4.2.3.3 X-ray diffraction (XRD)

To determine which phases are present after nitriding, XRD was applied using a Philips X'Pert diffractometer. Measurements were made using Cu Kα and Co Kα radiations and employing the Bragg-Brentano geometry with a graphite monochromator in the diffracted beam. The diffraction angle (2Θ) range scanned was 10 – 150°, with a step size of 0.05°. The X-ray diffractograms were recorded from specimen surfaces as obtained after nitriding. To identify the phases from the positions of the diffraction peaks, data from the JCPDS data base were used [25].

4.2.3.4 Electron probe microanalysis (EPMA)

To determine the composition of the nitrided zones of the samples after nitriding, EPMA was performed employing a Cameca SX100 instrument. Cross-sections of the nitrided alloys, similar to those as described above for light and scanning electron microscopy, were analyzed, but in this case no etching after polishing was applied. A focused electron beam at an accelerating voltage of 15 kV and a current of 100 nA was applied. To obtain the element contents in the specimens, the intensity of the characteristic Fe Kβ, V Kβ, N Kα, and O Kα X-ray emission peaks was determined at points along lines across the cross-sections (single measurement points at a distance of 2 μm). The intensities obtained from the nitrided samples were divided by the intensities obtained from standard samples of pure Fe (Fe Kβ), pure V (V Kβ), andradite/$Ca_3Fe_2(SiO_4)_3$ (O Kα), and γ'-Fe_4N (N Kα). Concentration values were calculated from the intensity ratios applying the $\Phi(\rho z)$ approach according to Ref. [26].

4.3 Precipitation behavior; “continuous” versus “discontinuous”

4.3.1 Nitriding of Fe-4wt.%V

A light optical micrograph of an etched cross-section of a thin (thickness of 0.2 mm) Fe-4wt.%V specimen nitrided at 580 ºC for 24 hrs is shown in Fig. 4.1a; the corresponding hardness-depth profile is presented in Fig. 4.1b. Almost the entire specimen is composed of grains with a dark appearance, except a few grains, which appear bright in the light optical micrograph (Fig. 4.1a). The dark grains in the through nitrided specimens show much lower hardness values (from 650 to 770 HV0.1) than the bright grains (about 1200 HV0.1) (Fig. 4.1b).

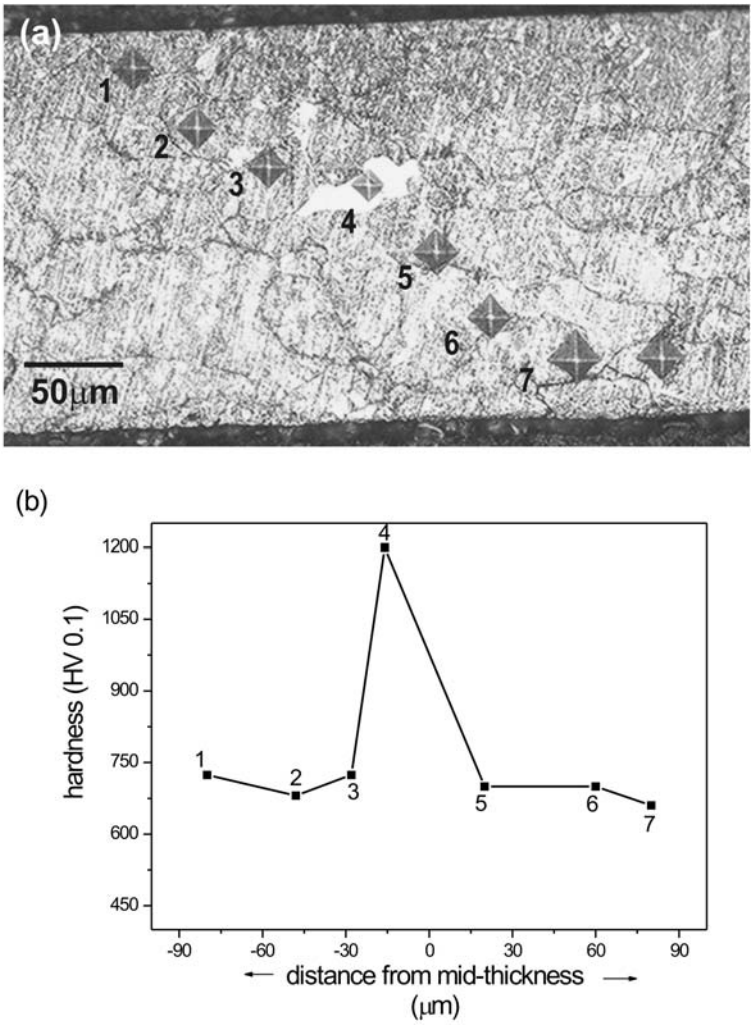

Fig. 4.1: Light optical micrograph of the etched cross-section of the thin (thickness of 0.2 mm) Fe-4wt.%V specimen nitrided at 580 ºC for 24h at a nitriding potential of 0.103 $atm^{-1/2}$ (a). The hardness values corresponding to the indentations numbered 1-7 are presented in (b).

A light optical micrograph of the cross section of a nitrided thick specimen (thickness of 1.0 mm) of Fe-4wt.%V is shown in Fig. 4.2. The nitrided zone of this *not* through nitrided specimen is composed of a layer near the surface, which contains mainly dark grains, and a layer below with bright grains.

An enlargement of a dark grain reveals the presence of a lamellar morphology (see the SEM micrograph shown in Fig. 4.3b); the observed lamellar spacing ranges from 25 to 40 nm. Considering an original grain of the nitrided Fe-4wt.%V alloy that had been partially transformed, it could be shown that the dark part with the lamellar morphology has a much lower hardness than the bright part (for which such a lamellar morphology could not be detected): see the differences in size of the hardness indentations in Fig. 4.4. This result is consistent with the hardness-depth profile of the thick, nitrided Fe-4wt.%V specimen shown in Fig. 4.2b: the surface adjacent region is composed of dark grains and exhibits a relatively low hardness.

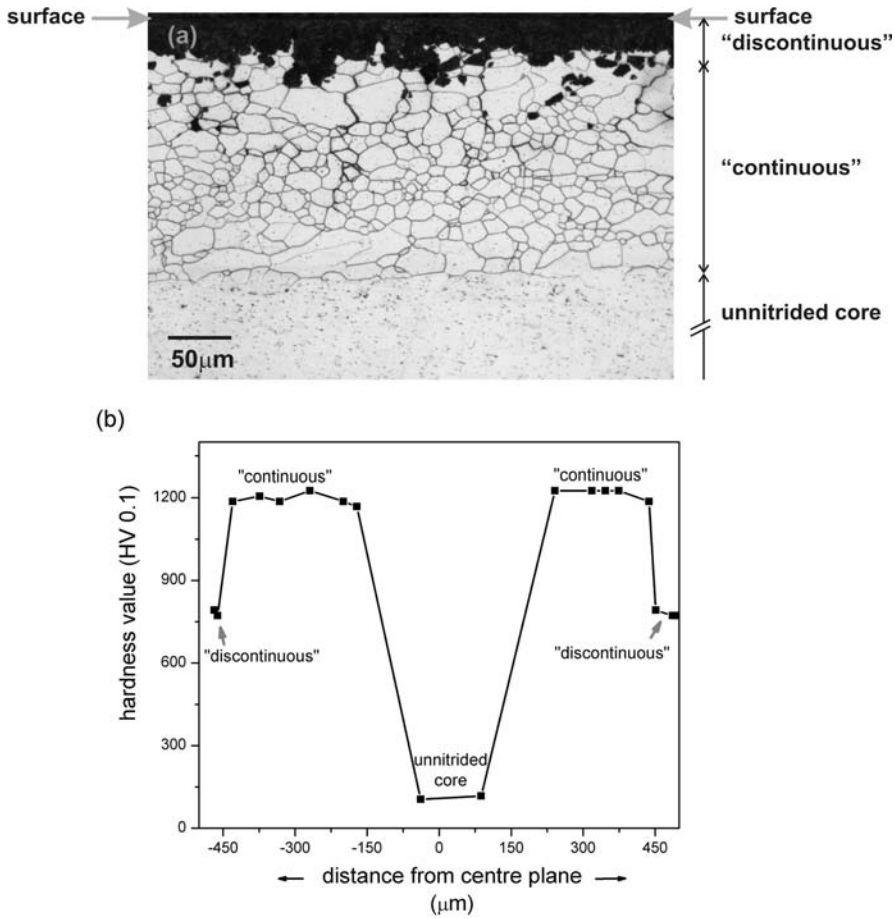

Fig. 4.2: (a) Light optical micrograph of the etched cross section of the thick (thickness of 1.0 mm) Fe-4wt.%V specimen nitrided at 580 ºC for 10h at a nitriding potential of 0.103 $atm^{-1/2}$. The three zones of different morphology have been indicated. (b) Hardness-depth profile of the same specimen.

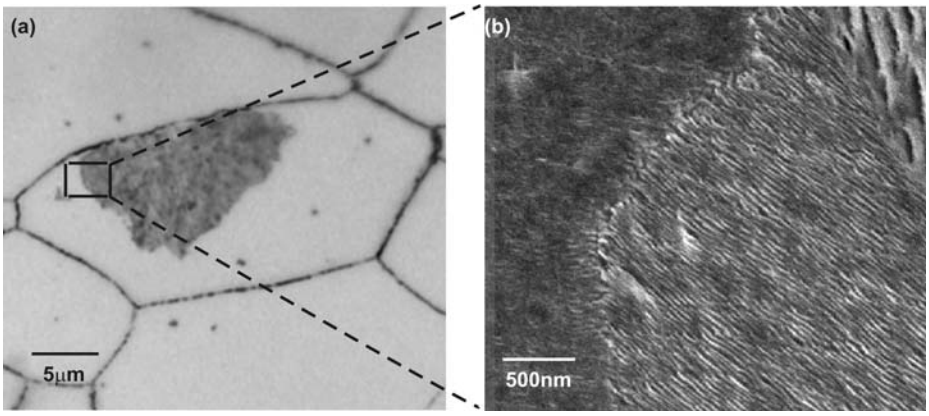

Fig. 4.3: An original grain of the Fe-4wt.%V alloy (10h of nitriding at 580 ºC for a nitriding potential of 0.103 $atm^{-1/2}$), that after nitriding had partially transformed by the discontinuous coarsening reaction. (a) Light optical micrograph; (b) SEM micrograph of the part indicated in (a), which clearly reveals the lamellar morphology of the part of the grain that had experienced the discontinuous coarsening.

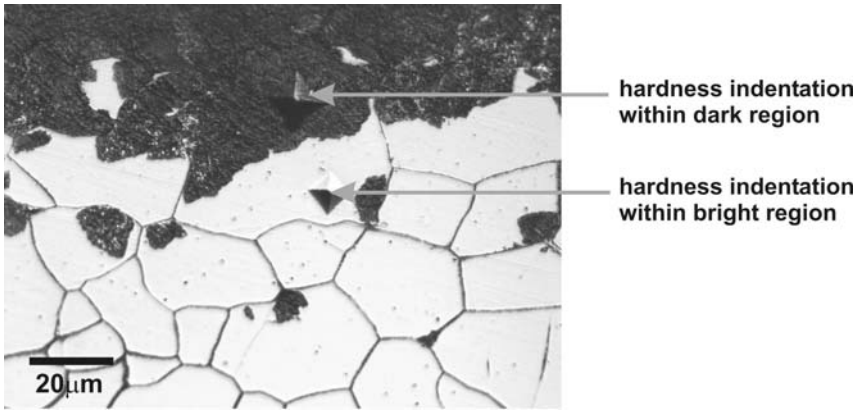

Fig. 4.4: Light optical micrograph showing two hardness indentations (performed with the same load) in one original grain of the thick nitrided Fe-4wt.%V alloy: the dark region of the grain exhibits a much larger indentation (i.e. possesses a much lower hardness) than the bright part of the grain.

The X-ray diffractograms recorded from the surfaces of the nitrided Fe-4wt.%V specimen show diffraction peaks of the phases α-Fe and VN (e.g. see Fig. 4.5).

The results shown in Figs. 4.1-4.5 can be interpreted such as that apparently two precipitation morphologies in nitrided Fe-4wt.%V occur: one characterized with very fine precipitates (not detectable with light optical and scanning electron microscopy), associated with a very high hardness, and one characterized with a lamellar morphology, associated with a relatively low hardness. In view of similar observations made in the past for nitrided Fe-Cr alloys [20] and the discussion given in section 4.4.1, both precipitation morphologies will be denoted “continuous” and “discontinuous” in the following.

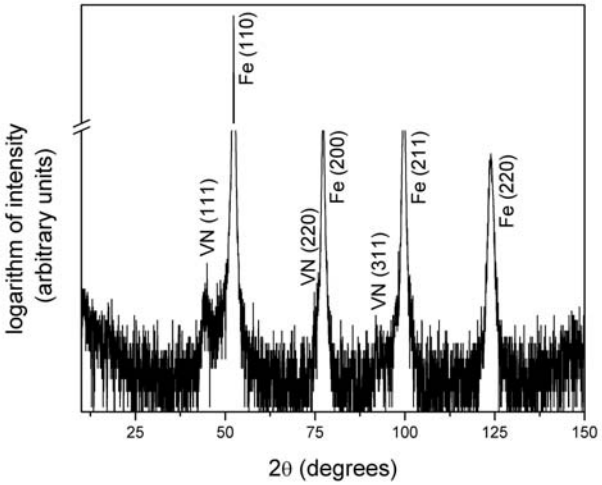

Fig. 4.5: X-ray diffractogram (CoKα-radiation) recorded from the surface of an Fe-4wt.%V specimen nitrided at 580 ºC for 10h at a nitriding potential of 0.103 $atm^{-1/2}$. The locations of the possible α-Fe and VN reflections have been indicated.

The elemental concentration-depth profiles of the nitrided layer of the nitrided Fe-4wt.%V specimen are presented in Fig. 4.6 (EPMA data). Evidently, a distinct uptake of nitrogen has occurred in the nitrided zone (Fig. 4.6a). An overall decrease of nitrogen content, from surface to interface with the unnitrided core, can be observed. However, additionally, at the location of discontinuously transformed regions/grains a significantly lower nitrogen content is observed (see Figs. 4.6b and c). This result of nitrogen uptake in the nitrided region of Fe-4wt.%V differs strikingly from that observed for nitrided Fe-Cr alloys (containing 4, 7, 13, 20 wt.% Cr), which show a nitrogen uptake in the nitrided region independent of measurements made in discontinuously transformed or continuously precipitated regions [21-24].

Further, the nitrogen concentration in the nitrided zone is larger than compatible with (i) the precipitation of all vanadium as VN, and (ii) the equilibrium solubility of nitrogen in the (remaining) ferrite matrix (see the horizontal, grey line drawn in Fig. 4.6a). The difference between the experimentally obtained total amount of nitrogen in the nitrided zone and this "normal" amount of nitrogen uptake is defined as "excess" nitrogen. Note that excess nitrogen is present in both the discontinuously transformed regions and in the continuously precipitated regions.

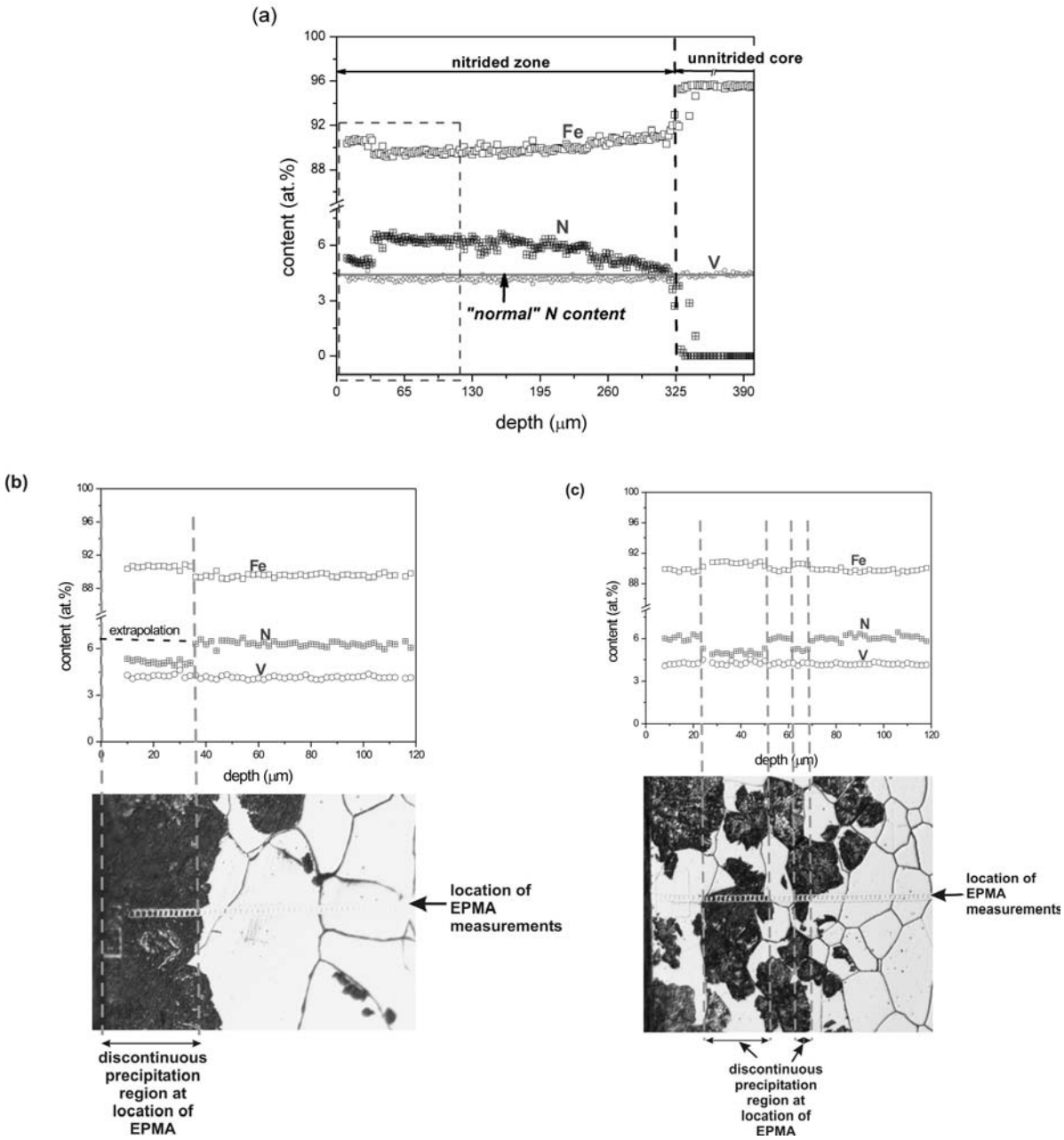

Fig. 4.6: (a) Elemental (N, V, Fe) concentration-depth profiles of the Fe-4wt.%V alloy nitrided at 580 ºC for 10h at a nitriding potential of 0.103 $atm^{-1/2}$. The horizontal, grey line indicates the "normal" amount of nitrogen uptake. (b) Enlargement of part of the depth profile, indicated by the dashed rectangle in (a), together with the light optical micrograph of the cross-section analyzed (which was etched after EPMA analysis) showing the location of the EPMA measurements (as revealed by the usual track of carbon contamination). Clearly, the nitrogen concentration in the surface adjacent dark part of the nitrided zone is smaller than in the bright part of the nitrided zone. (d) Part of elemental concentration-depth profile recorded at another location of the same specimen, together with the light optical micrograph of the cross-section analyzed (which was etched after EPMA analysis) showing the location of the EPMA measurements. Clearly, the nitrogen concentration at the location of dark grains ("discontinuously" transformed grains) is smaller than in the bright grains ("continuously" precipitated grains).

4.3.2 Nitriding of Fe-2wt.%V

A light optical micrograph of the etched cross-section of a Fe-2wt.%V specimen nitrided at 580 ºC for 10h at a nitriding potential of 0.103 $atm^{-1/2}$ is shown in Fig. 4.7a. As compared with the nitrided zone of the Fe-4wt.%V alloy (see Fig. 4.2a), only the presence of bright, and no dark, grains can be observed for the Fe-2wt.%V alloy (see Fig. 4.7a). Indeed the measured, corresponding hardness-depth profile reveals a constant, very high value for the hardness in the nitrided zone (1000-1050 HV0.1; Fig. 4.7b). Note that the hardness of the bright grains in the nitrided Fe-4wt.%V alloy is (even) somewhat higher (cf. Figs. 4.2b and 4.7b), reflecting the larger amount of V, and thus vanadium nitride, in nitrided Fe-4wt.%V.

Apparently, only "continuous" precipitation of very fine nitride precipitates occurs in the Fe-2wt.%V alloy upon nitriding.

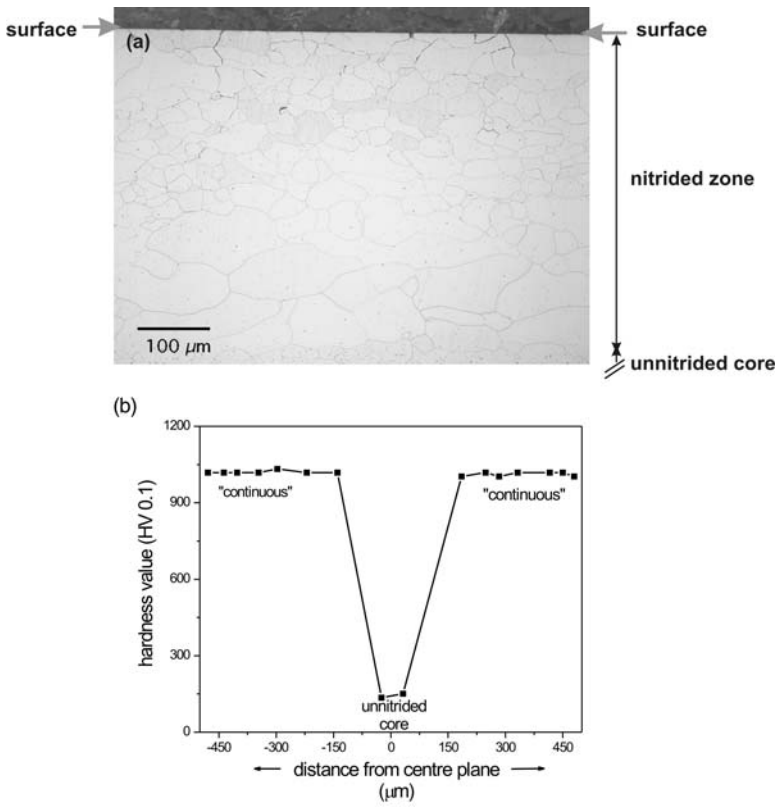

Fig. 4.7: (a) Light optical micrograph of the etched cross-section of the thick (thickness of 1.0 mm) Fe-2wt.%V specimen nitrided at 580 ºC for 10h at a nitriding potential of 0.103 $atm^{-1/2}$. (b) Hardness-depth profile of the same specimen.

The X-ray diffractogram recorded from the surface of the nitrided Fe-2wt.%V specimen is shown in Fig. 4.8. The X-ray diffractogram shows only the presence of reflections of α-Fe. These reflections are strongly, asymmetrically broadened: see Fig. 4.8b, where the (200) α-Fe reflections of nitrided Fe-4wt.%V and of nitrided Fe-2wt.%V can be compared. This type of

broadening (note the occurrence of "side-bands" for the Fe-2wt.%V alloy) can be ascribed to the presence of coherent misfitting nitride precipitates diffracting coherently with the α-Fe matrix [17]. Analysis of this type of diffraction – line broadening is not straightforward [27].

The elemental concentration-depth profiles of the nitrided layer of the nitrided Fe-2wt.%V alloy are presented in Fig. 4.9. In contrast with the nitrided zone of the Fe-4wt.%V alloy, here an undisturbed gradual decrease of nitrogen content from surface to the unnitrided core can be observed. The "normal" amount of nitrogen, which should be present in the nitrided zone if no excess nitrogen would occur, has been indicated in Fig. 4.9 with a horizontal grey line. Evidently, a significant amount of excess nitrogen is also taken up by the Fe-2wt.%V alloy upon nitriding.

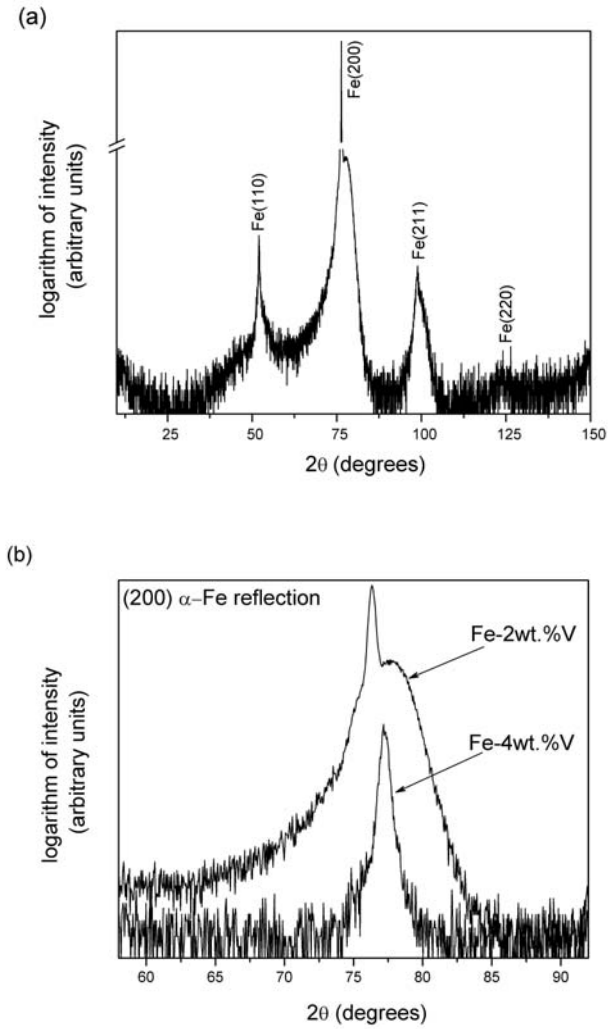

Fig. 4.8: (a) X-ray diffractogram (CoKα-radiation) recorded from the surface of the Fe-2wt.%V specimen, nitrided at 580 ºC for 10 hrs at a nitriding potential 0.103 $atm^{-1/2}$; (b) comparison of the (200) α-Fe reflections as recorded from nitrided Fe-4wt.%V (cf. Fig. 4.5) and from nitrided Fe-2wt.%V.

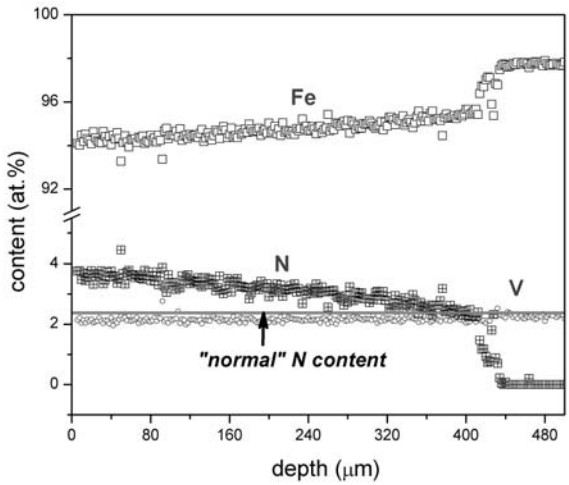

Fig. 4.9: Elemental (N, V, Fe) concentration-depth profiles of the Fe-2wt.%V alloy nitrided at 580 ºC for 10h at a nitriding potential of 0.103 $atm^{-1/2}$. The horizontal, grey line indicates the "normal" amount of nitrogen uptake.

4.4 Discussion

4.4.1 Precipitation morphology

On the basis of the results obtained for nitrided Fe-4wt.%V and with reference to literature data for nitrided Fe-Cr [20, 21], the mechanism for the discontinuous coarsening in nitrided Fe-4wt.%V can be described as follows.

Upon nitriding, initially the vanadium nitride is formed as finely dispersed precipitates, as platelets which are probably coherent with the α-Fe matrix (see high resolution transmission electron microscopical (HRTEM) analysis of a VN platelet in nitrided Fe-2at.%V in Ref. [17]). The misfit-induced stress fields associated with these precipitates [28] are very likely responsible for the very high hardness values observed for the ferrite matrix containing these "continuous" precipitates. On prolonged treatment a coarsening of the VN precipitates occurs, driven by the reduction of the Gibbs energy as a result of, in any case, relaxation of the internal long-range stress fields and of reduction of the precipitate/matrix interfacial area. This coarsening can of course in general be realized by continuous growth of the (largest) precipitates ("Ostwald ripening"), but, for the Fe-4wt.%V alloy, it can in particular occur by a discontinuous coarsening of the former continuous precipitates, involving growth of α-Fe and VN lamellae from nucleation sites as surfaces and grain boundaries. The discontinuous coarsening mechanism operating here can be of the following type:

$$\alpha^{|} + \beta^{|} \rightarrow \alpha + \beta \qquad (4.1)$$

where $\beta^{|}$ denotes coherent VN precipitates in a supersaturated matrix ($\alpha^{|}$). The reaction consists of replacing the submicroscopical, coherent, VN precipitates by VN lamellae ($\beta^{|} \rightarrow \beta$) under simultaneous elimination of the (nitrogen) supersaturation of the matrix ($\alpha^{|} \rightarrow \alpha$).

Thus, upon nitriding of Fe-4wt.%V alloys two reaction fronts can be expected, the first one is due to inward diffusion of nitrogen and the reaction of V and N to finely dispersed VN precipitates, and the second one is due to the subsequent discontinuous coarsening of the precipitates (see Fig. 4.2a). The hardness of the grains showing discontinuous precipitation is significantly lower than that of the grains showing continuous precipitation (Fig. 4.2b and Fig. 4.4), which is a direct consequence of the coarsening with the associated loss of coherency.

The driving force for the discontinuous coarsening reaction will be the larger the larger the amount of VN precipitates. Hence it can be anticipated that upon nitriding the driving force for discontinuous coarsening is larger for the Fe-4wt.%V alloy than for the Fe-2wt.%V alloy. Thus the absence of discontinuous coarsening in case of the nitrided Fe-2wt.%V alloy can be understood.

4.4.2 Excess nitrogen

The measured nitrogen concentration-depth profiles of the nitrided Fe-4wt.%V (Fig. 4.6a) and Fe-2wt.%V (Fig. 4.9) specimens reveal the presence of excess nitrogen within the nitrided zone. The origin of excess nitrogen can be understood as follows.

Long range strain fields are provoked by the coherent (or partly coherent) interfaces between matrix and the continuously precipitated, finely dispersed VN particles [17]. These long range strain fields, in particular the associated hydrostatic component of stress, cause a pronounced increase of the solubility of nitrogen in the matrix [28]. Clear examples of this phenomenon have been given in Refs. [20, 28, 29]. The ferrite lattice solubility can be enhanced with 100% and more as a result of this effect. It should however be recognized that the strain-induced increase of the lattice parameter of the matrix is not a direct quantitative indication of the amount of excess nitrogen.

A significant part of the excess nitrogen in nitrided Fe-V alloys may be adsorbed at the nitride-matrix interfaces [7, 28]. The amount of interfacial nitrogen depends not only on the total precipitate-matrix interface area but also on the interface structure. A VN precipitate with excess nitrogen adsorbed at the interface with the matrix can thus be regarded as a VN_x compound, i.e. (x-1) nitrogen atoms per VN_x molecule are bonded / adsorbed to the coherent faces of the particle / platelet. The magnitude of x depends on the size of the particles assuming that at every octahedral interstice adjacent to the $(001)_{\alpha\text{-Fe}}$ // $(001)_{VN}$ interface [17]

one excess nitrogen atom is trapped; the maximal value of x equals 3 and occurs for a monolayer of VN [7, 28].

Upon (discontinuous) coarsening relaxation of long range strain fields occurs. Thereby the capacity for excess nitrogen uptake is lost. The fate of the original excess nitrogen can then be as follows. Within the discontinuously coarsened regions, either (i) it diffuses inward, to contribute to further increase of the nitrided zone, or (ii) it diffuses outward (appears only feasible for the surface adjacent grains, in view of the nitrogen-concentration gradient within the nitrided zone), or (iii) it precipitates as nitrogen gas (development of pores at grain boundaries; see Refs. [20 and 21]). In particular processes (i) and (ii) could explain the occurrence of an amount of (residual) excess nitrogen within the discontinuously transformed grains (appearing dark in the light optical micrographs) somewhat smaller than in the grains with the fine, coherent precipitates (appearing bright in the light optical micrographs) (see Figs. 4.6b and c).

With a view to the kinetic analysis in section 4.4.3, the amount of total "excess" nitrogen at the surface of the nitrided zone can be calculated as follows. The equilibrium solubility of nitrogen in stress-free ferrite, $c_{N_\alpha}^{S,0}$, is given by data in Refs. [1 and 2]. The experimental amount of surface nitrogen content in ferrite, $c_{N_\alpha}^{S}$, has been determined for the nitrided Fe-2wt.%V alloy by EPMA, as average value from the (first) three data points closest to the surface (Fig. 4.9) after subtracting the amount of nitrogen incorporated in VN from the total measured N content. An estimate for the total amount of excess nitrogen at the surface of the nitrided Fe-4wt.%V alloy cannot be based on (EPMA) measurements of the nitrogen content in the surface adjacent region because the surface adjacent region had experienced the discontinuous coarsening reaction with the associated decrease of excess nitrogen content (see above discussion; Fig. 4.6). Therefore a crude estimate of the surface-nitrogen content for the Fe-4wt.%V alloy has been based on extrapolation to the surface of the nitrogen-concentration profile as measured for the region of "continuous" precipitation (for example, see Fig. 4.6b). The difference between the thus determined values for $c_{N_\alpha}^{S}$ and $c_{N_\alpha}^{S,0}$ gives the total amount of "excess" nitrogen (row 3 in Table 4.2).

4.4.3 Growth kinetics of the nitrided layers

The most simple quantitative description of growth of the nitrided zone is based on a model originally meant for "internal oxidation" (Ref. [30]; see also Ref. [23]). Applying this model to internal nitriding, the following assumptions must hold:

(i) The nitrogen dissolved in the ferrite matrix (α) exhibits Henrian behavior. This implies that the diffusion coefficient of nitrogen in the ferrite matrix is independent of the dissolved nitrogen content.

(ii) The reaction of dissolved nitrogen with dissolved V, leading to the nitride VN, takes place only and completely at a sharp interface between the nitrided zone and the not nitrided core.

(iii) The amount of nitrogen which is required for building up the concentration profile in the ferrite matrix of the nitrided zone is negligible in comparison to the amount of nitrogen which is consumed at the reaction interface.

(iv) Diffusion of V can be neglected and is not nitriding-rate determining.

(v) Local equilibrium prevails at the nitriding medium / specimen interface, so that the surface concentration $c^S_{N_\alpha}$ is equal to the lattice solubility of nitrogen, as given by the chemical potential of nitrogen in the nitriding atmosphere.

With these assumptions and approximating the concentration gradient of dissolved nitrogen with $-c^S_{N_\alpha}/z$, the amount of nitrogen (per unit area) which reaches the reaction front in the time period dt is equal to $\left(c^S_{N_\alpha} \cdot D_{N_\alpha} / z\right) dt$, where z is the depth coordinate of the reaction front and D_{N_α} is the diffusivity of nitrogen in α-Fe. This nitrogen amount must equal the nitrogen amount required to move the reaction front a distance dz, i.e.: $c_V \cdot dz$, where c_V is the vanadium concentration. Upon integration of the resulting differential equation for constant temperature it is obtained:

$$z^2 = \left(\frac{2 \cdot c^S_{N_\alpha} \cdot D_{N_\alpha}}{c_V} \right) \cdot t \tag{4.2}$$

The expected nitriding depths for the Fe-4wt.%V and Fe-2wt.%V specimens can now be calculated from Eq. (4.2) by using the following data: diffusivity of nitrogen in α-Fe (D_{N_α}) at 580ºC = $1.135 \cdot 10^{-11}$ m^2 sec^{-1} [31], equilibrium nitrogen content in α-Fe ($c^{S,0}_{N_\alpha}$) at 580 ºC for a nitriding potential of 0.103 $atm^{-1/2}$ = 0.24 at.% [1, 2]. Then, according to Eq. (4.2), it is obtained for the predicted values of nitriding depth (z) for 10h nitriding at 580 ºC: 210 μm and 296 μm for Fe-4wt.%V and Fe-2wt.%V respectively.

Experimental values for the thickness of the nitrided regions of the Fe-4wt.%V and Fe-2wt.%V specimens have been obtained from the concentration-depth profiles measured by EPMA. The experimental nitriding depth has been defined as the distance between the surface

and the location where the nitrogen content reaches half the vanadium content present in the alloys [22].

Comparison of the thus predicted and experimental values of nitriding depth (Table 4.2) shows that, the experimental nitriding depths are much larger than the values predicted as described above. This is just another indication that the true lattice solubility in the nitrided zone is larger than the equilibrium solubility, which is the consequence of dissolved excess nitrogen (this effect has been discussed detailedly for nitrided Fe-Cr in Refs. [23 and 24]).

Reversely, adopting the experimental values for the nitriding depth, values of $c^{S}_{N_\alpha}$ can be obtained for the Fe-4wt.%V and Fe-2wt.%V specimens applying Eq. (4.2). The difference between the thus determined values of $c^{S}_{N_\alpha}$ and the values of $c^{S,0}_{N_\alpha}$ calculated using literature data [1, 2] represents the amount of dissolved excess nitrogen (see row 6 in Table 4.2). Evidently, the amount of dissolved excess nitrogen is of the same order of magnitude as the equilibrium nitrogen solubility and is responsible for a pronounced, extra increase of the nitriding depth. Therefore the dissolved excess nitrogen is called *mobile* excess nitrogen. The presence of a larger amount of dissolved excess nitrogen in Fe-4wt.%V as compared to Fe-2wt.%V (see row 6 in Table 4.2) is due to a higher amount of vanadium nitrides in Fe-4wt.%V, associated with a more severally strained matrix.

The difference between the total amount of excess nitrogen and the amount of dissolved excess nitrogen gives the amount of excess nitrogen "adsorbed" at the precipitate / matrix interfaces (see row 7 in Table 4.2). The adsorbed precipitate / matrix interfacial nitrogen is called *immobile* excess nitrogen as it does not diffuse and does not contribute to (additional) growth of the nitrided zone. The corresponding ratio N:V in the vanadium nitride precipitate (x in VN_x; see section 4.4.2) for Fe-4wt.%V is about 1.5 and for Fe-2wt.%V is about 1.4, which implies (cf. Ref. [7]) that the nitride platelet thickness is about 4 monolayers (≈ 0.8 nm) for both alloys.

Table 4.2: Tabular presentation of the expected nitriding depth as calculated using Eq. (4.2) with $c^{S}_{N_\alpha} = c^{S,0}_{N_\alpha}$, the measured nitriding depth as determined from the experimental (EPMA) data, the total amount of excess nitrogen at the surface determined as described in section 4.4.2, the equilibrium nitrogen content in (stress-free) α-Fe ($c^{S,0}_{N_\alpha}$), the nitrogen content in α-Fe at the surface as calculated using Eq. (4.2) with experimental values for the nitriding depths ($c^{S}_{N_\alpha}$), the amount of dissolved, mobile excess nitrogen ($=c^{S}_{N_\alpha} - c^{S,0}_{N_\alpha}$) and the amount of immobile, adsorbed at precipitate / matrix interfaces, excess nitrogen. All results have been given for the Fe-4wt.%V and Fe-2wt.%V alloys, nitrided at 580 ºC for 10h at a nitriding potential of 0.103 $atm^{-1/2}$.

		Fe-4wt.%V	*Fe-2wt.%V*
(1)	**Expected nitriding depth (Eq. (4.2) with $c^{S}_{N_\alpha} = c^{S,0}_{N_\alpha}$) (µm)**	210	296
(2)	**Measured nitriding depth (experimental (EPMA) results) (µm)**	322	425
(3)	**Total excess nitrogen at surface (measured from EPMA) (at.%)**	2.31*	1.15
(4)	**Equilibrium nitrogen content in α-Fe, $c^{S,0}_{N_\alpha}$ (Refs. 1 and 2) (at.%)**	0.24	0.24
(5)	**Nitrogen content in α-Fe at the surface, $c^{S}_{N_\alpha}$ (Eq. (4.2) with experimental values for nitriding depths, z) (at.%)**	0.56	0.49
(6)=(5)-(4)	**Dissolved (i.e. mobile) excess nitrogen ($=c^{S}_{N_\alpha} - c^{S,0}_{N_\alpha}$) (at.%)**	0.32	0.25
(7)=(3)-(6)	**Adsorbed precipitate / matrix interfacial (i.e. immobile) excess nitrogen (at.%)**	1.99	0.91

* *estimate; see text in section 4.4.2*

4.5. Conclusions

1. Upon nitriding Fe-V alloys two precipitation morphologies have been observed for the first time: Near the surface of nitrided Fe-4wt.%V alloys a lamellar microstructure composed of α-Fe and VN lamellae occurs; at larger depths in the nitrided zone very finely dispersed, submicroscopical VN precipitates occur, which cannot be detected by light optical and scanning electron microscopy. The lamellar morphology is characterized by a relatively low hardness and the presence of α-Fe and VN reflections in X-ray diffractograms. The very finely dispersed, submicroscopical precipitation

morphology is characterized by a very high hardness and the absence of separate VN reflections in X-ray diffractograms.

2. The lamellar precipitation morphology is the result of a discontinuous coarsening reaction: the initial, continuous precipitation morphology, i.e. finely dispersed (semi-) coherent VN precipitates in an α-Fe matrix, is replaced by a discontinuous precipitation morphology by growth of α-Fe and VN lamella colonies starting from grain boundaries (and the free surface). This discontinuous coarsening is driven by the decrease of precipitate / matrix misfit strain and the reduction of precipitate / matrix interface area, and the elimination of supersaturation of the ferrite matrix by dissolved "excess" nitrogen (see next conclusion). The driving force for the discontinuous coarsening depends on the vanadium content of the alloy. For nitriding at 580 ºC, the driving force in the Fe-2wt.%V alloy is too small for the occurrence of discontinuous coarsening.
3. The nitrided zone of the Fe-V alloys contains more nitrogen than necessary for precipitation of all vanadium as nitride and equilibrium saturation with nitrogen of the ferrite matrix. This additional nitrogen is called "excess nitrogen".
4. The analysis of the growth kinetics of the nitrided zone in the Fe-V alloys shows that mobile (i.e. dissolved in ferrite) excess nitrogen and immobile excess nitrogen (as adsorbed at the interface between nitride precipitate and ferrite matrix) occur. The mobile (dissolved) excess nitrogen is responsible for pronounced additional increase of the thickness of the nitrided zone, as compared to the thickness of the nitrided zone expected if only the equilibrium solubility of nitrogen in ferrite would occur.

Acknowledgements

We are grateful to Mr. P. Kress and Mr. J. Koehler for assistance with the nitriding experiments and also to Mrs. S. Haug for assistance with the electron probe microanalysis measurements.

References

[1] Mittemeijer EJ, Slycke JT. Surface Engineering 1996;12:152.

[2] Mittemeijer EJ, Somers MAJ. Surface Engineering 1997;13:483.

[3] Jack DH. Acta Metall 1976;24:137.

[4] Podgurski HH, Davis FN. Acta Metall 1981;29: 1.

[5] Rickerby DS, Henderson S, Hendry A, Jack KH. Acta Metall 1986;34:1687.

[6] Podgurski HH, Oriani RA, Davis NA, with Appendix by Li JCM and Chou YT. Trans Metall Soc AIME 1969;245:1603.

[7] Biglari MH, Brakman CM, Mittemeijer EJ, van der Zwaag S. Phil Mag A 1995;72:931.

[8] Biglari MH, Brakman CM, Somers MAJ, Sloof WG, Mittemeijer EJ. Z Metallkd 1993;84:124.

[9] Steenaert JS, Biglari MH, Brakman CM, Mittemeijer EJ, van der Zwaag S. Z Metallkd 1995;86:700.

[10] Biglari MH, Brakman CM, Mittemeijer EJ, van der Zwaag S. Metall Mater Trans A 1995;26:765.

[11] Biglari MH, Brakman CM, Mittemeijer EJ. Phil Mag A 1995;72:1281.

[12] Philipps A, Seybolt AU. Trans Metall Soc AIME 1968;242:2415.

[13] Pope M, Grieveson P, Jack KH. Scandinavian Journal of Metallurgy 1973;2:29.

[14] Welch WD, Carpenter SH. Acta Metall 1973;21:1169.

[15] Krawitz A. Scripta Metall 1977;11:117.

[16] Yang MM, Krawitz AD. Metall Trans A 1984;15:1545.

[17] Bor TC, Kempen ATW, Tichelaar FD, Mittemeijer EJ, van der Giessen E. Phil Mag A 2002;82:971.

[18] Djeghlal ME, Barrallier L. Ann Chim Sci Mat 2003;28:43.

[19] Gouné M, Belmonte T, Redjaimia A, Weisbecker P, Fiorani JM, Michel H. Materials Science and Engineering A 2003;351:23.

[20] Hekker PM, Rozendaal HCF, Mittemeijer EJ. Journal of Materials Science 1985;20:718.

[21] Schacherl RE, Graat PCJ, Mittemeijer EJ. Z Metalld 2002;93:468.

[22] Schacherl RE, Graat PCJ, Mittemeijer EJ. Proceedings of the Symposium on Nitriding (April 2002 Aachen, Germany), (Eds.) Grosch J, Mittemeijer EJ.

Arbeitsgemeinschaft Wärmebehandlung und Werkstofftechnik (AWT), Schlangenbad, Germany 2002, 51.

[23] Schacherl RE, Graat PCJ, Mittemeijer EJ. Metall Mater Trans A 2004;35:3387.

[24] Hosmani SS, Schacherl RE, Mittemeijer EJ. Materials Science and Technology 2005;21:113. (Chapter 2).

[25] JCPDS-International Center for Diffraction Data (1999), PCPDFWIN, Version 202.

[26] Pouchau JL, Pichoir F. La Recherche Aerospatial 1984;3:167.

[27] Vives-Diaz N, Hosmani SS, Schacherl RE, Mittemeijer EJ. in preparation.

[28] Somers MAJ, Lankreijer RM, Mittemeijer EJ. Phil Mag A 1989;59:353.

[29] Chechenin NG, Chezan AR, Craus CB, Roerma DO, Bronsveld PM, Hosson JThMDe. Metall Mater Trans A 2002;33:3075.

[30] Meijering JL. Advances in Material Research (Wiley Interscience, New York) 1971;5:1.

[31] Fast JD, Verrijp MB. Journal of the Iron and Steel Institute 1954;176:24.

Chapter 5

Nitrogen uptake by an Fe-V alloy; quantitative analysis of excess nitrogen

S.S. Hosmani, R.E. Schacherl and E.J. Mittemeijer

Abstract

Nitrogen absorption isotherms of Fe-2wt.%V alloys were determined experimentally to study the differences in chemical bonding for various types of absorbed nitrogen. It was observed that the nitrogen uptake was larger than necessary for precipitation of all vanadium as nitride and for equilibrium dissolution of nitrogen in the ferrite matrix: uptake of excess nitrogen. Three types of absorbed nitrogen could be distinguished: (i) nitrogen in the stoichiometric vanadium nitride, (ii) nitrogen adsorbed at the VN precipitate / α-Fe matrix interface, and (iii) nitrogen dissolved interstitially in the ferrite matrix. Quantitative analysis of the nitrogen absorption isotherms was possible adopting a model that incorporates (immobile) excess nitrogen, identical to nitrogen adsorbed at the nitride/matrix interface, and (mobile) excess nitrogen, identical to the surplus nitrogen solubility of the ferrite matrix due to the misfit-stress field surrounding the nitride precipitates.

5.1 Introduction

Nitriding is a thermochemical surface engineering process by which nitrogen is introduced into the surface region of ferritic iron-based (steel) workpieces at temperatures in the range 500-580°C. The industrial importance of nitriding is great because it improves the fatigue strength, the tribological properties and/or the corrosion resistance. These properties result from the development of an outer (compound) layer composed of (largely) iron nitrides and a diffusion zone underneath where alloying element nitrides can occur.

There are several nitriding methods: e.g. plasma nitriding, salt bath nitriding and gaseous nitriding. The most well-known method to introduce nitrogen into a (ferritic) workpiece is gaseous nitriding. Nitriding in NH_3/H_2 gas mixtures is equivalent to nitriding in N_2 at a pressure of a number of thousands atm (thermodynamic argument [1]) and is possible due to the slow thermal decomposition of NH_3 (kinetic argument [2]).

During internal nitriding, if the iron matrix (substrate) contains alloying elements with a relatively high affinity for nitrogen, like Ti, Al, V and Cr, alloying element nitride precipitates can develop (in the "diffusion zone"), which leads to a pronounced increase of the hardness. A number of studies have been devoted to the nitriding of binary iron-based alloys: see for Fe-Ti, Refs. [3-5], for Fe-Al, Refs. [6-11], for Fe-V, Refs. [12-20], for Fe-Cr, Refs. [21-25]. The increase in e.g. hardness or fatigue resistance depends on the chemical composition of the precipitates, their coherency with the matrix, their size and their morphology.

Results from previous work on the nitriding of iron-vanadium alloys [12-20], of relevance to the present work, can be summarized as follows. Nitriding of low vanadium containing Fe-V alloy (say, 2 wt.% V (or below): see Ref. [20]) shows the formation of finely distributed, plate-like precipitates of vanadium nitride (typically about 40 Å long with a thickness of about 10 Å, precipitated along $\{001\}_\alpha$ matrix planes; see Refs. [12, 17]). The coherent VN precipitates induce strain fields in the surrounding ferrite matrix and thereby influence the nitrogen solubility of the ferrite matrix. It appears that the nitrided Fe-V alloys have a considerable capacity for the uptake of so-called excess nitrogen (i.e. more nitrogen than necessary for (i) precipitation of all vanadium as nitride and (ii) equilibrium saturation of the ferrite matrix; e.g. see Refs. [19, 20]). The total amount of excess nitrogen can be divided into two types: mobile and immobile excess nitrogen (for detailed discussion see Refs. [20, 24, 25]).

The analysis of nitrogen absorption isotherms* allows distinction of the various kinds of differently (chemically) bonded nitrogen, as has been shown by applying this technique to nitrided Fe-Al alloy [7]. Nitrogen absorption isotherms were first determined in detail for pure iron by Lehrer (see Ref. [26]) and for Fe-Al alloy by Podgurski et al. (see Ref. [6]).

Until now the direct compositional analysis of the coherent, extremely tiny, thin nitride precipitate platelets (see above) has appeared impossible. Doubts have been raised that the composition of the nitrides would not be purely MeN (here VN) but (Me, Fe)N, which would simply explain the observation of excess nitrogen [27, 28].

Possibly similar to the occurrence of excess nitrogen in Fe-Me alloys, excess oxygen can be taken up in internally oxidized metal alloys (see section 5.4.3.1): During internal oxidation of Cu-, Ag- and Pb-alloys uptake of excess oxygen occurred and was ascribed to oxygen segregated at oxide/matrix interfaces [29-34].

This study has been performed to investigate in detail the various types and their amounts of absorbed nitrogen, and thereby also to settle the nature of the excess nitrogen (see next to one paragraph above), at least for the Fe-V alloys considered here.

5.2 Theoretical background

5.2.1 Nitrogen uptake in Fe-V alloys

If an Fe-V alloy is nitrided such that no iron nitrides can be formed at the surface (i.e. the nitriding potential is sufficiently low [1, 2]; see section 5.2.2), only a diffusion zone containing VN precipitates develops ("internal nitriding").

The total nitrogen uptake, c_N, of internally nitrided Fe-V alloys can be given as:

$$c_N = [N]_\alpha^0 + [N]_{VN} + [N]_{strain} + [N]_{dislocation} + [N]_{interface} \tag{5.1}$$

where, $[N]_\alpha^0$ is the equilibrium solubility of nitrogen in unstrained α-Fe corresponding to the temperature T and the applied nitriding potential $r_n = \frac{p_{NH_3}}{p_{H_2}^{3/2}}$ (see Ref. [1] and section 5.2.2), $[N]_{VN}$ is the amount of nitrogen incorporated in the equilibrium vanadium nitride, $[N]_{strain}$ is the additional (excess) nitrogen dissolved due to the misfit stress field in the iron-matrix lattice, $[N]_{dislocation}$ is the (excess) nitrogen trapped at dislocations and $[N]_{interface}$ is the (excess) nitrogen adsorbed at the precipitate-matrix interface.

* A nitrogen absorption isotherm shows the dependence of the amount of nitrogen taken up by a (homogeneously) nitrided specimen as a function of the nitriding potential (directly related to the chemical potential of the nitriding atmosphere).

In Eq. (5.1), $([N]_{\alpha}^{0}+[N]_{VN})$ represents the "normal" capacity of nitrogen uptake and $([N]_{strain}+[N]_{dislocation}+[N]_{interface})$ is the total amount of "excess" nitrogen. The total amount of excess nitrogen can be divided into two types: mobile excess nitrogen, i.e. $[N]_{strain}$, and immobile excess nitrogen, i.e. $[N]_{dislocation}$ and $[N]_{interface}$. Due to the relatively low dislocation densities in recrystallized samples (which pertains to the current experiments) the amount of $[N]_{dislocation}$ can be neglected here.

5.2.1.1 Nitrogen adsorbed at the precipitate-matrix interfaces

It has been suggested [3-5, 7, 35] that a significant part of the excess nitrogen in nitrided binary iron-based alloys is adsorbed at the nitride-matrix interfaces, $[N]_{interface}$. The amount of interfacial nitrogen depends not only on the total precipitate-matrix interfacial area but also on the interface structure (for VN in α-Fe the nitride platelet faces have the orientation $(001)_{\alpha\text{-Fe}}$ // $(001)_{VN}$, which is compatible with the Bain orientation relationship [17]). A VN precipitate with excess nitrogen adsorbed at the interface with the matrix can be regarded as a VN_X compound, i.e. (X-1) nitrogen atoms per VN_X molecule are bonded / adsorbed to the coherent faces of the particle / platelet (see Fig. 5.1b), i.e.:

$$X = \frac{[N]_{VN}+[N]_{interface}}{[N]_{VN}} \tag{5.2}$$

The magnitude of X depends on the thickness of the platelets assuming that at every octahedral interstice adjacent to the $(001)_{\alpha\text{-Fe}}$ // $(001)_{VN}$ interface (see above) one excess nitrogen atom is trapped; the maximal value of X equals 3 and occurs for a monolayer of VN.

5.2.1.2 Nitrogen dissolved in the strained iron lattice

Due to elastic accommodation of the misfit between a (coherent) nitride particle and the iron matrix, a dilatation of the lattice of the matrix occurs [4, 35]. Straining of the matrix influences the solubility of nitrogen in the ferrite matrix. A model predicting the amount of nitrogen dissolved in ferrite containing misfitting nitride particles has been described in Ref. [35]. The essence of that model is summarised briefly below.

A vanadium-nitride precipitate developing in the ferrite matrix experiences a positive volume misfit. Then, supposing fully elastic accommodation, the treatment by Eshelby [36] for a finite matrix shows that a positive dilation of the matrix occurs. The matrix lattice dilation generated by the misfitting nitrides, induced by the hydrostatic component of the

image-stress field of finite bodies, provides a geometrical understanding for the occurrence of enhanced solubility of nitrogen. This dilation is not a direct function of temperature. The actually occurring, temperature dependent amount of (mobile) excess nitrogen can then be estimated applying the thermodynamics of (hydrostatically) stressed solids [35]. Thus, the enhancement of the lattice solubility $[N]_{strain}$ with respect to that of the reference state $[N]_{\alpha}^{ref}$ is given by [35]:

$$[N]_{strain} = [N]_{\alpha}^{ref}\left\{\exp\left[\frac{\bar{V}_N}{RT}\left(\frac{4\varepsilon G_{\alpha}}{(1+\varepsilon)^3}CY_{VN_x}^0 - \sigma_{\alpha}^{ref}\right)\right]-1\right\} \tag{5.3}$$

with

misfit parameter: $$\varepsilon = \frac{\left[V_{VN} + (X-1)fV_{VN}\right]^{1/3} - \left(V_{\alpha}\right)^{1/3}}{\left(V_{\alpha}\right)^{1/3}} \tag{5.4}$$

constant: $$C = \frac{3K_{VN}}{\left(3K_{VN} + 4G_{\alpha}\right)} \tag{5.5}$$

volume fraction of VN_X precipitates: $$Y_{VN_x}^0 = \frac{V\left(V_{VN} + (X-1)fV_{VN}\right)}{(1-V)V_{\alpha} + V\left(V_{VN} + (X-1)fV_{VN}\right)} \tag{5.6}$$

where $\bar{V}_N$ is the partial molar volume of nitrogen in iron, V_{α} and V_{VN} are the molar volumes of the matrix and the VN precipitate, G_{α} is the shear modulus of the iron matrix, K_{VN} is the bulk modulus of VN precipitate, σ_{α}^{ref} is a hydrostatic pressure for a specific reference state and V (= [V]/100) is the atomic fraction of vanadium in the specimen. The reference state is taken as ferrite (α-Fe) with the equilibrium nitrogen solubility for the same nitriding potential, same temperature and same external (atmospheric) pressure as for the Fe-V alloys considered (i.e. $[N]_{\alpha}^{ref} = [N]_{\alpha}^{0}$ and hence $\sigma_{\alpha}^{ref} = 0$). The parameter f describes the extent to which the full misfit due to building out of the lattice of the VN particle by the adsorbed nitrogen atoms, which act as an entity with the particle, is experienced ($0 \leq f \leq 1$; see further Ref. [35]). The following values for some of the parameters mentioned above can be taken from Refs. [35 and 37]):

$\bar{V}_N$ = 5.12 $cm^3\ mol^{-1}$; V_{α} = 7.092 $cm^3\ mol^{-1}$; G_{α} = 81.6 GPa; K_{VN} = 338 GPa ; V_{VN} = 10.68 $cm^3\ mol^{-1}$.

5.2.2 The nitrogen absorption isotherm

The nitrogen uptake by ferrite upon nitriding in an NH_3/H_2 gas mixture can generally be described by the equilibrium:

$$NH_3 \Leftrightarrow N_\alpha + \frac{3}{2}H_2 \tag{5.7a}$$

where N_α is the nitrogen dissolved interstitially in ferrite matrix. The solubility of nitrogen in ferrite matrix, $[N]_\alpha$, is proportional to the nitriding potential, r_n (= $\frac{p_{NH_3}}{p_{H_2}^{3/2}}$, with p as partial pressure), according to

$$[N]_\alpha = K \cdot r_n \tag{5.7b}$$

where K is the equilibrium constant for Eq. (5.7a) and where it has been assumed that the activity coefficient of the nitrogen atoms is constant and has been incorporated in K [1].

Any point on a nitrogen absorption isotherm indicates the equilibrium amount of nitrogen absorbed by the specimen at the specific nitriding potential selected. To determine experimentally nitrogen absorption isotherms, a prerequisite is the establishment of a homogeneous, constant nitrogen content throughout the cross-section of the specimen. Further, the precipitation morphology should not change during determination of the absorption isotherm. Therefore it is preferred to pre-nitride at a temperature above the temperature of the isotherm concerned, thereby fixing the precipitate morphology.

The nitrogen absorption isotherm as determined for the Fe-V system (see results presented in section 5.4) can be schematically presented as in Fig. 5.1a. Three types of absorbed nitrogen atoms can be discerned (see also section 5.4):

(i) Type I: nitrogen strongly bonded to vanadium in the corresponding stoichiometric VN. As compared with nitrogen of types II and III, this nitrogen cannot be removed easily by de-nitriding in a pure H_2 atmosphere. Type I nitrogen is indicated by level ‘A’ in Fig. 5.1a.

(ii) Type II: nitrogen adsorbed at the nitride/matrix interface (Fig. 5.1b; section 5.2.1.1). As compared to type I nitrogen, this nitrogen is less strongly bonded and can be removed by de-nitriding. This nitrogen is called immobile excess nitrogen as it does not diffuse [20, 24]. Type II nitrogen corresponds with the difference between levels ‘B’ and ‘A’ in Fig. 5.1a.

(iii) Type III: nitrogen dissolved in the octahedral interstices of the ferrite matrix surrounding the precipitates (Fig. 5.1c). According to Eq. (5.7b) the amount of interstitially dissolved nitrogen increases linearly with r_n, provided the activity coefficient for the dissolved nitrogen is constant. Thus the straight line dependence above level 'B' in Fig. 5.1a represents nitrogen dissolved interstitially in the ferrite matrix, i.e. type III nitrogen. This type of nitrogen is the sum of $[N]_\alpha^0$ and $[N]_{strain}$ (section 5.2.1). This is mobile nitrogen which takes part in the nitrogen diffusion process. $[N]_{strain}$ is dissolved nitrogen in excess of $[N]_\alpha^0$ and thus also called mobile excess nitrogen. All nitrogen of type III can be removed easily by de-nitriding.

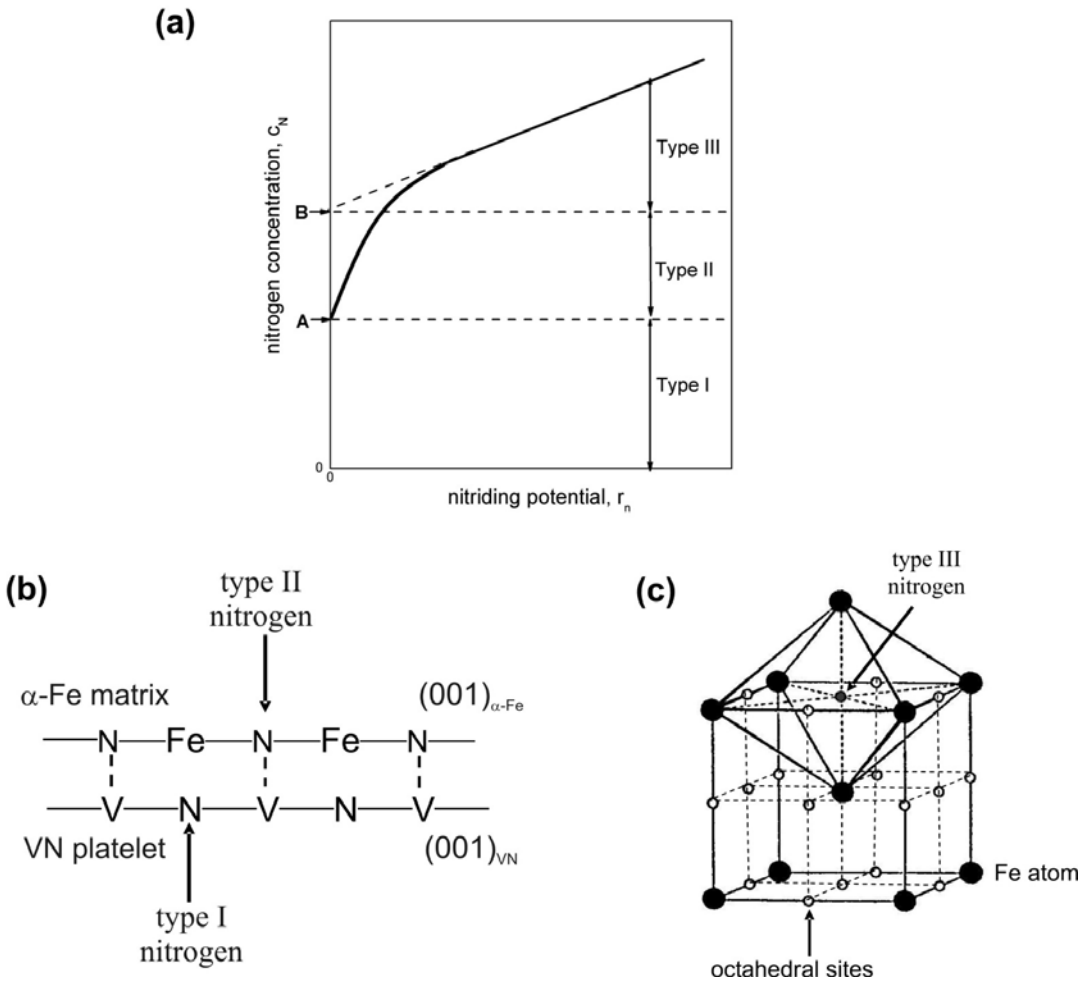

Fig. 5.1: (a) Schematic presentation of a nitrogen absorption isotherm: the total amount of nitrogen uptake, c_N , as a function of nitriding potential, r_n. (b) The $(001)_{VN}$ // $(001)_{\alpha\text{-Fe}}$ VN / α-Fe interface: nitrogen in octahedral interstices of the α-Fe matrix is adsorbed at the interface in direct contact with V atom at the interface in the VN platelet: type II nitrogen. (c) Type III nitrogen is dissolved in the α-Fe matrix and is incorporated in octahedral interstices of the α-Fe matrix.

5.3 Experimental

5.3.1 Specimen preparation

Iron rods were prepared from pure Fe (99.98 wt.%) in an inductive furnace under argon atmosphere (99.999 vol. %). Fe-2wt.%V alloys were prepared from pure Fe (99.98 wt.%) and pure V (99.80 wt. %) in a Al_2O_3 crucible in an inductive furnace under argon atmosphere (99.999 vol. %). The amounts of vanadium and impurities like oxygen, nitrogen, carbon and sulphur were determined by chemical analysis (inductive-coupled plasma-optic emission spectroscopy). The alloy composition is shown in Table 5.1. From now on the alloy used is denoted in this paper as Fe-2V.

Table 5.1: Amounts of vanadium and light element impurities for the alloy used in this work.

Alloy	V (wt.%)	V (at.%)	O (µg/g)	N (µg/g)	C (µg/g)	S (µg/g)
Fe-2V	2.04 ± 0.05	2.23 ± 0.05	170 ± 10	< 6	6 ± 2	6 ± 3

After casting the pure Fe and the Fe-2V alloy had a cylindrical shape with a diameter of 10 mm and a length of 100 mm. The cast rods of both pure Fe and Fe-2V alloy were cold rolled to sheets with a thickness of 1.0 mm. These sheets were annealed for 2h at 700 ºC to obtain a recrystallized grain structure. After this annealing the sheets were cold rolled to foils with a thickness of about 0.2 mm. The obtained foils of pure Fe and Fe-2V alloy were cut into rectangular pieces with a lateral dimensions of 1.5 x 2.0 cm^2. These pieces were annealed for 2h at 700 ºC to obtain a recrystallized grain structure. After annealing the grains have an average diameter of about 40 µm. Before nitriding the samples were ground, polished (last step: 1µm diamond paste) and cleaned in an ultrasonic bath filled with ethanol.

5.3.2 Nitriding

For nitriding the specimen were suspended at a quartz fibre in a vertical tube furnace. To start the nitriding process the specimen were placed in the middle of the nitriding furnace. The nitriding experiments were performed in an ammonia/hydrogen gas flux (purity: H_2: 99,999 vol.%, NH_3: >99,998 vol.%). The fluxes of both gases were adjusted with mass flow controllers and amounted together 500 ml/min, which corresponds to a linear gas velocity of 1.35 cm/s (inner diameter of the furnace: 2.8cm).

5.3.3 Determination of nitrogen absorption isotherms

To obtain a homogenous precipitation morphology throughout the Fe-2V sample cross-section a pre- and de-nitriding step was performed prior to the determination of the absorption isotherms. Pre-nitridings were performed at 580 ºC for 24h, at 550 ºC for 26h and at 530 ºC for 30h in an ammonia/hydrogen gas flow. The applied nitriding potential amounted 0.103 $atm^{-1/2}$ (455 ml/min hydrogen and 45 ml/min ammonia) for all samples investigated. Under these nitriding conditions no iron nitrides can be formed at the surface [2]. The pre-nitriding led to fully, homogeneously nitrided specimens. At the end of the nitriding process, the samples were quenched in water.

After pre-nitriding the samples were de-nitrided in pure H_2 at 470 ºC for 42h and then cooled to room temperature in a H_2 atmosphere.

Nitrogen absorption isotherms were determined using the nitriding furnace (cf. section 5.3.2). After the consecutive pre- and de-nitriding treatments, nitrogen absorption isotherms were determined at temperatures below the pre-nitriding temperature (cf. Table 5.2) to avoid any change of the precipitation morphology. Nitriding parameters which were used for the determination of the absorption isotherms for the different samples have been summarised in Table 5.2. The pure Fe specimens were nitrided together with the Fe-2V alloy specimens to ensure that the same nitriding conditions hold for both types of specimen (for nitriding parameters, see Table 5.2). The nitriding potentials applied for determination of the nitrogen absorption isotherms (also) do not allow the formation of iron nitrides [2].

The nitrogen uptake or loss was determined by weight measurements after and before nitriding or de-nitriding, respectively, using a Mettler microbalance with an accuracy of 1μg. To determine accurately each weight difference, the average value of five weight measurements was taken. The error bars indicated in Figs. 5.2-5.4 represent the maximal deviation from the average value calculated on the basis of the five weight measurements before (de)nitriding and the five weight measurements after (de)nitriding.

Hot extraction analysis of the hydrogen content before and after nitriding indicated that no significant hydrogen uptake had occurred upon nitriding (i.e. the hydrogen uptake must be less than 0.001 (± 0.0007) wt.%).

Table 5.2: Summary of the nitriding parameters used for the determination of the absorption isotherms.

Pre- and de-nitrided (see section 5.3.3) Sample	Determination of absorption isotherms			
	Temperature (°C)	Time (h)	NH_3 (ml/min)	H_2 (ml/min)
V-1 pre-nitrided at 580 °C; de-nitrided at 470 °C	570	24	25	475
			40	460
			50	450
			58	442
	550	24	25	475
			40	460
			50	450
			65	435
V-2 pre-nitrided at 550 °C; de-nitrided at 470 °C	540	26	25	475
			40	460
			50	450
			65	435
	510	26	25	475
			40	460
			50	450
			65	435
V-3 pre-nitrided at 530 °C; de-nitrided at 470 °C	520	30	25	475
			40	460
			50	450
			65	435
	500	48	25	475
			40	460
			50	450
			65	435

5.4 Results and discussion

5.4.1 Pre-nitriding

A homogenous precipitation morphology is maintained during the nitrogen absorption isotherm measurements by pre-nitriding at a temperature higher than the temperatures at which nitrogen absorption isotherms are determined subsequently (cf. section 5.3.1). To determine a nitriding time, at the chosen pre-nitriding temperature, which is sufficiently long to establish through nitriding of the specimen foil so that a constant nitrogen concentration occurs over the whole thickness of the specimen, a series of experiments for variable nitriding time were performed. The results of such series, performed at the pre-nitriding temperatures of 580, 550 and 530°C, are shown in Fig. 5.2.

The horizontal dashed-lines in Fig. 5.2 indicate the normal capacity for the nitrogen uptake $[N]_{nor}$, which is defined as the sum of the amount of nitrogen required for the formation of VN (for the amount of vanadium which takes part in the formation of VN, see section 5.4.2) and the amount of nitrogen dissolved in the unstrained ferrite matrix (see Table 5.3). The experimentally obtained nitrogen uptake, c_N, is larger than $[N]_{nor}$ (Fig. 5.2). Hence excess nitrogen has been absorbed.

It is observed that the nitrogen uptake in Fe-2V specimens is relatively high at relatively short nitriding times (see Fig. 5.2a) and decreases somewhat (most pronouncedly at the highest pre-nitriding temperature; see Fig. 5.2a) on prolonged nitriding, until a constant nitrogen level occurs. This phenomenon can be ascribed to a small decrease of the total amount of excess nitrogen recognising that in the initial stage of nitriding, very fine VN platelets with a fully coherent interface with the ferrite matrix will be formed, which coarsen somewhat upon continued nitriding which process is associated with a decrease of the capacity for excess nitrogen uptake. Nitriding times longer than 20h did not lead to a further, continued decrease of the nitrogen uptake. This result is compatible with earlier high resolution transmission electron microscopical (HREM) analysis [17] of a VN platelet in Fe-2at.%V specimen, nitrided for 25h at the relatively high temperature of 640 °C, which revealed the occurrence of only a few misfit dislocations for a relatively large VN precipitate.

From the results shown in Fig. 5.2 it follows that, nitriding times of 24h, 26h and 30h suffice to obtain a constant nitrogen uptake throughout the sample cross section at the pre-nitriding temperatures of 580, 550 and 530 °C, respectively (also see section 5.3.3). The corresponding N uptakes after pre-nitriding Fe-2V specimens and nitriding pure Fe specimens have been gathered in Table 5.3.

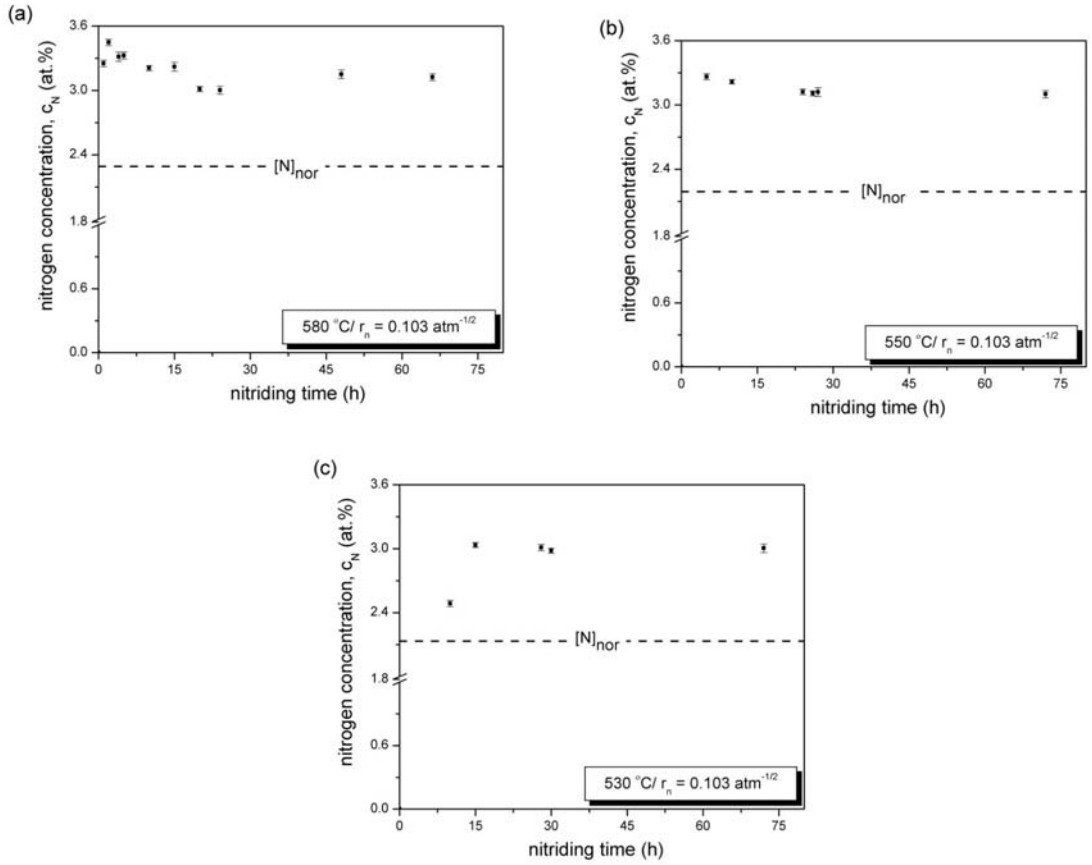

Fig. 5.2: Total nitrogen uptake as a function of nitriding time for Fe-2V specimens nitrided at (a) 580 ºC, (b) 550 ºC and (c) 530 ºC with a nitriding potential of r_n=0.103 atm$^{-1/2}$. The horizontal dashed line indicates the normal capacity of nitrogen uptake.

Table 5.3: The nitrogen uptake by Fe-2V specimens after pre-nitriding, at r_n= 0.103 atm$^{-1/2}$, and the nitrogen uptake by pure Fe under the same nitriding conditions.

Sample	Nitriding temperature (ºC)	N uptake in Fe-2V (at.%)	N uptake in pure Fe (at.%)
V-1	580	3.00 (± 0.04)	0.30 (± 0.004)
V-2	550	3.08 (± 0.02)	0.20 (± 0.006)
V-3	530	2.98 (± 0.02)	0.14 (± 0.003)

5.4.2 De-nitriding

Subsequent to the pre-nitriding treatment, the Fe-2V specimens were de-nitrided at 470 ºC in pure H_2 (500 ml/min) for about 42h (see section 5.3.3). After the de-nitriding treatment the nitrogen content which remains in the sample was determined by weighing. The remaining nitrogen content in the Fe-2V alloy amounts 2.00 (± 0.03) at.% (for error determination, see section 5.3.3) and can be fully attributed to nitrogen which is strongly bonded to V in the

corresponding VN. This indicates that the dissolved nitrogen present in interstitial α-Fe matrix plus the nitrogen adsorbed at the nitride/matrix interface (immobile excess nitrogen) are removed from the specimen during de-nitriding process.

Recognizing that 2.00 at.% (type I) nitrogen is bonded to V to form VN precipitates, (see above), it holds:

$$[Fe] + [V] + [N]_{VN} = 96 \text{ at.\%} + 2.00 \text{ at.\%} + 2.00 \text{ at.\%} = 100 \text{ at.\%}$$

Therefore, the vanadium content in the original Fe-V alloy that takes part in the formation of VN is $\approx \frac{2.00 \times 100}{98}$ = 2.04 (±0.03) at.% (where the error is based on the experimental error in the nitrogen content (see above)). Chemical analysis of the investigated alloys yielded a V content of 2.23 (±0.05) at.% before nitriding (Table 5.1). Apparently, 0.19 (±0.08) at.% V did not take part in the formation of VN, possibly because it is present in the form of oxides already before nitriding (oxides are generally more stable than nitrides).

5.4.3 Nitrogen absorption isotherms

Nitrogen absorption isotherms as determined for the Fe-V alloys for various pre-nitriding and nitriding temperatures (see Table 5.2) are shown in Figs. 5.3a-c. Nitrogen absorption isotherms determined for pure iron for the same nitriding temperatures are presented in Fig. 5.4. The nitrogen level indicated with 'A' in Fig. 5.3 represents the amount of nitrogen required for the formation of stoichiometric VN and corresponds with the amount of nitrogen left in the specimen after de-nitriding (see section 5.4.2). The nitrogen level indicated with 'B' follows from the intercept at $r_n = 0$, as obtained by extrapolating the linear portion of the absorption isotherm (see section 5.2.2). The nitrogen uptake recorded at the lowest nitriding potential (r_n= 0.050 $atm^{-1/2}$) does not comply with the linear relation between c_N and r_n as observed for larger nitriding potentials. The reason for this could be that at low nitriding potential saturation is not achieved for both (i) nitrogen adsorbed at the precipitate/matrix interface and (thereby; cf. Eqs. (5.3-5.6)) (ii) excess nitrogen dissolved interstitially in the ferrite matrix.

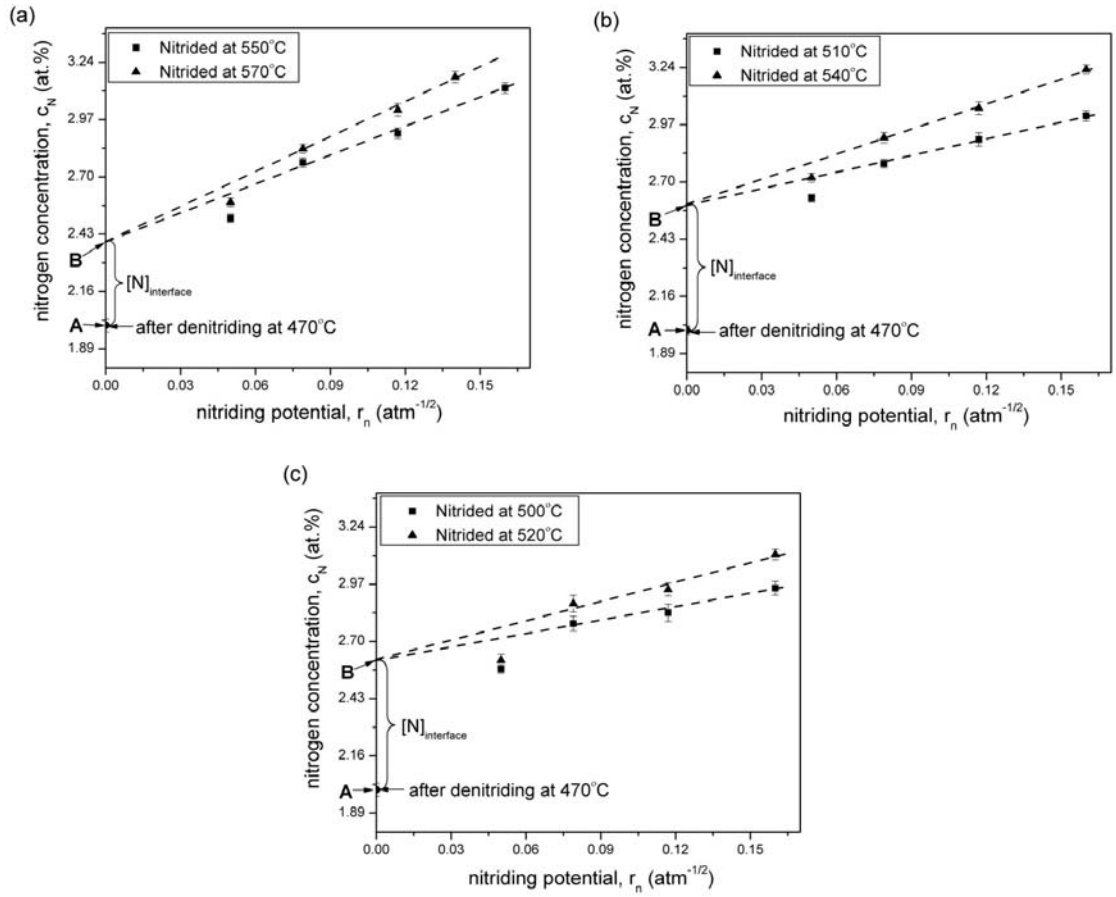

Fig. 5.3: Nitrogen absorption isotherms as observed for pre- and de-nitrided Fe-2V specimens (see Tables 5.2): (a) at 570 and 550 ºC after pre-nitriding at 580 ºC, (b) at 540 and 510 ºC after pre-nitriding at 550 ºC and (c) at 520 and 500 ºC after pre-nitriding at 530 ºC. The nitrogen levels after de-nitriding have been indicated by 'A'. The linear portions of the absorption isotherms have been indicated by the dotted lines which intersect the ordinates at $r_n = 0$ at nitrogen levels indicated by 'B'.

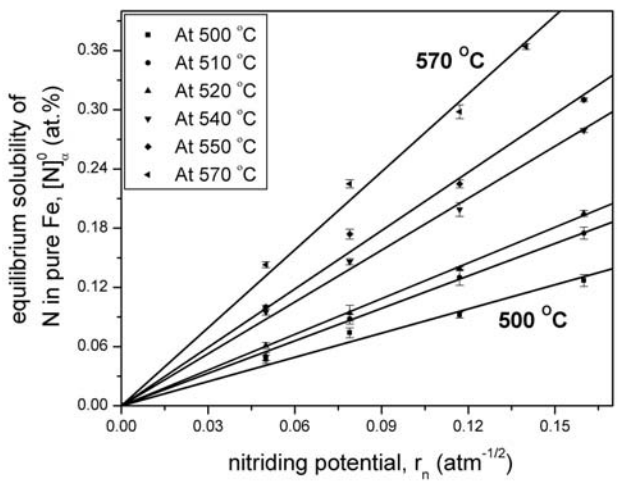

Fig. 5.4: Nitrogen absorption isotherms for pure iron recorded at various temperatures. Straight lines shown represent the (least squares) fits of straight lines (forced to pass through the origin) to the experimental data.

5.4.3.1 Interfacial, adsorbed nitrogen, $[N]_{interface}$

Note that the linear parts of the absorption isotherms extrapolate to the same amount of nitrogen taken up at $r_n = 0$ (level 'B') *independent of* the temperature at which the absorption isotherms were determined, as long as the pre-nitriding temperature is constant (see Figs. 5.3a-c). Evidently, the nitrogen level labelled 'B' represents the sum of the nitrogen present in stoichiometric VN ($[N]_{VN}$) and the (excess) nitrogen adsorbed at the VN precipitate / α-Fe matrix interfaces ($[N]_{interface}$) (see also section 5.2.2). The difference between the nitrogen level 'B' and the nitrogen level 'A' is the amount of $[N]_{interface}$. Describing the composition of a vanadium-nitride precipitate with excess nitrogen adsorbed at the interface with VN_X, the value (X-1) represents the number of nitrogen atoms per VN_X molecule bonded / adsorbed at the (coherent) interfaces of the VN particles. Hence:

$$X = \frac{[N]_{VN} + [N]_{interface}}{[N]_{VN}} = \frac{\text{Level B}}{\text{Level A}} \tag{5.8}$$

The results for X thus obtained have been gathered in Table 5.4. It follows that X decreases with an increasing pre-nitriding temperature. This phenomenon can be discussed as follows. The morphology of the VN precipitates depends on the pre-nitriding temperature, and not on the temperatures at which the absorption isotherms were determined, recognizing that the temperature at which the nitrogen absorption isotherms were determined are lower than the pre-nitriding temperature of the specimen considered. For higher pre-nitriding temperatures the vanadium-nitride platelets are expected to be coarser (i.e. a smaller precipitate/matrix interface area) than for lower pre-nitriding temperatures. Consequently, a relatively high pre-nitriding temperature, corresponds with a relatively small capacity for adsorbed nitrogen and thus X decreases with increasing pre-nitriding temperature.

The value of X gives indirect information on the average thickness of the precipitate platelet. VN precipitates develop as plate-like, cubic (NaCl-type), precipitates along $\{001\}_{\alpha}$ matrix planes with $\{001\}_{\alpha\text{-Fe}}$ // $\{001\}_{VN}$ [17]. With $\{001\}_{VN}$ as the habit plane, the thickness of a monolayer of VN equals one half of the lattice parameter of the face-centred cubic (fcc) unit cell of VN, a_{VN}. Assuming that at every octahedral interstice in the ferrite matrix at the interface one excess nitrogen atom is trapped (cf. Fig. 5.1b), it follows:

$$X = \frac{n+2}{n}. \tag{5.9}$$

where n is the number of VN monolayers comprising the VN platelet. Accordingly, the thickness of the VN platelet is given by,

$$\text{thickness} = \text{n} \cdot \left(\frac{a_{VN}}{2} \right) = \frac{2}{(\text{X}-1)} \cdot \frac{a_{VN}}{2} \tag{5.10}$$

Such results, obtained with a_{VN} = 0.410 nm [38], have been given in Table 5.4. The thickness values obtained are compatible with data obtained by direct analysis in the transmission electron microscope [17].

Upon internal oxidation of an Ag-Mg alloy, MgO precipitates developed with excess oxygen atoms segregating at the oxide/matrix interface [31]. Electron energy loss spectroscopy (EELS) indicated a charge (electron) transfer from Ag atom to these excess O atoms [31]. Although the interfacial planes are different for both systems ($\{111\}_{\text{Ag}}$ planes for MgO/Ag and $\{001\}_{\alpha\text{-Fe}}$ planes for VN/Fe; whereas both MgO and VN have a rocksalt (NaCl) crystal structure), and thus the bonding situation for the excess O may largely differ from that for the excess N (see Fig. 5.1b), such charge (electron) transfer (from V atoms, which can, more easily than Mg, donate electrons, or from Fe atoms) may also occur for the adsorbed excess N.

Table 5.4: The value of X in VN_X and the estimated average thickness of VN platelets (calculated using Eq. (5.10)) for specimens pre-nitrided at different temperatures.

Sample **Pre-nitriding temperature (°C)**	**V-1** **580**	**V-2** **550**	**V-3** **530**
X in VN_X	1.21 (± 0.01)	1.30 (± 0.02)	1.32 (± 0.02)
Average thickness of VN precipitates (see Eq. (5.10)) (nm)	2.0	1.4	1.3

5.4.3.2 Dissolved nitrogen, $[N]_\alpha^0 + [N]_{strain}$

The amount of nitrogen dissolved in the ferrite matrix can be written as $[\text{N}]_\alpha \equiv [\text{N}]_\alpha^0 + [\text{N}]_{\text{strain}} = [\text{N}]_\alpha^{\text{ref}} + [\text{N}]_{\text{strain}}$ (cf. section 5.2.1.2) and thus (cf. Eq. (5.3)):

$$\frac{[\text{N}]_\alpha}{[\text{N}]_\alpha^0} = \left\{ \exp\left[\frac{\bar{\text{V}}_\text{N}}{\text{RT}} \left(\frac{4\varepsilon \text{G}_\alpha}{(1+\varepsilon)^3} \text{CY}_{\text{VN}_\text{x}}^0 - \sigma_\alpha^{\text{ref}} \right) \right] \right\} \tag{5.11}$$

Experimental values for $\frac{[N]_\alpha}{[N]_\alpha^0}$, at nitriding temperatures T, follow from the slopes, S_{Fe-2V} and S_{Fe} , of the linear parts of the absorption isotherms determined at the same temperature for the Fe-V alloy (Fig. 5.3) and for pure-Fe (Fig. 5.4), respectively:

$$\frac{[N]_\alpha}{[N]_\alpha^0} = \frac{(\Delta[N]_\alpha / \Delta r_n)}{(\Delta[N]_\alpha^0 / \Delta r_n)} = \frac{S_{Fe-2V}}{S_{Fe}} \tag{5.12}$$

The absorption isotherm slope ratio, $\frac{S_{Fe-2V}}{S_{Fe}}$, for the different nitriding temperatures for samples pre-nitrided at different temperatures have been summarized in Table 5.5.

The values of all constants at the right-hand side of Eq. (5.11), except X and f (cf. Eqs. (5.4) and (5.6)), are known (cf. section 5.2.1.2). The values of X have been determined in section 5.4.3.1. Hence, applying Eq. (5.11), the values for f can be straightforwardly calculated from $\frac{S_{Fe-2V}}{S_{Fe}}$. The results thus obtained for f have been gathered in Table 5.6. Within experimental accuracy, the values obtained for f are the same for the same pre-nitriding temperature, in accordance with a precipitation morphology that is determined by the pre-nitriding temperature (which is higher than the temperature used for determination of the nitrogen absorption isotherms; see discussion in section 5.4.3.1). Furthermore, f does not significantly depend on the pre-nitriding temperature in the investigated temperature range (530-580 °C).

Table 5.5: Nitrogen absorption isotherm slope ratio, $\frac{S_{Fe-2V}}{S_{Fe}}$, for different nitriding temperatures for Fe-V samples pre-nitrided at different temperatures, where, S_{Fe-2V} and S_{Fe} are the slopes of the linear parts of the nitrogen absorption isotherms for Fe-2V (Fig. 5.3) and for pure iron (Fig. 5.4) at the same temperature.

Sample	Pre-nitriding temperature (ºC)	$\frac{S_{Fe-2V}}{S_{Fe}}$ at the nitriding temperatures used for determination of the absorption isotherms					
		570 ºC	550 ºC	540 ºC	520 ºC	510 ºC	500 ºC
V-1	**580**	2.08 (± 0.24)	2.21 (± 0.23)	-	-	-	-
V-2	**550**	-	-	2.27 (± 0.13)	-	2.53 (± 0.14)	-
V-3	**530**	-	-	-	2.39 (± 0.51)	-	2.54 (± 0.56)

Table 5.6: The value of f (cf. Eqs. (5.4) and (5.6)) for Fe-2V specimens pre-nitrided at different temperatures.

Sample	**V-1**	**V-2**	**V-3**
Pre-nitriding temperature (°C)	**580**	**550**	**530**
f	0.81 (± 0.08)	0.76 (± 0.10)	0.77 (± 0.10)

5.4.3.3 Concluding remarks on excess nitrogen

Because of the capacity to take up excess nitrogen in the form of interfacial nitrogen, at the (coherent) nitride/matrix interface, and interstitially dissolved nitrogen in the ferrite matrix, due to the hydrostatic tensile misfit stress component, the total amount of nitrogen absorbed by the Fe-V alloy can be considerably larger than expected naively: see the summary of results provided by Tables 5.7 and 5.8. It follows that, (i) an amount of nitrogen as large as 30% of the amount of nitrogen bonded to V in VN_X can be adsorbed as interfacial excess nitrogen at the nitride/matrix interface and (ii) the equilibrium solubility of nitrogen in the ferrite matrix can be increased with 50%.

Finally, it should be recognized that the nitride precipitates formed in the Fe-V alloy apparently have the composition VN, as indicated by the nitrogen level ‘A’ (cf. Fig. 5.3) as obtained by de-nitriding. This rules out the possible explanation of excess nitrogen as due to the development of (Fe, V)N, instead of VN precipitates.

Table 5.7: The amount of nitrogen bonded in VN (type I nitrogen; $[N]_{VN}$) and excess nitrogen adsorbed at the nitride/matrix interface (type II nitrogen; $[N]_{interface}$) for the Fe-2V alloy pre-nitrided at different temperatures, as derived from the nitrogen absorption isotherms (Fig. 5.3).

Sample	**V-1**	**V-2**	**V-3**
Pre-nitriding temperature (°C)	**580**	**550**	**530**
$[N]_{VN}$ **(at.%)**	2.00	2.00	2.00
$[N]_{interface}$ **(at.%)**	0.40	0.60	0.64

Table 5.8: The amount of nitrogen dissolved in the ferrite matrix (type III nitrogen; $[N]_{\alpha}$), the equilibrium solubility of nitrogen in unstrained ferrite ($[N]_{\alpha}^{0}$) and dissolved excess nitrogen ($[N]_{strain}$) at 570, 540 and 520 ºC, and at 0.103 $atm^{-1/2}$ nitriding potential for specimens pre-nitrided at 580, 550 and 530 ºC, respectively, and as derived from the nitrogen absorption isotherms (Figs. 5.3 and 5.4).

	Sample	**V-1**	**V-2**	**V-3**
	Pre-nitriding temperature (°C)	**580**	**550**	**530**
	Nitriding temperature for absorption isotherm (ºC)	**570**	**540**	**520**
(1)	$[N]_{\alpha}^{0}+[N]_{strain}$ **(at.%)**	0.56	0.41	0.31
(2)	$[N]_{\alpha}^{0}$ **(see Fig. 5.4) (at.%)**	0.27	0.18	0.13
(3)=(1)-(2)	$[N]_{strain}$ **(at.%)**	0.29	0.23	0.18

5.5 Conclusions

(i) Upon nitriding Fe-V alloy three types of absorbed nitrogen can be distinguished, in order of decreasing strength of the chemical bonding: (a) nitrogen contained in VN precipitates, (b) nitrogen adsorbed at the (coherent) nitride/matrix interface and (c) nitrogen dissolved interstitially in the ferrite matrix.

(ii) The distribution of the nitrogen over the different types of sites can be determined by quantitative analysis of nitrogen absorption isotherms and verified by using specimens pre-nitrided at different temperatures corresponding to different nitride-precipitate morphologies.

(iii) The values determined for the amounts of excess nitrogen adsorbed at the nitride/matrix interface lead to estimates for the nitride platelet thickness compatible with experimental observations.

(iv) The values determined for the amounts of excess nitrogen dissolved in the ferrite matrix can be quantitatively described as the result of the hydrostatic tensile stress component induced by fully elastic accommodation of the misfit between nitride and matrix.

Acknowledgements

We are grateful to Mr. P. Kress and Mr. J. Koehler (both at Max Planck Institute for Metals Research) for assistance with the nitriding experiments.

References

[1] Mittemeijer EJ, Slycke JT. Surface Engineering 1996;12:152.

[2] Mittemeijer EJ, Somers MAJ. Surface Engineering 1997;13:483.

[3] Jack DH. Acta Metall 1976;24:137.

[4] Podgurski HH, Davis FN. Acta Metall 1981;29:1.

[5] Rickerby DS, Henderson S, Hendry A, Jack KH. Acta Metall 1986;34:1687.

[6] Podgurski HH, Oriani RA, Davis NA, with Appendix by Li JCM and Chou YT. Trans Metall Soc AIME 1969;245:1603.

[7] Biglari MH, Brakman CM, Mittemeijer EJ, van der Zwaag S. Phil Mag A 1995;72:931.

[8] Biglari MH, Brakman CM, Somers MAJ, Sloof WG, Mittemeijer EJ. Z Metallkd 1993;84:124.

[9] Steenaert JS, Biglari MH, Brakman CM, Mittemeijer EJ, van der Zwaag S. Z Metallkd 1995;86:700.

[10] Biglari MH, Brakman CM, Mittemeijer EJ, van der Zwaag S. Metall Mater Trans A 1995;26:765.

[11] Biglari MH, Brakman CM, Mittemeijer EJ. Phil Mag A 1995;72:1281.

[12] Philipps VA, Seybolt AU. Trans Metall Soc AIME 1968;242:2415.

[13] Pope M, Grieveson P, Jack KH. Scandinavian Journal of Metallurgy 1973;2:29.

[14] Welch WD, Carpenter SH. Acta Metall 1973;21:1169.

[15] Krawitz A. Scripta Metall 1977;11:117.

[16] Yang MM, Krawitz AD. Metall Trans A 1984;15:1545.

[17] Bor TC, Kempen ATW, Tichelaar FD, Mittemeijer EJ, van der Giessen E. Phil Mag A 2002;82:971.

[18] Djeghlal ME, Barrallier L. Ann Chim Sci Mat 2003;28:43.

[19] Gouné M, Belmonte T, Redjaimia A, Weisbecker P, Fiorani JM, Michel H. Materials Science and Engineering A 2003;351:23.

[20] Hosmani SS, Schacherl RE, Mittemeijer EJ. Acta Materialia 2005;53:2069. (Chapter 4).

[21] Hekker PM, Rozendaal HCF, Mittemeijer EJ. Journal of Materials Science 1985;20:718.

[22] Schacherl RE, Graat PCJ, Mittemeijer EJ. Z Metalld 2002;93:468.

[23] Schacherl RE, Graat PCJ, Mittemeijer EJ. Proceedings of the Symposium on Nitriding (April 2002 Aachen, Germany), (Eds.) Grosch J, Mittemeijer EJ. Arbeitsgemeinschaft Wärmebehandlung und Werkstofftechnik (AWT), Schlangenbad, Germany 2002, 51.

[24] Schacherl RE, Graat PCJ, Mittemeijer EJ. Metall Mater Trans A 2004;35:3387.

[25] Hosmani SS, Schacherl RE, Mittemeijer EJ. Materials Science and Technology 2005;21:113. (Chapter 2).

[26] Lehrer E. Zeitschrift fuer Elektrochemie 1930;36:383.

[27] Danoix F, Danoix R, Hazotte A, Dulcy J, Vu Dinh J. Revue de Metallurgie 2000;SF2M JA:121.

[28] Danoix R, Legras L, Hannoyer B, Dulcy J, Danoix F. Presentation at "PMT-2005 - International Conference on Solid-Solid Transformations in Inorganic Materials", Phoenix, Arizona, USA, May 29-June 03, 2005.

[29] Charrin L, Combe A, Cabane J. Oxidation of Metals 1992;37:65.

[30] Charrin L, Combe A, Cabane F, Cabane J. Oxidation of Metals 1993;40:483.

[31] Pippel E, Woltersdorf J, Gegner J, Kirchheim R. Acta Materialia 2000;48:2571.

[32] Backhaus-Ricoult M, Samet L, Thomas M, Trichet MF, Imhoff D. Acta Materialia 2002;50:4191.

[33] Backhaus-Ricoult M, Samet L, Trichet MF, Hÿtch MJ, Imhoff D. Journal of Solid State Chemistry 2003;173:172.

[34] Kirchheim R, Pundt A, Al-Kassab T, Wang F, Kluthe C. Z Metallkd 2003;94:266.

[35] Somers MAJ, Lankreijer RM, Mittemeijer EJ. Phil Mag A 1989;59:353.

[36] Eshelby JD. Solid State Physics 1956;3:79.

[37] Grossman JC, Mizel A, Côté M, Cohen ML, Louie SG. Physical Review B 1999;60:6343.

[38] Pearson WB. A Handbook of Lattice Spacings and Structures of Metals, vol.2. London: Pergamon Press, 1968.

Chapter 6

Kinetics of nitriding Fe-2wt.%V alloy; mobile and immobile excess nitrogen

S.S. Hosmani, R.E. Schacherl and E.J. Mittemeijer

Abstract

The kinetics of nitriding of Fe-2wt.%V alloy was investigated as a function of time and temperature by exposing the alloy to a gas mixture of ammonia and hydrogen at constant nitriding potential 0.103 $atm^{-1/2}$ at different nitriding temperatures, 520, 550, 580, 600 ºC, for times up to 10h, 10h, 10h and 07h, respectively. The nitrided zone contains finely dispersed small vanadium-nitride precipitates in ferrite (α-Fe) grains. The nitrogen content within the nitrided zone is larger than expected on the basis of the vanadium content and the solubility of nitrogen in (stress-free) ferrite: excess nitrogen occurs. A model was developed that adequately predicts the evolution of the nitrogen concentration-depth profile of the nitrided layer. The model distinguishes quantitatively between the effects of mobile and immobile excess nitrogen, where immobile excess nitrogen is nitrogen adsorbed at the nitride platelet/matrix interface and mobile excess nitrogen is nitrogen dissolved in the matrix. The model has as important (fit) parameters: the composition of the precipitated vanadium nitride, the effective diffusivity of nitrogen in the ferrite matrix surrounding the precipitates and the solubility product of dissolved vanadium and dissolved nitrogen in the ferrite matrix. Analysis of the concentration-depth profile data at various nitriding temperatures exhibited the effect of the nitriding temperature on the amounts of mobile and immobile excess nitrogen.

6.1 Introduction

Nitriding of (ferritic) steels is a technologically important thermochemical surface treatment leading to a hard surface layer giving rise to large improvement in mechanical (fatigue and wear resistance) and chemical (corrosion resistance) properties [1]. The presence of alloying elements Me with a strong affinity for nitrogen, as, Ti, V, Cr and Al, leads to the precipitation of tiny MeN_n precipitates that are largely responsible for the hardness increase.

In particular recent research [2, 3, 4] has made it clear that upon nitriding of such Fe-Me alloys more nitrogen is taken up than necessary for (i) precipitation of all Me as MeN_n nitride and (ii) equilibrium saturation of the ferrite matrix. These amounts of *excess nitrogen* can be as large as 3.6 at.% (Fe-13wt.%Cr [3]) and 2.3 at.% (Fe-4wt.%V [5]).

Until now attempts to model the nitriding kinetics, involving the prediction of the nitrogen concentration-depth profile as a function of time and temperature, have been unsatisfactory or were restricted to simple prescriptions of the extent of the nitrided zone by a simple parabolic growth law [6-8]. The main reason for this unsatisfactory situation is the lack of recognition of the important role that the excess nitrogen has on the nitriding kinetics.

The purpose of this work is to develop a model for the nitriding kinetics of Fe-Me alloys that incorporates the role of the excess nitrogen. The model departs from the basis provided by Ref. [3] and now incorporates a quantitative description for the enhanced nitrogen solubility of the matrix (excess nitrogen) due to the nitride-precipitate/matrix misfit stress field. The model is applied to the nitriding of Fe-2wt.%V alloy. Previous work [5, 9-16] has shown that nitriding of low vanadium containing Fe-V alloy (say 2 wt.% (or below) V: see Ref. [5]) leads to the formation of finely distributed, plate-like precipitates of vanadium nitride (typically about 40 Å long with a thickness of about 10 Å, precipitated along $\{001\}_\alpha$ matrix planes; see Refs. [9, 14]). The coherent VN precipitates induce strain fields in the surrounding ferrite matrix and thereby influence the nitrogen solubility of the ferrite matrix [5].

6.2 Model for the kinetics of diffusion zone growth: theoretical background

6.2.1 Nitrogen uptake in Fe-Me alloys

A full description of the theoretical background can be found in Refs. [17, 18, 19]. Here, the essentials necessary for the current paper are briefly summarized.

The total nitrogen uptake, c_N, of an internally nitrided Fe-Me alloy can be given as [20]:

$$c_N = [N]_\alpha^0 + [N]_{MeN_n} + [N]_{strain} + [N]_{dislocation} + [N]_{interface} \tag{6.1}$$

where, $[N]_\alpha^0$ is the equilibrium solubility of nitrogen in unstrained α-Fe corresponding to the temperature T and the applied nitriding potential $r_n = \frac{p_{NH_3}}{p_{H_2}^{3/2}}$ (see Ref. [21]), $[N]_{MeN_n}$ is the amount of nitrogen incorporated in the equilibrium element nitride, $[N]_{strain}$ is the additional (excess) nitrogen dissolved due to the misfit-stress field in the iron-matrix lattice, $[N]_{dislocation}$ is the (excess) nitrogen trapped at dislocations and $[N]_{interface}$ is the (excess) nitrogen adsorbed at the precipitate-matrix interface.

In Eq. (6.1), $([N]_\alpha^0 + [N]_{MeN_n})$ is the "normal" capacity of nitrogen uptake and $([N]_{strain} + [N]_{dislocation} + [N]_{interface})$ is the total amount of "excess" nitrogen. The total amount of excess nitrogen can be divided into two types: mobile excess nitrogen, i.e. $[N]_{strain}$, and immobile excess nitrogen, i.e. $[N]_{dislocation}$ and $[N]_{interface}$. Due to the relatively low dislocation densities in recrystallized samples (which pertains to the current experiments) the amount of $[N]_{dislocation}$ can be neglected here.

A MeN_n precipitate with excess nitrogen adsorbed at the interface with the matrix can be regarded as a MeN_X compound, i.e. (X-n) nitrogen atoms per MeN_X molecule are bonded / adsorbed to the coherent faces of the particle / platelet, i.e.:

$$X = \frac{[N]_{MeN_n} + [N]_{interface}}{[N]_{MeN_n}} \tag{6.2}$$

The magnitude of X depends on the thickness of the platelets assuming that at every octahedral interstice adjacent to the $(001)_{\alpha\text{-Fe}}$ // $(001)_{MeNn}$ interface [14] one excess nitrogen atom is trapped; the maximal value of X equals 3 and occurs for a monolayer of MeN_n.

A MeN_n precipitate developing in the ferrite matrix experiences a positive volume misfit. Supposing fully elastic accommodation, the strain-induced enhancement of the lattice solubility $[N]_{strain}$ with respect to that of the reference state $[N]_\alpha^{ref}$ is given by [18]:

$$[N]_{strain} = [N]_\alpha^{ref} \left\{ \exp\left[\frac{\bar{V}_N}{RT} \left(\frac{4\varepsilon G_\alpha}{(1+\varepsilon)^3} C Y_{MeN_x}^0 - \sigma_\alpha^{ref} \right) \right] - 1 \right\} \tag{6.3}$$

with

misfit parameter: $$\varepsilon = \frac{\left[V_{MeN_n} + (X-n)fV_{MeN_n}\right]^{1/3} - \left(V_\alpha\right)^{1/3}}{\left(V_\alpha\right)^{1/3}} \quad (6.4)$$

constant: $$C = \frac{3K_{MeN_n}}{\left(3K_{MeN_n} + 4G_\alpha\right)} \quad (6.5)$$

volume fraction of MeN_X precipitates: $$Y^0_{MeN_x} = \frac{Me\left(V_{MeN_n} + (X-n)fV_{MeN_n}\right)}{(1-Me)V_\alpha + Me\left(V_{MeN_n} + (X-n)fV_{MeN_n}\right)} \quad (6.6)$$

where $\bar{V}_N$ is the partial molar volume of nitrogen in iron, V_α and V_{MeNn} are the molar volumes of the matrix and MeN_n precipitate, G_α is the shear modulus of the iron matrix, K_{MeN_n} is the bulk modulus of MeN_n precipitate, σ_α^{ref} is a hydrostatic pressure for a specific reference state and Me is the atomic fraction of the alloying element in the specimen. The reference state is taken as unstrained ferrite (α-Fe) with the equilibrium nitrogen solubility for the same nitriding potential, same temperature and same external (atmospheric) pressure as for the Fe-Me alloys considered (i.e. $[N]_\alpha^{ref} = [N]_\alpha^0$ and hence $\sigma_\alpha^{ref} = 0$). The parameter f describes the extent to which the full misfit due to building out of the lattice of the MeN_n particle by the adsorbed nitrogen atoms, which act as an entity with the particle, is experienced ($0 \le f \le 1$; see further Ref. [18]). The following values for some of the parameters mentioned above were taken from Refs. [18 and 22]):

$\bar{V}_N$ = 5.12 $cm^3\ mol^{-1}$; V_α = 7.092 $cm^3\ mol^{-1}$; G_α = 81.6 GPa; R = 8.314 J $mol^{-1}\ K^{-1}$; K_{MeN_n} = 338 GPa (for VN precipitate), 361 GPa (for CrN precipitate), 304 GPa (for TiN precipitate); V_{MeNn} = 10.68 $cm^3\ mol^{-1}$ (for VN precipitate), 10.75 $cm^3\ mol^{-1}$ (for CrN precipitate), 11.51 $cm^3\ mol^{-1}$ (for TiN precipitate).

6.2.2 Modelling the nitrogen depth profile of the diffusion zone of nitrided Fe-Me alloys

The inward diffusion of nitrogen in the α-Fe matrix can be described with Fick's second law:

$$\frac{\partial c_{N_\alpha}(z,t)}{\partial t} = D_N \cdot \frac{\partial^2 c_{N_\alpha}(z,t)}{\partial z^2} \quad (6.7)$$

$c_{N_\alpha}(z,t)$ is the nitrogen dissolved in the α-Fe matrix at the depth z at time t and at temperature T. D_N is the diffusion coefficient of nitrogen in α-Fe, which can be taken as concentration

independent [1, 21]. The formation of nitrides MeN_n of possibly present alloying elements Me removes dissolved, mobile nitrogen from the matrix. This nitrogen is then trapped as immobile nitrogen in the nitrides MeN_n. The formation of MeN_n can be expressed with the following equation:

$$Me_\alpha + nN_\alpha \Leftrightarrow MeN_n \tag{6.8}$$

where Me_α and N_α denote alloying element and nitrogen dissolved in the α-Fe matrix. The equilibrium constant of the above reaction, K_e, obeys

$$K_e = \frac{1}{[Me_\alpha]\cdot[N]^n} = \frac{1}{K_{MeN_n}} \quad \text{with} \quad K_{MeN_n} = [Me_\alpha]\cdot[N_\alpha]^n \tag{6.9}$$

where $[Me_\alpha]$ and $[N_\alpha]$ denote the concentrations of dissolved Me and dissolved N in the α-Fe matrix and K_{MeN_n} is the corresponding solubility product of Me_α and N_α. The precipitation of MeN_n will take place at a certain location if there it holds

$$[Me_\alpha][N_\alpha]^n > K_{MeN_n} \tag{6.10}$$

In solving Fick's second law (Eq. (6.7)) it must be tested at every location (depth z) for every time (step) if the solubility product, K_{MeN_n}, is surpassed. If this is the case, precipitation of MeN_n, at the location considered, should be allowed for until $[Me_\alpha][N_\alpha]^n = K_{MeN_n}$. On this basis a numerical finite difference (explicit method) solution method can be developed to solve Fick's second law, subject to the prevailing boundary conditions. This has been described in Ref. [3].

The MeN_n precipitates, which are present in the nitrided zone, could act as obstacles for the inward diffusing nitrogen in the ferrite matrix. To consider this effect, the diffusion coefficient of nitrogen in α-Fe, D_N, can be multiplied with a so-called labyrinth factor (see Refs. [23, 24]). The labyrinth factor depends on the fraction of particles, their morphology, and their size distribution function [23].

The amount of mobile excess nitrogen, which is equivalent to $[N]_{strain}$, is determined using the parameters X and f (from Eqs. (6.3)-(6.6)). The equilibrium solubility of nitrogen in α-Fe ($[N]_\alpha^0$) was determined experimentally in this work by nitriding pure Fe under the same conditions as for the Fe-Me alloys considered. The surface nitrogen content dissolved in ferrite, $c_{N_\alpha}^S$, which is mobile nitrogen (i.e. taking part in diffusion process), can then be calculated from:

$$c^{S}_{N_\alpha} = [N]^{0}_{\alpha} + [N]_{strain} \tag{6.11}$$

The fitting parameters used are: X, D^{eff}_{N} and K_{MeN_n}. The value of f can be taken as constant (≈ 0.8) at the different nitriding temperatures, as shown in Ref. [2].

The presence of immobile excess nitrogen is recognised by replacing the stoichiometric parameter n in MeN_n by X=n+x, with x as the contribution of the immobile excess nitrogen. Using Eq. (6.2) it is possible to calculate at each time step the amount of nitrogen adsorbed at the precipitate/matrix interface, $[N]_{interface}$ (i.e. immobile excess nitrogen) at the depths where the condition $[Me_\alpha][N_\alpha]^n > K_{MeN_n}$ is satisfied. The complete scheme of calculating the nitrogen concentration–depth profile is shown in Fig. 6.1a. An example of the various contributions of mobile nitrogen and immobile nitrogen to the total nitrogen concentration-depth profile is shown in Fig. 6.1b for the nitrided Fe-2wt.%V alloy.

According to Eqs. (6.3)-(6.6) and (6.11), the amount of mobile nitrogen at the surface, $c^{S}_{N_\alpha}$, is a function of X and f. The influence of the parameters X and f on the nitrogen concentration-depth profile (see Figs. 6.2 and 6.3) can be explained as follows:

a. *Effect of X*: If the value of X increases, the *total* nitrogen content, c_N (Eq. (6.1)), at the surface increases in particular because the amount of adsorbed nitrogen increases especially (see Fig. 6.2). Increase of X means that not only the value of $[N]_{interface}$ (see Eq. (6.2)) but also that of $[N]_{strain}$ increases (see Eqs. (6.3)-(6.6)). Due to the moderate increase of $[N]_{strain}$ (which pertains to mobile nitrogen), there is a small increase in the nitriding depth with increase in X value (because of a larger nitrogen-concentration gradient: see Fig. 6.2).

b. *Effect of f*: If f increases from 0 to 1, there is an increase in particular of the surface nitrogen content dissolved in ferrite, $c^{S}_{N_\alpha}$ (Fig. 6.3). The pronounced increase in nitriding depth with increasing f is due to the significant increase of mobile nitrogen at the specimen surface.

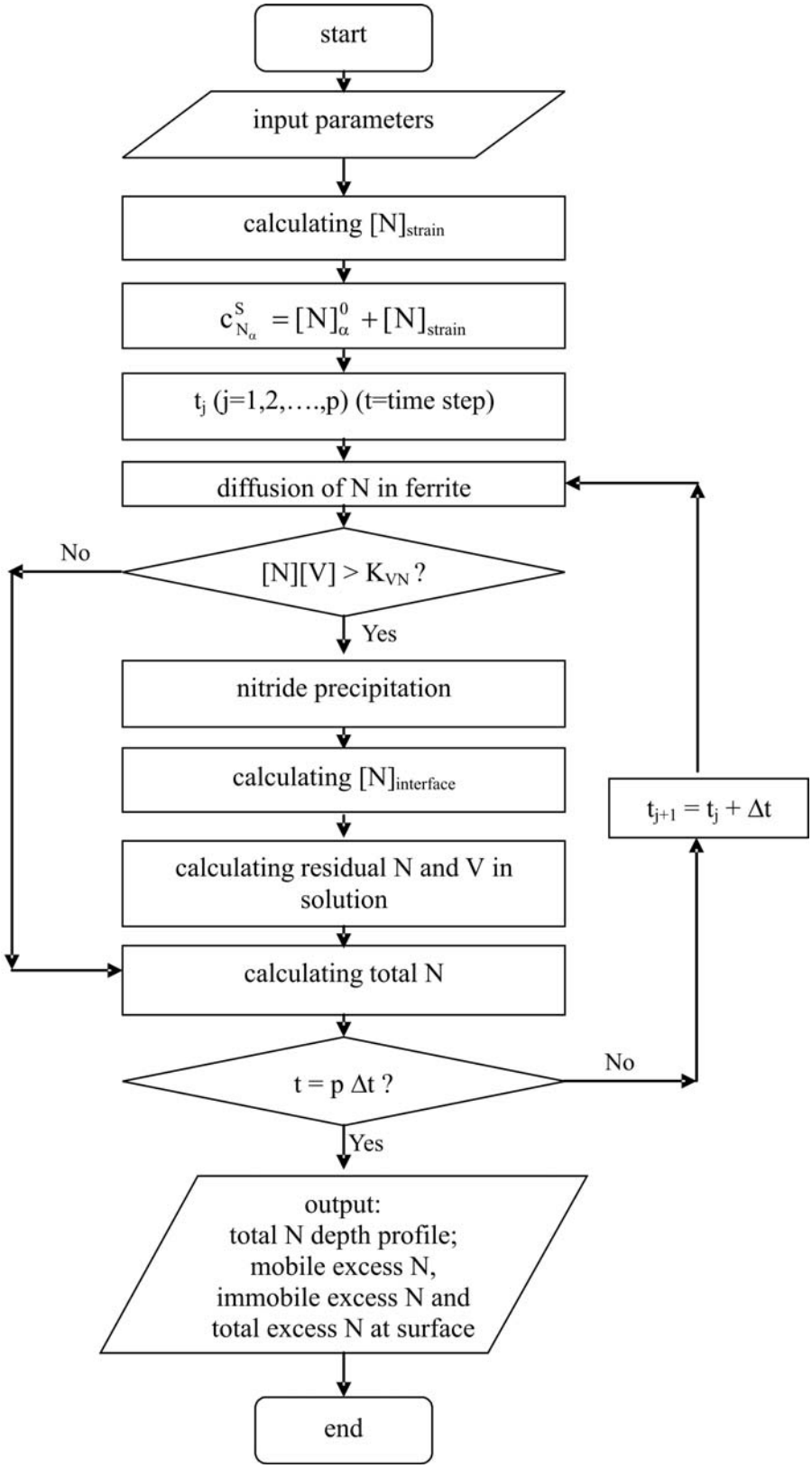

Fig. 6.1: (a) Flow chart showing the calculation of the nitrogen concentration-depth profile.

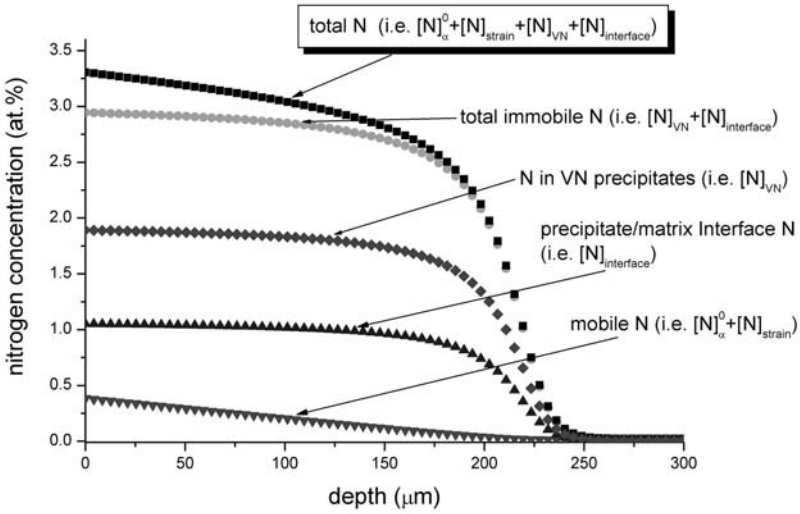

Fig. 6.1: (b) An example of the contributions of mobile and immobile nitrogen to the total nitrogen concentration-depth profile (profiles have been calculated using the algorithm indicated in Fig. 6.1a) for nitrided Fe-2wt.%V alloy nitrided at 520 ºC for 10h at a nitriding potential of 0.103 $atm^{-1/2}$.

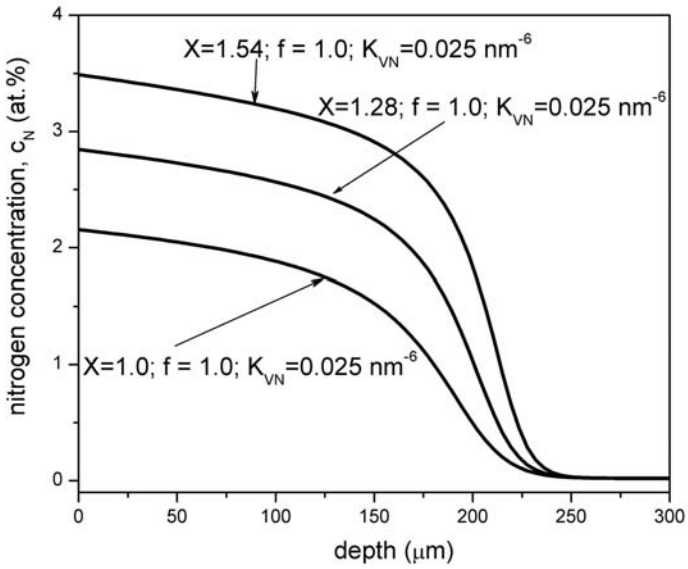

Fig. 6.2: The nitrogen concentration-depth profiles for different X values (keeping f, D_N^{eff} and K_{VN} constant) for Fe-2wt.%V specimens nitrided at 520 ºC for 10h at a nitriding potential of 0.103 $atm^{-1/2}$.

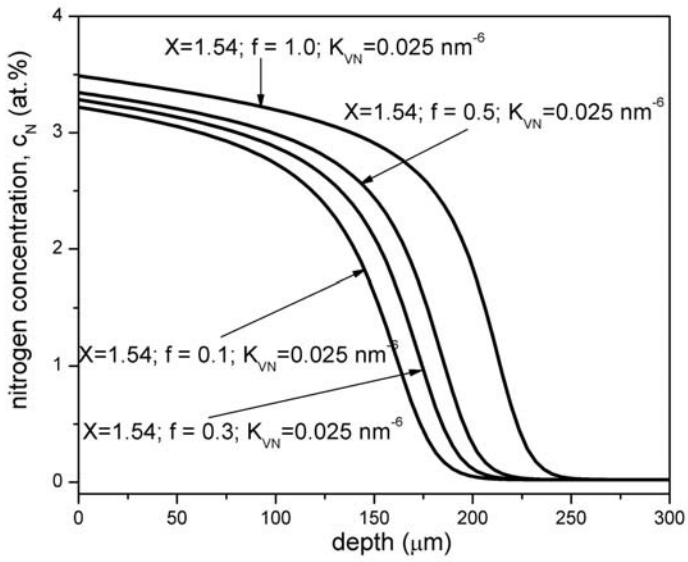

Fig. 6.3: The nitrogen concentration-depth profiles for different f values (keeping X, D_N^{eff} and K_{VN} constant) for Fe-2wt.%V specimens nitrided at 520 ºC for 10h at a nitriding potential of 0.103 $atm^{-1/2}$.

6.3 Experimental

6.3.1 Specimen preparation

Fe-2wt.%V alloys were prepared from pure Fe (99.98 wt.%) and pure V (99.80 wt. %) in a Al_2O_3 crucible in an inductive furnace under a protective argon atmosphere (99.999 vol. %). The amounts of vanadium and impurities like oxygen, nitrogen, carbon and sulphur in the produced alloys were determined by chemical analysis (inductive-coupled plasma-optic emission spectroscopy). The alloy compositions are shown in Table 6.1.

Table 6.1: Amounts of vanadium and light element impurities for the alloy used in this work.

Alloy	V (wt.%)	V (at.%)	O (μg/g)	N (μg/g)	C (μg/g)	S (μg/g)
Fe-2wt.%V	2.04 ± 0.05	2.23 ± 0.05	142 ± 10	< 6	6 ± 2	6 ± 3

After casting the Fe-2wt.%V alloys had a cylindrical shape with a diameter of 10 mm and a length of 100 mm. The cast alloys were cold rolled to sheets with a thickness of 1.0 mm. The obtained sheets were cut into rectangular pieces of lateral dimensions 1.5 x 1.5 cm^2. These pieces were annealed for 2h at 700 ºC (within the α-phase region of the Fe-V diagram) to obtain a recrystallized grain structure. After annealing the grains of the Fe-2wt.%V alloys had an average diameter of about 55 μm. Before nitriding the specimens were ground, polished (last step: 1μm diamond paste) and cleaned in an ultrasonic bath filled with ethanol.

6.3.2 Nitriding

One method to introduce nitrogen in a (ferritic) workpiece is by gaseous nitriding, involving that nitrogen, from dissociating NH_3 at temperatures in the range 450–600 ºC, enters the workpiece through its surface. Nitriding in NH_3/H_2 gas mixtures is equivalent to nitriding in N_2 at a pressure of a number of thousands atm (thermodynamic argument [21]) and is possible due to the slow thermal decomposition of NH_3 (kinetic argument [1]).

In this project the specimen to be nitrided was suspended at a quartz fibre in a vertical quartz tube of inner diameter 28 mm in the nitriding furnace. To start the nitriding process the specimen was placed in the middle of the nitriding furnace. The nitriding experiments were performed at different temperatures and times (Table 6.2) in an ammonia/hydrogen gas flux (purity: H_2: 99.999 vol. %; NH_3: >99.998 vol. %). The fluxes of both gases were adjusted with mass flow controllers and amounted to 455 ml/min hydrogen and 45 ml/min ammonia (i.e. the nitriding potential (= $\frac{p_{NH_3}}{p_{H_2}^{3/2}}$, with p as partial pressure [21]) equalled 0.103 $atm^{-1/2}$). Under these nitriding conditions no iron nitrides can be formed. Nitriding parameters used are shown in Table 6.2. At the end of the nitriding process, the specimens were quenched in water.

Table 6.2: Applied nitriding parameters (nitriding potential = 0.103 $atm^{-1/2}$).

Nitriding temperature =>	**520 ºC**	**550 ºC**	**580 ºC**	**600 ºC**
Nitriding time =>	10h	10h	10h	7h

6.3.3 Specimen characterization

6.3.3.1 Light microscopy

For light microscopical investigation, pieces were cut from the specimens and prepared to cross sections, by subsequent embedding (PolyFast, Buehler GmbH), polishing (last step: 1 µm diamond paste) and etching with 2.5% nital (2.5 vol.% HNO_3 in ethanol) for about 5 s. These cross sections were investigated with light optical microscopy applying a Leica DMRM microscope. The light micrographs were recorded with a digital camera (Jenoptik Progres 3008).

6.3.3.2 Hardness measurement

Hardness-depth profiles were obtained by carrying out hardness measurements across the cross-sections of the nitrided specimens using a Leitz Durimet hardness tester, applying a load of 100 g. The hardness values presented are average values of four measurements.

6.3.3.3 Electron probe microanalysis (EPMA)

To determine the composition of the nitrided zones of the samples after nitriding, EPMA was performed employing a Cameca SX100 instrument. Cross-sections of the nitrided alloys, similar to those as described above for light and scanning electron microscopy, were analyzed, but in this case no etching after polishing was applied. A focused electron beam at an accelerating voltage of 15 kV and a current of 100 nA was applied. To obtain the element contents in the specimens, the intensities of the characteristic Fe Kβ, V Kβ, N Kα, and O Kα X-ray emission peaks were determined at points along lines across the cross-sections (single measurement points at a distance of 2 or 3 μm). The intensities obtained from the nitrided specimens were divided by the intensities obtained from standard samples of pure Fe (Fe Kβ), pure V (V Kβ), andradite/$Ca_3Fe_2(SiO_4)_3$ (O Kα), and γ'-Fe_4N (N Kα). Concentration values were calculated from the intensity ratios applying the $\Phi(\rho z)$ approach according to Ref. [25].

6.4 Results and discussion

6.4.1 Morphology of the nitrided zone

The Fe-2wt.%V alloy shows only “continuous” precipitation of very fine nitride precipitates upon nitriding. A light optical micrograph of the etched cross-section of a Fe-2wt.%V specimen nitrided at 580 ºC for 10h at a nitriding potential of 0.103 $atm^{-1/2}$ is shown in Fig. 6.4a. The measured hardness-depth profile (Fig. 6.4b) reveals a constant (see also the hardness indentations within the nitrided zone in Fig. 6.4a), very high value for the hardness in the nitrided zone (1000-1050 HV0.1). For larger V contents discontinuous precipitation, a microstructure of VN/α-Fe lamellae, occurs upon nitriding (see Ref. [5] for detailed discussion).

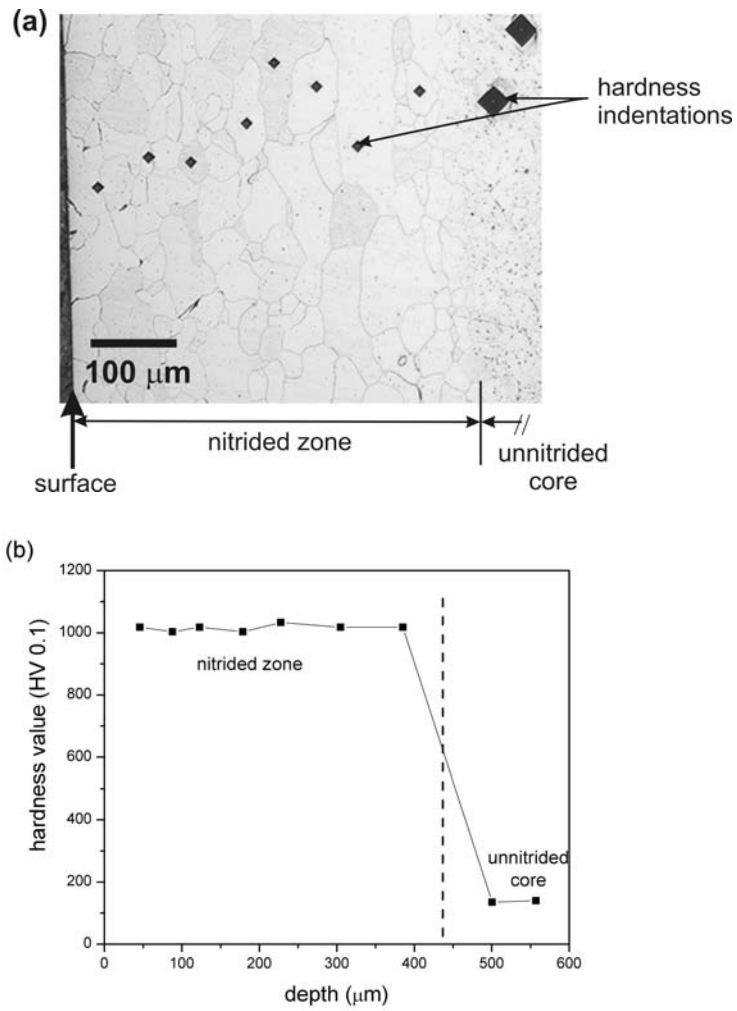

Fig. 6.4: (a) Light optical micrograph of the etched cross-section of the Fe-2wt.%V specimen (thickness of 1.0 mm) nitrided at 580 ºC for 10h at a nitriding potential of 0.103 $atm^{-1/2}$. Note the large difference in the size of the hardness indentations in the diffusion zone and in the unnitrided core. (b) Hardness-depth profile of the same specimen.

6.4.2 Nitrogen concentration-depth profiles: excess nitrogen

The nitrogen concentration-depth profiles, as determined by EPMA (section 6.3.3.3), for Fe-2wt.%V specimens nitrided at different temperatures and times at r_n = 0.103 $atm^{-1/2}$ are shown in Fig. 6.5. A gradual decrease of the nitrogen content from the surface to the interface with the unnitrided core can be observed. The horizontal lines in Fig. 6.5 indicate the "normal" capacity of nitrogen uptake, which consists of N in VN plus the amount of nitrogen dissolved in the unstrained ferrite matrix which is in equilibrium with the nitriding atmosphere at the given nitriding temperature (cf. section 6.2.1). The "normal" capacity of nitrogen uptake has been calculated recognizing that, indeed, 'pre-nitriding' → 'denitriding' experiments performed with thin (0.2 mm) Fe-2wt.%V specimens have shown that, about 2.00 at.% nitrogen is bound to V to form VN precipitates [2] and using data for the equilibrium

solubility of nitrogen in unstrained ferrite, $[N]_{\alpha}^{0}$, at 520, 550, 580 and 600 °C as measured separately in this project by performing nitriding experiments on thin (0.2 mm) pure Fe foils in NH_3/H_2 gas mixture having 0.103 $atm^{-1/2}$ nitriding potential (see Table 6.3). Comparing the actual amounts of absorbed nitrogen with the "normal" capacity for nitrogen uptake, it is evident that a significant amount of excess nitrogen is taken up by the Fe-2wt.%V alloy upon nitriding at different temperatures (see Fig. 6.5).

The experimental value of the surface nitrogen content in the ferrite matrix, $c_N^{s,exp}$ $(=[N]_{\alpha}^{0}+[N]_{strain}+[N]_{interface})$, for the Fe-2wt.%V specimens nitrided at the different nitriding temperatures has been determined from the EPMA results (obtained as average value from the (first) three data points closest to the surface) after subtracting the amount of nitrogen contained in the equilibrium VN (see Table 6.3). The difference between $c_N^{s,exp}$ and $[N]_{\alpha}^{0}$ then yields the amount of total "excess" nitrogen (Table 6.3). It should be recognized that, $c_N^{s,exp}$ incorporates both mobile and immobile excess nitrogen in addition to $[N]_{\alpha}^{0}$, and thus the value of $c_N^{s,exp}$ at the different nitriding temperatures not only varies because of changes in $[N]_{\alpha}^{0}$ but also because of changes in the contributions of mobile and immobile excess nitrogen (also see section 6.4.3). Therefore (although $[N]_{\alpha}^{0}$ increases monotonically with temperature; Table 6.3) one should not expect a monotonic increase of $c_N^{s,exp}$ with increasing temperature. For the present experiments it holds that the amount of total excess nitrogen is about the same at the different nitriding temperatures (Table 6.3).

Table 6.3: The experimental amount of nitrogen in the ferrite matrix at the surface, $c_N^{s,exp}$ (derived from the EPMA results after subtracting the amount of nitrogen contained in VN); the equilibrium solubility of nitrogen in stress-free ferrite, $[N]_\alpha^0$; and the total amount of excess nitrogen ($=c_N^{s,exp}$ - $[N]_\alpha^0$). Data pertain to Fe-2wt.%V specimens nitrided at the indicated temperatures at a nitriding potential of 0.103 $atm^{-1/2}$.

nitriding temperature (ºC) / time (h)	$c_N^{s,exp}$ **(from EPMA data) (at%)**	$[N]_\alpha^0$ **(experiments; from mass-increase) (at%)**	**total amount of excess nitrogen ($c_N^{s,exp}$ -$[N]_\alpha^0$) (at%)**
520 / 10	1.1	0.13	1.0
550 / 10	1.5	0.21	1.3
580 / 10	1.5	0.30	1.2
600 / 07	1.4	0.35	1.1

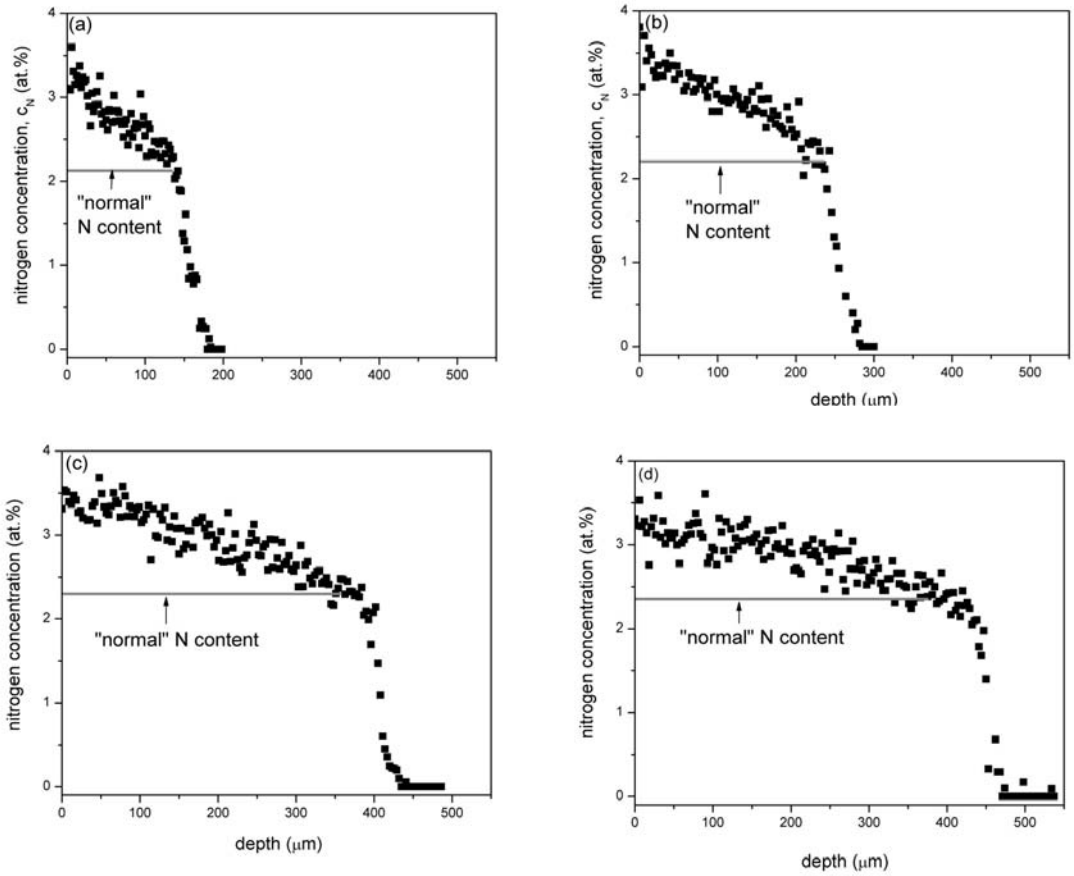

Fig. 6.5: Nitrogen concentration-depth profiles as measured with EPMA (black dots) for Fe-2wt.%V specimens nitrided at r_n = 0.103 $atm^{-1/2}$ at (a) 520 ºC for 10h; (b) 550 ºC for 10h; (c) 580 ºC for 10h and (d) 600 ºC for 7h. The horizontally drawn lines in these figures indicate the "normal" capacity for nitrogen uptake (see text).

6.4.3 Model fitting: the effect of temperature on excess nitrogen and nitrogen diffusivity

Nitrogen concentration-depth profiles, as calculated using the model as described in section 6.2, were fitted to the experimentally determined nitrogen concentration-depth profiles. In the model fitting X, D_N^{eff} and K_{VN} were the fit parameters.

Four nitrogen concentration-depth profiles were measured for each experiment at a specific nitriding temperature for a specific time (at r_n = 0.103 $atm^{-1/2}$). First, the nitrogen concentration-depth profiles were fitted individually. At constant temperature the solubility product K_{VN} should not depend on nitriding time, nitriding potential and vanadium content. Accordingly, at each nitriding temperature, the average values of K_{VN}, determined from the thus analysed four nitrogen concentration-depth profiles at each nitriding temperature are shown in Table 6.4. Secondly, using these values of K_{VN}, the definitive fittings at each nitriding temperature were performed, where only X and D_N^{eff} were the fit parameters. On this basis good fits were obtained. Examples of thus fitted nitrogen concentration-depth profiles are shown in Fig. 6.6. The results (averages of 4 data for each temperature) obtained for the nitride-particle composition parameter, X, and the effective diffusion coefficient of nitrogen in the ferrite matrix surrounding the VN precipitates, D_N^{eff}, have been gathered in Table 6.4. Finally, the values of the amounts of mobile excess nitrogen, immobile excess nitrogen and total excess nitrogen at the surface of the specimen have been gathered too in Table 6.4.

Table 6.4: Tabular presentation of the values obtained for the fit parameters: X, D_N^{eff} and K_{VN}. The resulting values of the amounts of mobile excess nitrogen at the surface ($[N]_{mob,exc}$), immobile excess nitrogen at the surface ($[N]_{imm,exc}$) and total excess nitrogen at the surface ($[N]_{total\ exc}$). Results pertain to Fe-2wt.%V specimens nitrided at the indicated temperatures and times at a nitriding potential of 0.103 $atm^{-1/2}$. See Table 6.6 for the literature values of the nitrogen diffusion coefficients for α-Fe at 520, 550 ºC, 580 and 600 ºC.

nitriding temperature (ºC) / time (h)	**X**	D_N^{eff} **($\times 10^{-11}$) ($m^2\ sec^{-1}$)**	**K_{VN} (nm^{-6})**	$[N]_{mob,exc}$ **(at.%)**	$[N]_{imm,exc}$ **(at.%)**	$[N]_{total\ exc}$ **(at.%)**
520 / 10	1.44	0.27	0.020	0.22	0.86	1.08
550 / 10	1.42	0.48	0.021	0.33	0.83	1.16
580 / 10	1.38	0.88	0.023	0.42	0.75	1.17
600 / 07	1.32	1.40	0.024	0.44	0.64	1.08

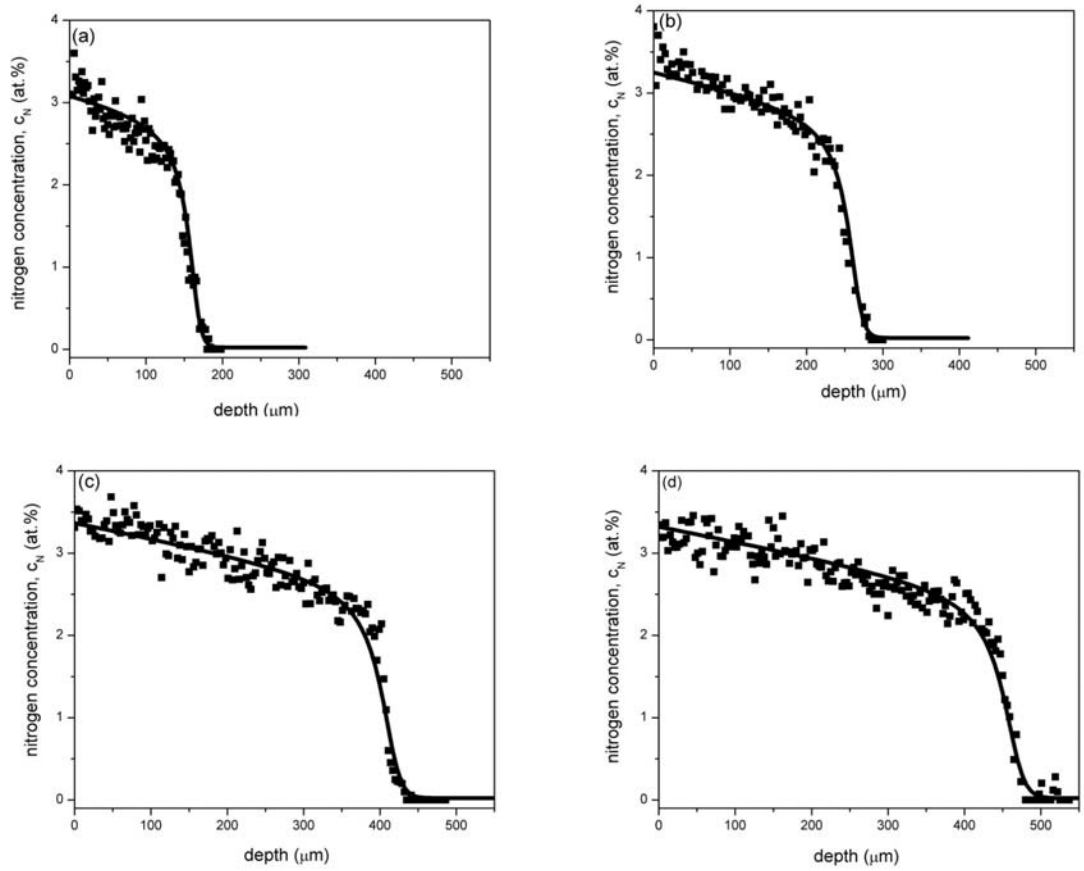

Fig. 6.6: Nitrogen concentration-depth profiles of nitrided Fe-2wt.%Cr specimens nitrided at r_n = 0.103 $atm^{-1/2}$, as measured with EPMA (black dots) and as calculated profiles (lines) by the model applying the parameters: (a) X = 1.44; D_N^{eff} = 0.27 × 10^{-11}; K_{VN} = 0.020 for 520 ºC for 10h. (b) X = 1.42; D_N^{eff} = 0.48 × 10^{-11}; K_{VN} = 0.021 for 550 ºC for 10h. (c) X = 1.38; D_N^{eff} = 0.88 × 10^{-11}; K_{VN} = 0.023 for 580 ºC for 10h. (d) X = 1.32; D_N^{eff} = 1.40 × 10^{-11}; K_{VN} = 0.024 for 600 ºC for 7h.

The value of X decreases with increasing nitriding temperature (Table 6.4). This phenomenon can be discussed as follows:

- The interaction between vanadium and nitrogen can be expressed by the interaction parameter, I [18],

$$I \equiv \frac{-\Delta G_{VN}}{W_{VN/\alpha-Fe}} \tag{6.12}$$

where ΔG_{VN} is the chemical Gibbs free energy for precipitation of VN and $W_{VN/\alpha-Fe}$ is the strain energy per unit volume of specimen introduced by a misfitting VN particle. A decrease in X can be due to a decrease in vanadium – nitrogen interaction. Indeed I becomes smaller for increasing temperature (ΔG_{VN} becomes less negative for increasing temperature [18]).

- At higher nitriding temperatures the vanadium-nitride platelets are coarser (i.e. a smaller precipitate/matrix interface area occur) than at lower nitriding temperatures. A smaller

nitride/matrix interfacial area implies a smaller capacity for adsorbed nitrogen and thus X decreases with increasing nitriding temperature.

The decrease of X with increasing nitriding temperature implies a decrease of $[N]_{interface}$ (cf. Eq. (2)), i.e. immobile excess nitrogen, $[N]_{imm,exc}$, decreases with increasing temperature (Table 6.4).

The value of X provides indirect information on the average thickness of the precipitate platelet. VN precipitates develop as plate-like, cubic (NaCl-type), precipitates along $\{001\}_{\alpha}$ matrix planes with $\{001\}_{\alpha\text{-Fe}}$ // $\{001\}_{VN}$ [14]. With $\{001\}_{VN}$ as the habit plane, the thickness of a monolayer of VN equals one half of the lattice parameter of the face-centred cubic (fcc) unit cell of VN, a_{VN}. Assuming that at every octahedral interstice in the ferrite matrix at the nitride/matrix interface one excess nitrogen atom is trapped, it follows:

$$X = \frac{n+2}{n}. \tag{6.13}$$

where n is the number of VN monolayers comprising the VN platelet. Accordingly, the thickness of the VN platelet is given by,

$$\text{thickness} = n \cdot \left(\frac{a_{VN}}{2}\right) = \frac{2}{(X-1)} \cdot \frac{a_{VN}}{2} \tag{6.14}$$

Such results, obtained with a_{VN} = 0.410 nm [26], have been gathered in Table 6.5. The thickness values obtained are compatible with thickness data obtained by direct analysis in the transmission electron microscope [14].

It is observed that the amount of mobile excess nitrogen, $[N]_{mob,exc}$ (= $[N]_{strain}$; cf. Eqs. (6.1) and (6.11)), increases distinctly with increasing nitriding temperature (Table 6.4). This is due to the increase in the thermodynamic capacity for dissolved nitrogen uptake by the strained matrix with increasing temperature (see also section 4.5 of Ref. [18]).

The effective diffusion coefficient of nitrogen for nitrided Fe-2wt.%V, D_N^{eff}, increases with temperature, as expected (see Table 6.4). The usual temperature dependence for the diffusion coefficient (D) reads:

$$D = D_0 \cdot \exp\left(\frac{-Q}{RT}\right) \tag{6.15}$$

where D_0 is pre-exponential factor; Q is the activation energy for diffusion and R is the universal gas constant (=1.9872 cal mol^{-1} K^{-1}). An Arrhenius plot (ln D vs. 1/T) for the obtained values for the nitrogen diffusion coefficient is shown in Fig. 6.7. The straight line fitted to the data can be given as:

$$D_N^{eff} = (1.4 \times 10^{-4}) \cdot \exp\left(\frac{-28.1}{RT}\right) \qquad m^2\ sec^{-1} \qquad (6.16)$$

where $D_0 = 1.4 \times 10^{-4}$ m^2 sec^{-1} and Q = 28.1 kcal mol^{-1}. The Arrhenius plot for the diffusion coefficient according to literature data for diffusion of nitrogen in pure ferrite [27] is also shown in Fig. 6.7 (dashed line). It is seen that there is a small difference (especially, at lower temperatures) between the obtained values for the diffusion coefficient of nitrogen in the ferrite matrix for the Fe-2wt.%V alloy as compared to the values for pure Fe (see Fig. 6.7 and Table 6.6). The difference can be discussed as follows.

Occurrence of a labyrinth factor, due to the presence of nitride particles as obstacles for nitrogen diffusion in the ferrite matrix (cf. section 6.2.2), should lead to a smaller value for the nitrogen diffusion coefficient, in accordance with the experimental observation. The reduction of the diffusion coefficient is relatively strong at the lower nitriding temperatures. This may be related to a more homogeneous nitride distribution (more finely dispersed), as the nitride particles are distinctly smaller at the lower nitriding temperatures (see also the above discussion of the X values).

Alternatively, inwardly diffusing nitrogen could be successively "trapped, de-trapped and re-trapped" etc., in Fe-V-N configurations [28], in particular in the transition region where not all V has already been precipitated as nitride. This leads to a reduction of the effective nitrogen diffusion coefficient, especially, given a constant number of trapping possibilities, at relatively low nitrogen concentrations (cf. Ref. [28]).

Both effects discussed above lead to a relatively strong reduction of the nitrogen diffusion coefficient at the lower nitriding temperatures. Consequently, the effective activation energy observed for D_N^{eff} (28.1 kcal mol^{-1}) is larger than the activation energy for D_N in pure α-Fe (18.6 kcal mol^{-1}) [27].

Table 6.5: The value of X in VN_X and the estimated average thickness of VN platelets (calculated using Eq. (6.14)) for specimens nitrided at different temperatures.

nitriding temperature (ºC)	X	Average thickness of VN precipitates (see Eq. (6.14)) (nm)
520	1.44	0.9
550	1.42	1.0
580	1.38	1.1
600	1.32	1.3

Table 6.6: The effective diffusion coefficient of nitrogen for nitrided Fe-2wt.%V, D_N^{eff} (obtained from the model fitting: cf. Table 6.4), and the diffusion coefficient of nitrogen in pure α-Fe, D_N (from literature data: Ref. [27]).

nitriding temperature (°C)	D_N^{eff} **(×10^{-11}) (from model fitting) (m^2 sec^{-1})**	D_N **(×10^{-11}) (from literature)** (m^2 sec^{-1})	$\frac{D_N^{eff}}{D_N}$
520	0.27	0.49	0.55
550	0.48	0.76	0.63
580	0.88	1.13	0.78
600	1.40	1.46	0.96

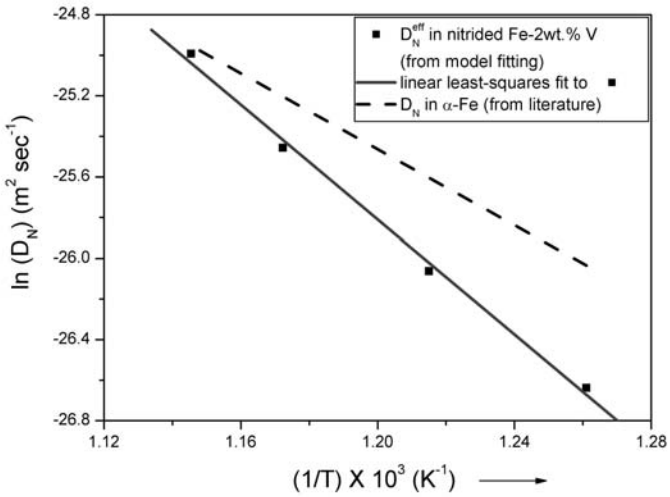

Fig. 6.7: Arrhenius plot for the diffusion coefficient of nitrogen in ferrite. Square dots represents the nitrogen diffusion coefficient values obtained from model fitting to EPMA nitrogen concentration-depth profiles measured at different nitriding temperatures for Fe-2wt.%V. The solid line is linear least-squares fit to these model-fit data. The dashed line indicates the Arrhenius plot for the diffusion coefficient of nitrogen in pure α-Fe as calculated from literature data (Ref. [27]).

6.5 Conclusions

The development of the nitrogen concentration-depth profile in Fe-2wt.%V alloy upon nitriding can be successfully modeled provided the occurrence of both *mobile* and *immobile* excess nitrogen is accounted for.

The model can be fitted to experimentally determined nitrogen concentration-depth profiles occurring in nitrided Fe-Me alloys employing three fit parameters: the composition parameter of the nitride, X, (recognizing the presence of nitrogen adsorbed at the nitride/matrix interface), the misfit parameter, f, and the solubility product, K. Whereas X

largely controls the overall nitrogen level in the nitrided zone, f > 0 significantly increases the nitriding depth and K influences the steepness of the nitrided zone / unnitrided core transition.

The value of X decreases with increasing temperature, reflecting a coarsening of the nitride precipitates with increasing temperature and, possibly, a decrease of the vanadium – nitrogen interaction with increasing temperature.

The diffusion coefficient of nitrogen in the ferrite matrix of nitrided Fe-2wt.%V alloy is somewhat smaller than the diffusion coefficient of nitrogen in pure α-Fe, in particular at lower nitriding temperatures, reflecting the finer dispersion of nitride precipitates at lower nitriding temperatures and/or the trapping of nitrogen in Fe-V-N configurations, in particular in the transition region where not all vanadium has already been precipitated as nitride, which is relatively most pronounced for lower (dissolved) nitrogen contents as occurring at lower temperatures.

References

[1] Mittemeijer EJ, Somers MAJ. Surface Engineering 1997;13:483.

[2] Hosmani SS, Schacherl RE, Mittemeijer EJ. Acta Materialia; 2006;54:2783. (Chapter 5).

[3] Schacherl RE, Graat PCJ, Mittemeijer EJ. Metall Mater Trans A 2004;35:3387.

[4] Biglari MH, Brakman CM, Mittemeijer EJ, van der Zwaag S. Phil Mag A 1995;72:931.

[5] Hosmani SS, Schacherl RE, Mittemeijer EJ. Acta Materialia 2005;53:2069. (Chapter 4).

[6] Hekker PM, Rozendaal HCF, Mittemeijer EJ. Journal of Materials Science 1985;20:718.

[7] Lightfoot BJ, Jack DH. Proceedings on the Conference on Heat Treatment 1973, The metals society, London 1975, pp. 59-65.

[8] Alves C, de Anchieta Rodrigues J, Eduardo Martinelli A. Mater. Sci Eng 2000;279:10.

[9] Philipps VA, Seybolt AU. Trans Metall Soc AIME 1968;242:2415.

[10] Pope M, Grieveson P, Jack KH. Scandinavian Journal of Metallurgy 1973;2:29.

[11] Welch WD, Carpenter SH. Acta Metall 1973;21:1169.

[12] Krawitz A. Scripta Metall 1977;11:117.

[13] Yang MM, Krawitz AD. Metall Trans A 1984;15:1545.

[14] Bor TC, Kempen ATW, Tichelaar FD, Mittemeijer EJ, van der Giessen E. Phil Mag A 2002;82:971.

[15] Djeghlal ME, Barrallier L. Ann Chim Sci Mat 2003;28:43.

[16] Gouné M, Belmonte T, Redjaimia A, Weisbecker P, Fiorani JM, Michel H. Materials Science and Engineering A 2003;351:23.

[17] Podgurski HH, Davis FN. Acta Metall 1981;29: 1.

[18] Somers MAJ, Lankreijer RM, Mittemeijer EJ. Phil Mag A 1989;59:353.

[19] Biglari MH, Brakman CM, Mittemeijer EJ. Phil Mag A 1995;72:1281.

[20] Biglari MH, Brakman CM, Somers MAJ, Sloof WG, Mittemeijer EJ. Z Metallkd 1993;84:124.

[21] Mittemeijer EJ, Slycke JT. Surface Engineering 1996;12:152.

[22] Grossman JC, Mizel A, Côté M, Cohen ML, Louie SG. Physical Review B 1999;60:6343.

[23] Engström A, Höglund L, Ågren J. Metall Mater Trans A 1994;25:1127.

[24] Garzón CM, Tschiptschin AP. Materials Science and Technology 2004;20:915.

[25] Pouchau JL, Pichoir F. La Recherche Aérospatial 1984;3:167-92.

[26] Pearson WB. A Handbook of Lattice Spacings and Structures of Metals, vol.2. London: Pergamon Press, 1968.

[27] Fast JD, Verrijp MB. Journal of the Iron and Steel Institute 1954;176:24.

[28] Kamminga JD, Klaver TPC, Nakata K, Thijsse BJ, Janssen GCAM. J. Computer-Aided Materials Design 2003;10:1.

Chapter 7

Zusammenfassung

7.1 Einleitung

Zur Optimierung von Ermüdungs-, Korrosions- und Verschleiß-Eigenschaft ist Nitrien das am weitesten verbreitete Verfahren. Während des Nitrierprozesses wird Stickstoff in die zu behandelnde Randschicht eines Bauteiles eingebracht. Eine Methode zur Aufstickung von Randschichten ist das Gasnitrieren. Dabei wird das zu behandelnde Bauteil in einer Gasatmosphäre, welche sich aus Ammoniak und Wasserstoff zusammensetzt, bei Temperaturen zwischen 450°C und 600°C ausgelagert. In Gegenwart von nitridbildenden Legierungselementen, wie beispielsweise Ti, Al, V und / oder Chrom, kann es zur Bildung von inneren Nitriden während des Nitrierprozesses kommen. Die Gegenwart von inneren Nitriden in einer Nitrierschicht ist mit einer deutlichen Zunahme der Härte verbunden. Das Ausmaß der Härtesteigerung hängt im Wesentlichen von der chemischen Zusammensetzung, der Kohärenz, der Größe sowie der Morphologie der Ausscheidungen ab.

Parallel zur ausscheidungsbedingten Härtesteigerung tritt eine deutlich erhöhte Stickstoffaufnahme auf. Die Differenz zwischen erwartungsgemäßer Stickstoffaufnahme (Stickstoff gelöst in Reineisen + Stickstoff gebunden in inneren Nitriden) und tatsächlicher Aufnahme wird als Überschussstickstoff bezeichnet. Überschussstickstoff kann, hinsichtlich der Wachstumskinetik von nitrierten Schichten, in mobilen und immobilen Stickstoff unterteilt werden. Mobiler Überschussstickstoff ist auf den Oktaederlücken des Ferrit Gitters gelöst (ist beweglich und kann zum weiteren Wachstum der Nitrierschicht beitragen), während immobiler Überschussstickstoff (ist nicht beweglich und kann somit nicht zum Wachstum der Nitrierschicht beitragen) an der Grenzfläche inneres Nitrid / Ferrit Matrix adsorbiert ist.

In dieser Dissertation werden schwerpunktmäßig Phasenumwandlungen in Nitrierschichten und die damit verbundenen Einflüsse auf die Wachstumskinetik untersucht.

7.2 Experimentelles

Fe-Cr und Fe-V Legierungen wurden aus reinem Fe (99,98 Gew.%), reinem Cr (99,999 Gew. %) und V (99,98 Gew.%) in einem Induktionsofen unter einer Ar Schutzatmosphäre hergestellt.

Nach dem Abgießen wurden die Legierungen zu Blechen mit einer Dicke von ca. 1 bzw. 0.2 mm gewalzt. Anschließend wurden die Bleche in rechteckige Probenstücke geschnitten und unter Schutzgas (Argon mit einer Reinheit von 99.999 vol. %) bei 700°C für ca. zwei Stunden rekristallisiert.

Vor dem Nitrieren wurden die Proben geschliffen, poliert (letzte Stufe 1µm) und im Ultraschallbad gereinigt. Das Nitrieren wurde in einem vertikal angeordneten Mehrzonenofen unter einem Ammoniak/Wasserstoff Gasstrom durchgeführt. Die Stickstoffaufnahme an der Probenoberfläche hängt vom Ammoniakanteil in der Nitrieratmosphäre ab. Der Ammoniakanteil kann über das Verhältnis der Strömungsgeschwindigkeiten von Ammoniak und Wasserstoff geregelt werden. Die Regelung der Gasströme erfolgt durch „Mass Flow – Controler“. Am Ende der Nitrierung wurden die Proben in Wasser abgeschreckt.

Die Mikrostruktur der nitrierten Schichten wurde durch Licht-, Elektronen-Mikroskopie, Härtemessungen und Röntgendiffraktometrie untersucht. Die Zusammensetzung der Nitrierschichten wurden mittels Elektronenstrahlmikroanalyse bestimmt.

7.3 Ergebnisse und Diskussion

7.3.1 Mikrostruktur der Nitrierschicht

Bei der Nitrierung von Fe-Cr und Fe-V Legierungen scheiden sich innere Nitride in der Nitrierschicht aus. Im Anfangsstadium weisen diese Nitride eine kohärente oder teilkohärente Grenzflächen zur umgebenden Ferrit Matrix auf. Bei fortschreitender Nitrierdauer tritt eine Vergröberung der ausgeschiedenen Nitride auf. Dabei können zwei Vergröberungsmechanismen unterschieden werden (i) Wachstum der Nitride kombiniert mit dem Verlust der Kohärenz zur Matrix (ii) diskontinuierliche Vergröberung, bei welcher die feinen Nitridausscheidungen durch eine lamellare Morphologie, bestehend aus Nitrid und Ferrit Lamellen, ersetzt werden. Nitrierschichten von Fe-7Gew.%Cr Proben weisen im Oberflächennahen Bereich diskontinuierlich vergröberte Nitridausscheidungen auf, im Bereich darunter herschen feine, kohärente Nitridausscheidungen vor. Erstmalig konnten beide Ausscheidungsformen auch in den Nitrierschichten von Fe-4Gew.%V Legierungen gezeigt werden. Triebkraft der diskontinuierlichen Vergröberung ist (i) sowohl die Verringerung der Fehlpassung zwischen Ausscheidung und umgebender Matrix, (ii) die damit verbundenen Spannungsfelder, sowie (iii)die Reduktion der Grenzfläche Ausscheidung / Matrix. Der diskontinuierliche Vergröberungsmechanismus kann im Allgemeinen wie folgt beschrieben werden:

$$\alpha^{|} + \beta^{|} \rightarrow \alpha + \beta \qquad (7.1)$$

$\beta^{|}$ bezeichnet hier die Nitrid-Ausscheidungen in der übersättigten Ferrit Matrix $\alpha^{|}$. Beim Ablauf der Vergröberungsreaktion werden die submikroskopischen Ausscheidungen durch eine relativ grobe lamellenförmige Ausscheidungsform ersetzt ($\beta^{|} \rightarrow \beta$). Dabei wird die Übersättigung in der Eisenmatrix eliminiert ($\alpha^{|} \rightarrow \alpha$). Die dabei entstehende lamellare Struktur kann durch Anätzen von Querschliffen sichtbar gemacht werden (siehe dunkle Bereiche in den Bildern 7.1 bis 7.3).

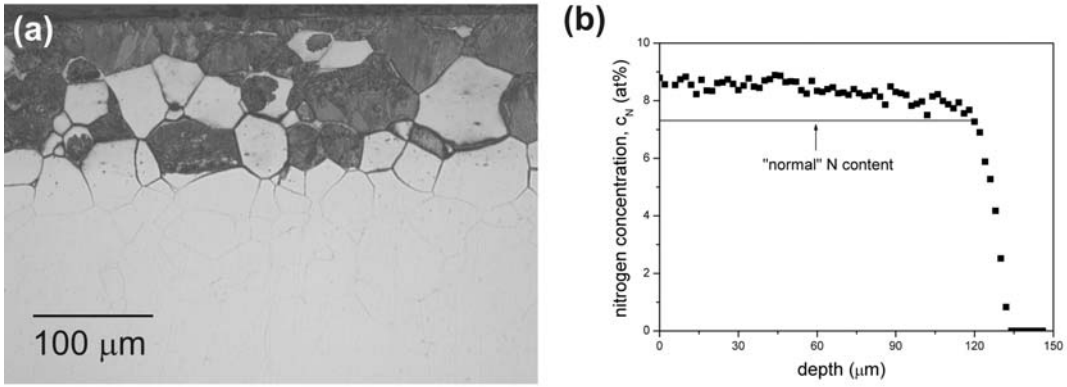

Bild 7.1: (a) Lichtmikroskopische Aufnahme eines geätzten Querschliffs einer Fe-7Gew. % Cr Probe, nitriert bei 580°C für 4h (r_n=0.16 atm$^{1/2}$). (b) Stickstoff Konzentrationstiefenprofil der in Abbildung (a) gezeigten Probe. Die horizontale graue Linie kennzeichnet die „normale“ Stickstoffaufnahme.

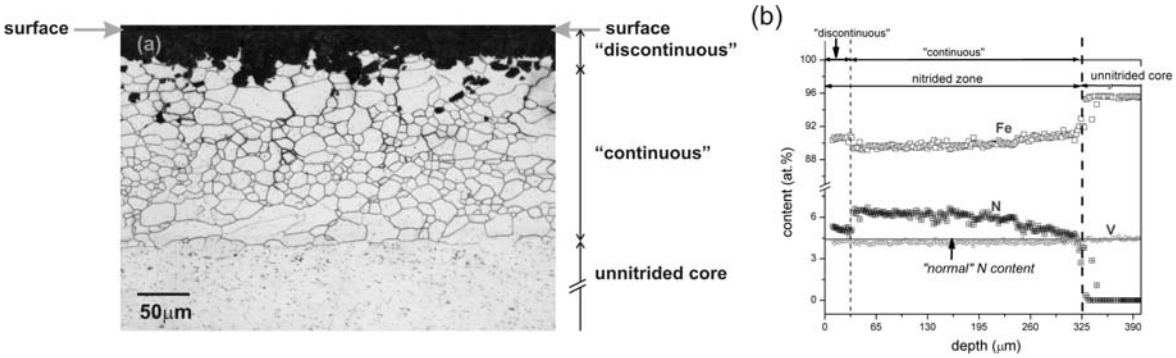

Bild 7.2: (a) Lichtmikroskopische Aufnahmen eines geätzten Querschliffs einer Fe-4Gew. % V Probe, nitriert bei 580°C für 10h (r_n=0.16 atm$^{1/2}$). (b) Konzentrationstiefenprofil (N, V, Fe) der in Abbildung (a) gezeigten Probe. Die horizontale graue Linie kennzeichnet die „normale“ Stickstoffaufnahme.

Die Nitrierschichten der Fe-7 Gew.%Cr und Fe-4 Gew.%V Legierungen setzen sich aus 2 Zonen zusammen. Zone I enthält zum größten Teil eine diskontinuierlich vergröberte Ausscheidungsstruktur und befindet sich direkt unterhalb der Probenoberfläche. Zone II enthält im wesentlichen submikroskopisch kohärente / teilkohärente Nitridausscheidungen (siehe Bild 7.1 und 7.2). Die Härte der diskontinuierlich vergröberten Bereiche ist im

Vergleich zu den Bereichen mit submikroskopischen Ausscheidungen deutlich geringer (siehe Bild 7.3). Dieser Unterschied bei der Härte kann auf den Verlust der Kohärenz während der Vergröberung zurückgeführt werden.

Die Triebkraft der diskontinuierlichen Vergröberung weist eine Abhängigkeit bezüglich der Konzentration des nitridbildenden Elementes auf. Die Nitrierschicht einer bei 580°C nitrierten Fe-2Gew.%V Legierung weist keinerlei diskontinuierlicher Vergröberung auf (die gesamte Schicht besteht aus hellen Körnern (siehe Bild 7.4)). Die Triebkraft zur Initiierung einer diskontinuierlichen Vergröberung ist bei dieser Legierungszusammensetzung offensichtlich zu gering.

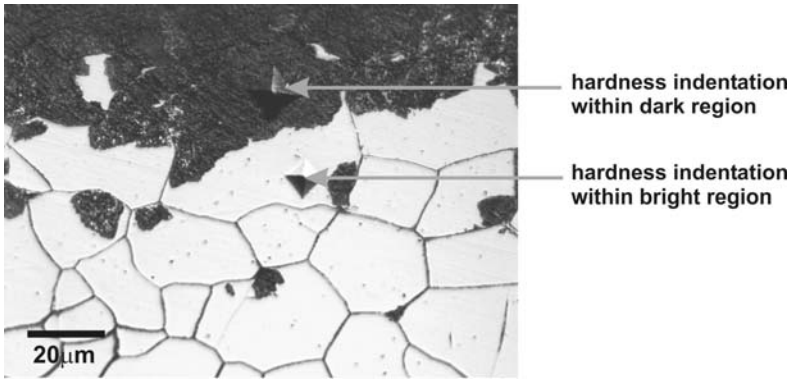

Bild 7.3: Lichtmikroskopische Aufnahme zweier Härteeindrücke im gleichen Korn (eingebracht mit dem gleichen Gewicht), mit diskontinuierlich vergröberten Ausscheidungen und submikroskopischen Ausscheidungen einer nitrierten Fe-4Gew.%Cr Legierung. Der Härteeindruck im dunkleren Bereich (diskontinuierlich vergröbert) ist deutlich größer im Vergleich zum Härteeindruck im hellen Bereich.

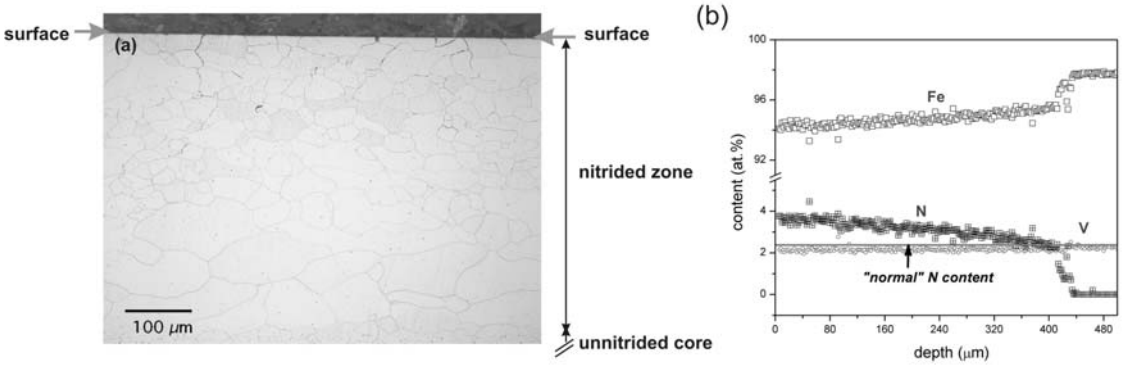

Bild 7.4: (a) Lichtmikroskopische Aufnahmen eines geätzten Querschliffs einer Fe-2Gew. % V Probe, nitriert bei 580°C für 10h (r_n=0.16 $atm^{1/2}$. (b) Konzentrationstiefenprofil (N, V, Fe) der in Abbildung (a) gezeigten Probe. Die horizontale graue Linie kennzeichnet die „normale“ Stickstoffaufnahme.

Die Aufnahme von Überschussstickstoff konnte sowohl in den Nitrierschichten der Fe-V als auch der Fe-Cr Legierungen beobachtet werden (siehe Bilder 7.1b, 7.2b und 7.4b). Im Gegensatz zu den Nitrierschichten der Fe-Cr Legierungen, hängt die Menge des Überschussstickstoffes, im Falle der Fe-V Legierungen von der Ausscheidungsform (lamellar

oder submikroskopisch) ab (siehe Bild 7.1b im Vergleich zu 7.2b). Im Falle der nitrierten Fe-V Legierungen weisen diskontinuierlich vergröberte Bereiche eine geringere Überschussstickstoffaufnahme auf (Bild 7.2b).

Bei hinreichend hohen Ammoniak Konzentrationen in der Nitrieratmosphäre können sich Eisennitride an der Probenoberfläche bilden. Ist die Ammoniak Konzentration ausreichend um dass stickstoffreiche ε-Eisennitrid zu bilden entsteht an der Probenoberfläche eine sogenannte Verbindungsschicht mit ε-Eisennitrid an der Oberfläche, gefolgt vom Stickstoffärmeren γ'-Eisennitrid. Unterhalb der Verbindungsschicht schließt sich die sogenannte Diffusionszone an, bestehend aus Ferrit mit gelöstem Stickstoff.

Fe-Cr Legierungen mit 7 Gew. % Cr wurden so nitriert, dass sich eine ε-Nitrid Schicht an der Oberfläche bilden konnte. Die Verbindungsschicht wurde mittels Röntgendiffraktometrie, Lichtmikroskopie, und Elektronenstrahlmikroanalyse untersucht. Zum ersten Mal konnte in einer Verbindungsschicht einer Fe-Cr Legierung die Präsens von CrN festgestellt werden. Auf Basis der gewonnen Resultate kann für die Nitrierschichtbildung auf den folgenden Mechanismus geschlossen werden: Die Eindiffusion des Stickstoffs geschieht durch Volumendiffusion. Während der Aufstickung bilden sich zunächst innere Chromnitride aus. Dies geschieht überwiegend an den Korngrenzen, da hier die Keimbildung schneller ablaufen kann. Wird die Löslichkeitsgrenze für Stickstoff in Ferrit im Bereich der Ausscheidungen überschritten, bildet sich die Stickstoffreichere γ' Phase. Die Phasenumwandlung Ferrit → γ' beginnt daher an der Korngrenze und schreitet in Richtung Kornmitte fort.

7.3.2 Überschussstickstoff; Absorptionsisothermen

Stickstoff in der Nitirierschicht einer Fe-Cr oder einer Fe-V Legierung kann in 3 Kategorien unterschieden werden: (i) Stickstoff in stöchiometrischem Cr- bzw. V- Nitrid (Typ I), (ii) Stickstoff adsorbiert an der Grenzfläche Nitrid / Ferrit Matrix (Typ II), (iii) Stickstoff gelöst auf den Zwischengitterplätzen der Ferrit Matrix (Typ III). Um die jeweiligen Anteile der Stickstoff Kategorien zu bestimmen wurden für das System Fe-V Stickstoffabsorptionsisotherme bestimmt. Bild 7.5 zeigt die Stickstoffabsorptionsisotherme bei einer Nitriertemperatur von 540°C für Fe-V und Reineisen. Der Stickstoffanteil, welcher in Bild 7.5 mit A gekennzeichnet ist, repräsentiert den Anteil im stöchiometrischen Vanadiumnitrid VN. Durch Extrapolation des linearen Verlaufes der Absorptionsisotherme erhält man auf der Y-Achse die mit B gekennzeichnete Stickstoffkonzentration. Diese Konzentration repräsentiert den Stickstoffanteil, welcher auf den Zwischengitterplätzen gelöst

ist (Typ III). Aus der Differenz B-A kann die Menge des Stickstoffs, adsorbiert an der Grenzfläche Nitrid / Matrix, bestimmt werden. Es konnte gezeigt werden, dass 30% der Stickstoffkonzentration im Nitrid VN, in Form von Überschussstickstoff an der Grenzfläche Nitrid / Matrix vorliegen (Typ II). Auf den Zwischengitterplätzen gelöster Überschussstickstoff, kann auf die Aufweitung der Eisenmatrix, verursacht durch die Fehlpassung der kohärent ausgeschiedenen Vanadiumnitrid Partickel, zurückgeführt werden. Die Menge des zusätzlich gelösten Stickstoffes des Typs III beträt 50%, bezüglich des Lösungsvermögens einer Reineisenmatrix, bei gleichen Nitrierbedingungen.

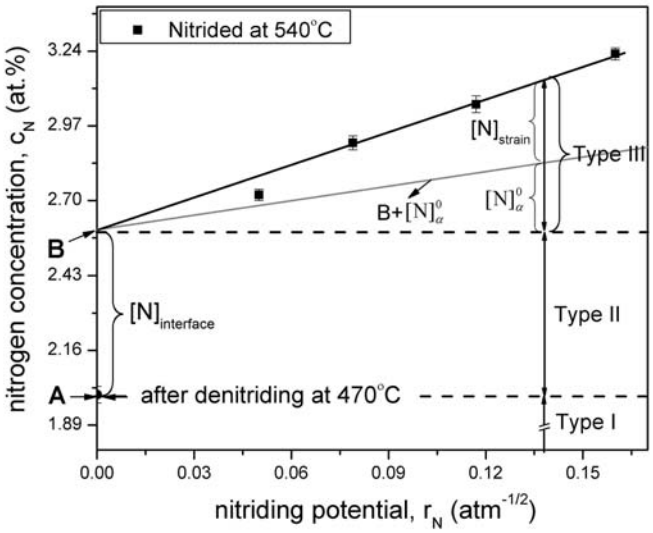

Bild 7.5: Stickstoffabsorbtionsisotherme ermittelt für eine Nitriertemperatur von 540°C.

7.3.3 Wachstumskinetik nitrierter Schichten

Zur Berechnung von Stickstoffkonzentrationsprofilen wurde ein neues Model entwickelt, welches die Präsenz von mobilem und immobilem Stickstoff in der Nitrierschicht von Fe-V bzw. Fe-Cr Legierungen berücksichtigt. Mobiler und immobiler Überschussstickstoff wird durch die Stickstofflöslichkeit in der Ferrit Matrix an der Probenoberfläche, sowie durch die Faktoren X und f im Model berücksichtigt. Der Faktor X beschreibt den Mengenanteil des an der Grenzfläche adsorbierten Stickstoffes, wohingegen f die Fehlpassung zwischen ausgeschiedenen Nitriden und der Ferrit Matrix angibt. Die Profilform im Übergangsbereich der nitrierten Schicht zum nicht nitrierten Bereich wird durch das Gleichgewichtslöslichkeitsprodukt K beschrieben. Durch Variation der Parameter X, f und K können berechnete Profile an experimentell bestimmte Stickstofftiefenprofile angepasst

werden. Der Einfluss der Parameter auf die Stickstofftiefenprofile ist in Abbildung 7.6 (Betrachtung von mobilem und immobilem Überschussstickstoff), Abbildung 7.7 und 7.8 dargestellt. Größere X Werte simulieren eine höhere Stickstoffkonzentration in der Grenzfläche Nitrid / Matrix, und damit verknüpft auch eine erhöhte Stickstoffaufnahme in der Nitrid umgebenden Ferrit Matrix. Die erhöhte Stickstoffaufnahme in der Ferrit Matrix kann auf die stärkere Aufweitung der Matrix durch die zusätzlich gelösten Grenzflächenstickstoffatome zurückgeführt werden. Beide Effekte resultieren in einer erhöhten Gesamtstickstoffaufnahme sowie einer etwas größeren Eindringtiefe des Stickstoffes. Die Erhöhung der f Werte führen zu einer größeren Stickstoffaufnahmekapazität auf den Zwischengitterplätzen der Ferrit Matrix. Durch die erhöhte Löslichkeit für Stickstoff in der Ferrit Matrix ergibt sich ein größerer Stickstoffkonzentrationsgradient für mobilen Stickstoff (gelöst auf den Oktaederlücken der Matrix). Dadurch erhöht sich die Nitriertiefe und somit die Dicke der Nitrierschicht.

Die MeN_n Ausscheidungen könnten Barrieren für den eindiffundierenden Stickstoff darstellen. Um diesen Effekt zu berücksichtigen kann ein Faktor für den Diffusionskoeffizienten von Stickstoff in Ferrit eingeführt werden. Dieser sogenannte Labyrinth Faktor hängt von der Form, der Größe und dem Volumenanteil der MeN_n Ausscheidungen ab.

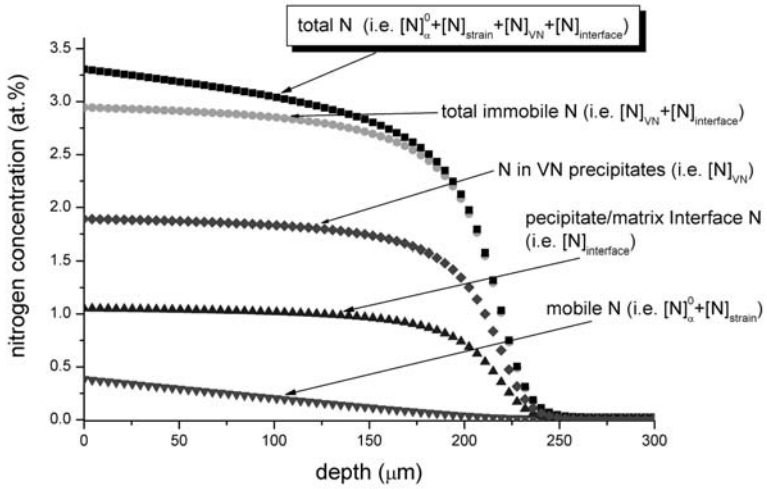

Bild 7.6: Beispiele für den Einfluss der Präsens von mobilem und immobilem Überschussstickstoff auf das Stickstofftiefenprofil einer nitrtierten Fe-2Gew.%V Legierung (nitriert bei 520°C für 10h; r_n= 0.103 $atm^{-1/2}$).

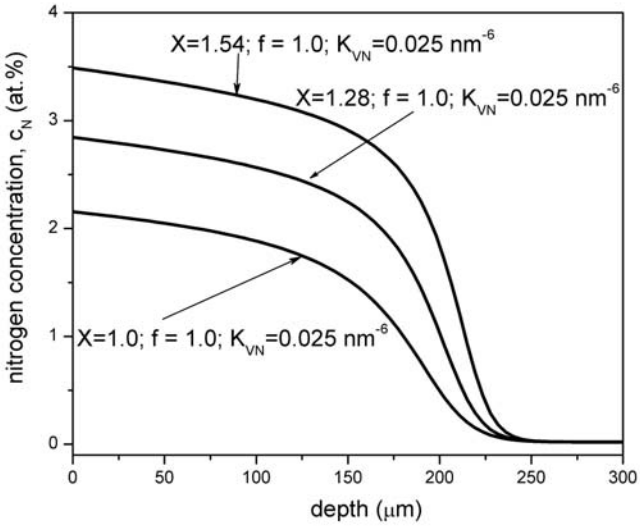

Bild 7.7: Einfluss des Parameters X (f, D und K sind konstant) auf das Stickstoffkonzentrationstiefenprofil einer Fe-2Gew.%V nitriert bei 520°C für 10h; r_n=0.103 $atm^{-1/2}$.

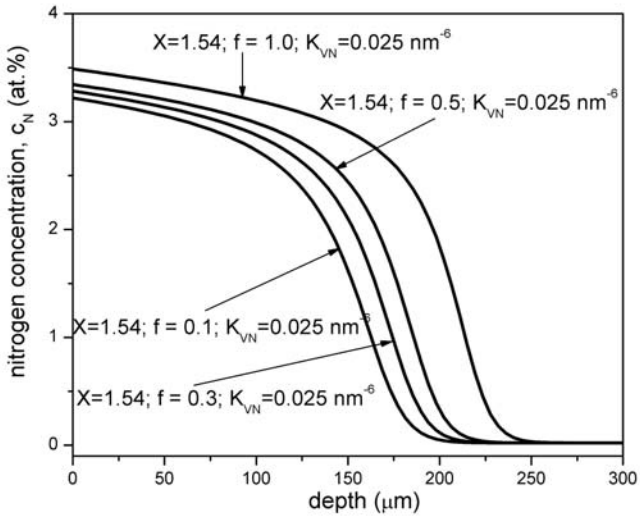

Bild 7.8: Einfluss des Parameters f (X, D und K sind konstant) auf das Stickstoffkonzentrationstiefenprofil einer Fe-2Gew.%V nitriert bei 520°C für 10h; r_n=0.103 $atm^{-1/2}$.

Die Wachstumskinetik nitrierter Schichten von Fe-2Gew.%V Legierungen wurden als Funktion der Temperatur untersucht. Hierzu wurden die Proben bei 520 (bis 10h), 550 (bis 10h), 580 (bis 10h) u. 600°C (bis 7h) bei einer Nitrierkennzahl von 0.103 $atm^{-1/2}$ nitriert und Stickstofftiefenprofile für jede Probe gemessen. An die gemessenen Stickstofftiefenprofile wurden gerechnete Profile angepasst. Anpassungsparameter waren X, D und K. In Bild 7.9 ist die Anpassung für eine Probe, welche bei 580°C für 10h nitriert wurde, dargestellt.

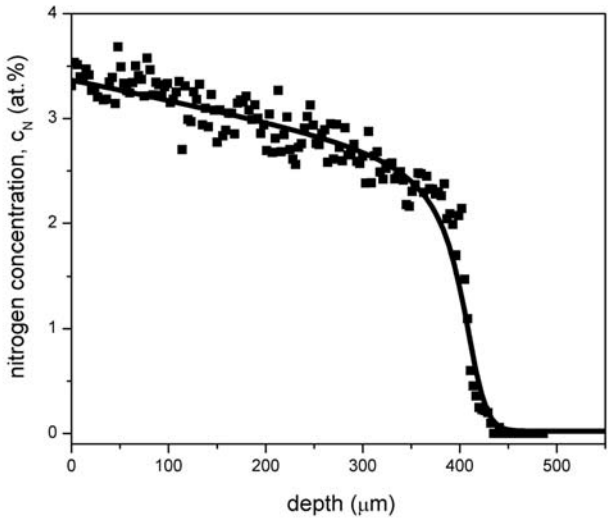

Bild 7.9: Stickstoffkonzentrationstiefenprofil einer nitriertne Fe-2Gew.%Cr probe, nitriert bei einer Kennzahl von r_n=0.103 $atm^{-1/2}$. Die rechteckigen Punkte stellen die Messwerte dar, während die durchgezogene Linie die angepasste Kurve angibt. Bei der Anpassung ergaben sich die folgenden Parameter: X=1.38; D=0.88x10^{-11}; K_{VN}=0.023 für 580°C bei einer Nitrierzeit von 10h.

Der Parameter X verringerte sich mit zunehmender Nitriertemperatur. Dies kann sowohl auf die schnellere Vergröberung als auch auf die verringerte Stickstoff – Vanadium Wechselwirkung bei höheren Temperaturen zurückgeführt werden. Der ermittelte Stickstoffdiffusionskoeffizient ist für die nitrierte Fe-2Gew.%V Legierung etwas geringer als für reines Eisen. Dies gilt speziell bei relativ geringen Nitriertemperaturen, da hier die Nitride vergleichsweise fein verteilt sind.

Curriculum Vitae

PERSONAL DATA

Name: Santosh Satappa Hosmani

Date of Birth: 22nd May 1980

Place of Birth: Belagam (Karnataka State, India)

Nationality: Indian

SCHOOLING

1995 **Maharashtra State Board of Secondary and Higher Secondary Education, Pune (Kolhapur Divisional Board), India**
Secondary School Certificate (S.S.C.) Examination (10-Year Course)

1997 **Maharashtra State Board of Secondary and Higher Secondary Education, Pune (Kolhapur Divisional Board), India**
Higher Secondary School Certificate (H.S.C.) Examination

HIGHER EDUCATION

1997-2001 **National Institute of Technology (formerly Regional College of Engineering) and Nagpur University, India**
B.Eng. (Metallurgy Engineering)
Thesis title: *Quality Evaluation of Centrifugally Spun Cast Iron Pipes.*

2001-2003 **Indian Institute of Technology, Bombay (Mumbai), India**
M.Tech. (Process Metallurgy)

05/2002-02/2003 **Universität Stuttgart, Germany**
M.Tech. thesis work, Under IIT-DAAD sandwich programme in Department Prof. Mittemeijer
Thesis title: *Gaseous Nitriding of Fe-Cr Alloys.*

05/2003-06/2006 **Department Prof. Mittemeijer, Max-Planck-Institut für Metallforschung and Universität Stuttgart, Germany**
PhD Student
Thesis title: *Nitriding of Iron-based Alloys; the Role of Excess Nitrogen.*

Acknowledgements

The present work was performed at the Institut für Metallkunde of the Universität Stuttgart and at the Max-Planck-Institut für Metallforschung, Stuttgart.

First of all I would like to thank my research supervisor Prof. Dr. Ir. E.J. Mittemeijer for accepting me as a PhD student in his department. I would like to thank him for his outstanding commitment, the continuous supervision and the numerous scientific discussions which have considerably contributed to the completion of this work. I have immensely benefited from his stimulating discussions, valuable inputs and continuous encouragement.

I am thankful to my daily supervisor Dr. R.E. Schacherl for his continuous co-operation in projects. He has considerably contributed to the successful completion of this work. My special thanks to him for taking the pain to write the German version of the summary.

My many thanks to all the colleagues of both the Max-Planck Institutes for their assistance during my research and hearty thanks to my friends who made my stay at Stuttgart pleasant and enjoyable.

Finally, I am extremely grateful to my beloved parents and sister who have always been a source of constant support and encouragement.